

Curriculum Vitae

Name: Naibo Zhang

Contact information: Naibo.zhang@som.umaryland.edu

Degree and Date: Ph.D., Oct 2025

Education

- | | |
|-------------|---|
| 2019-2025 | Ph.D. , School of Medicine, University of Maryland (UMB)
Major: Neuroscience |
| 2013-2015 | M.S. , Keck School of Medicine, University of Southern California (USC)
Major: Biochemistry and Molecular Biology |
| 2012 Summer | Exchange student, University of California Los Angeles (UCLA) |
| 2009-2013 | B.S. , Shandong University, China
Major: Biotechnology: Microbiology/Plant Physiology |

Publications

Finalizing:

1. (Targeting *PNAS*, 2025) Jaber, S.M., **Zhang, N. (Co-first author)**, Milstein, J.L., Hampton, B., Huang, W, Kane, M.A., Kingsbury, T.J., Yadava, N., Barrett, J.P., Loane, D.J., and Polster, B.M. “Inducible Nitric Oxide Synthase (iNOS)-catalyzed Reduction of the Coenzyme Q10 Analogue Idebenone Restores Mitochondrial Respiration in Pro-inflammatory Microglia.”
2. (Targeting *Neurotrauma Reports*, 2025) **Zhang, N.**, Saraswati, M., Piskoun, B., Robertson, C.L., and Polster, B.M. “Sex-Specific Acute Impairment of the Mitochondrial Respiratory Chain in a Rat Model of Pediatric Traumatic Brain Injury.”
3. (Review, targeting *Cells*, 2025) **Zhang, N.**, Freeman, D. and Polster, B.M. “BAX, VDAC, and permeability transition pores in inflammatory mitochondrial DNA release: is this the whole story?”
4. (2026) **Zhang, N.**, Vongdeuane, S., Wilson, S., Ding, J., Virata, G., Polster, B.M. “Nitric oxide (NO) and caspases inhibition rescues mitochondrial electron transport chain (ETC) Complex II and IV subunits degradation in pro-inflammatory microglia”

Published:

1. **Naibo Zhang**, Brian A. Roelofs, Evan A. Bordt, Boris Piskoun, Courtney L. Robertson, and Brian M. Polster, “CRABS-ROC, A Respirometry Protocol for Overcoming Substrate Limitations, Reveals Excess Brain Mitochondrial Complex I Capacity”, *Free Radical Biology and Medicine* 2025 Sep 9:241:24-31.
2. Hye Hyun Hwang, Chinmoy Sarkar, Boris Piskoun, **Naibo Zhang**, Apurva Borcar, Courtney L. Robertson, Marta M. Lipinski, Nagendra Yadava, Molly J. Goodfellow and Brian M. Polster, “Idebenone Mitigates Traumatic-Brain-Injury-Triggered Gene Expression Changes to Ephrin-A and Dopamine Signaling Pathways While Increasing Microglial Genes”, *Cells* 2025, 14, 824.
3. Evan A. Bordt, **Naibo Zhang**, Jaylyn Waddell and Brian M. Polster, “The Non-Specific Drp1 Inhibitor Mdivi-1 Has Modest Biochemical Antioxidant Activity”, *Antioxidants* 2022, 11(3), 450.
4. Aswathy Ammothumkandy, Kristine Ravina, Victoria Wolseley, Alexandria N Tartt, Pen-Ning Yu, Luis Corona, **Naibo Zhang**, George Nune, Laura Kalayjian, J. John Mann, Gorazd B. Rosoklija, Victoria Arango, Andrew J. Dwork, Brian Lee, Jason A D Smith, Dong Song, Theodore W Berger, Christianne Heck, Robert H Chow, Maura Boldrini, Charles Y Liu, Jonathan J Russin, and Michael A Bonaguidi, “Altered adult neurogenesis and gliogenesis in mesial temporal lobe epilepsy patients”, *Nature Neuroscience*, 2022 Apr;25(4):493-503.
5. Albina Ibrayeva, Maxwell Bay, Elbert Pu, David J Jörg, Lei Peng, Heechul Jun, **Naibo Zhang**, Daniel Aaron, Congrui Lin, Galen Resler, Axel Hidalgo, Mi-Hyeon Jang, Benjamin D Simons, Michael A Bonaguidi, “Early stem cell aging in the mature brain”, *Cell Stem Cell*, 2021 May 6;28(5):955-966.e7.
6. Byoung-San Moon, Aswathy Ammothumkandy, **Naibo Zhang**, Lei Peng, Albina Ibrayeva, Maxwell Bay, Athira Pratap, Hong Ju Park, Michael Anthony Bonaguidi, Wange Lu, “The Presence of Neural Stem Cells and Changes in Stem Cell-Like Activity With Age in Mouse Spiral Ganglion Cells In Vivo and In Vitro”, *Clinical and Experimental Otorhinolaryngology* 2018; 11(4): 224-232.
7. Xiaofeng Song, **Naibo Zhang**, Ping Han, Byoung-San Moon, Rose K. Lai, Kai Wang, Wange Lu, “Circular RNA profile in gliomas revealed by identification tool UROBORUS.” *Nucleic Acids Research*, 2016 May 19;44(9):e87.
8. Yang Zhao, Wei Dong, **Naibo Zhang**, Xinghui Ai, Mengcheng Wang, Zhigang Huang, Langtao Xiao, Guangmin Xia “A Wheat Allene Oxide Cyclase Gene Enhances Salinity Tolerance via Jasmonate Signaling” *Plant Physiology*, 164(2):1068-76, Feb, 2014.

Presentations

1. 2024 Poster presentation at National Neurotrauma Society (NNS)
 - *Mechanisms of mitochondrial dysfunction following traumatic brain injury-relevant pro-inflammatory microglial activation*
2. 2023 Poster presentation at Society for Neuroscience (SfN)
 - *Decoding the mechanisms of mitochondrial electron transport chain components loss upon pro-inflammatory microglial activation*
3. 2022 Poster presentation at National Neurotrauma Society (NNS)
 - *Acute, Sex-Specific Impairment of the Mitochondrial Respiratory Chain in a Juvenile Rat Model of Traumatic Brain Injury*
4. 2022 Short talk at Anesthesiology Research Retreat, University of Maryland, Baltimore
 - *Chemical reduction on the mitochondrial drug Idebenone to its active form is Catalyzed by iNOS in Pro-inflammatory Microglia*
5. 2021 Poster presentation (virtual) at Society for Redox Biology and Medicine (SfRBM)
 - *Stimulation of Mitochondrial Respiration by Idebenone in Pro-inflammatory Microglia is Catalyzed by iNOS*
6. 2018 Poster session at Society of Neuroscience (SfN)
 - *An improved cell culture system to recapitulate endogenous neural stem cell behavior*

Professional Society memberships

- 2018 member of Society of Neuroscience (SfN)
2021 member of Society for Redox Biology and Medicine (SfRBM)
2022 member of National Neurotrauma Society (NNS)
2023 member of Society of Neuroscience (SfN)
2024 member of National Neurotrauma Society (NNS)

Nationa Service

- 2023 Ad Hoc Reviewer, *Cell Reports Medicine*

Teaching and Montoring

Year	Name		Current
2015-2017	Talia Oughourlian	Undergrad, USC	PhD 2023, MSL
2016-2018	Justin Sheppard	Undergrad, USC	MD 2025, Resident physician
2017-2018	Rhea Koparde	Undergrad, USC	UI designer

2021-2023	Sitthixai Vongdeuane	Undergrad, UMBC	Research stuff UMB
2023	Jean Jouffroy	PhD rotation student, UMB	
2023	Geralin Virata	PhD rotation student, UMB	
2024	Yugantar Gera	PhD rotation student, UMB	
2024 summer	Shahana Wilson	Undergrad, UMBC	
2024 summer	Jennifer Ding	Undergrad, UMD College Park	

Abstract

Title: Mitochondria-Based Mechanisms and Interventions for Neurotrauma-relevant Neuroinflammatory Responses

Naibo Zhang, Doctor of Philosophy, 2025

Dissertation Directed by: Brian M. Polster, Ph.D., Professor, Department of Anesthesiology

In recent years, increased attention has been paid to the role of mitochondrial alterations in studies of traumatic brain injury (TBI). Mitochondria participate in the regulation of neuroinflammation after TBI. Disrupted mitochondrial respiration and impaired bioenergetics cause energy deficiency and reactive oxygen species (ROS) accumulation, facilitating the activation of pro-inflammatory signaling pathways in microglia, the innate immune cells of the brain. To robustly evaluate brain bioenergetics after TBI, we optimized a new Seahorse respirometry-based protocol, CRABS-ROC (Complex Respirometry Assay Bypassing Substrate-Restricted Oxygen Consumption). This protocol not only unmasks the full electron transport chain (ETC) Complex I-dependent respiratory capacity by bypassing substrate restrictions but also measures Complex-II- and IV-dependent respiration in the same experiment, on a variety of sample types. Using CRABS-ROC, we assessed ETC complex respiratory capacities in a rat pediatric TBI model, revealing sex-specific Complex I and IV deficiencies in males at an individual ETC complex level.

To restore impaired mitochondrial respiration in pro-inflammatory microglial cells, a Coenzyme Q10 (CoQ) short-chain analogue idebenone was employed. Idebenone supplies electron flux through ETC Complex III, bypassing a disruption at Complex I. To achieve this

activity, idebenone first requires a cytoplasmic reduction to its active form, idebenol. Previously, it was shown that the enzyme NAD(P)H quinone oxidoreductase 1 (NQO1) reduces idebenone in astrocytes. Here, we identified a different enzyme, inducible nitric oxide synthase (iNOS), which catalyzes most of the idebenone reduction in microglia.

Restoring impaired microglial respiratory function is predicted to inhibit pro-inflammatory signaling and mitigate secondary brain injury. Therefore, we also investigated ETC complex degradation mechanisms in microglia. We first observed that among representative subunits of each ETC complex, only the Complex III subunit UQCRC2 and the Complex V subunit ATPA5 remained unchanged in microglial cells stimulated to a pro-inflammatory state by lipopolysaccharide (LPS) and interferon-gamma (IFN- γ). Using iNOS-deficient *Nos2* knockout microglial cells, we found that nitric oxide (NO) regulates the degradation of the Complex II subunit SDHB and the Complex IV subunit MTCO1, but not the Complex I subunit NDUFB8. These findings indicate that multiple mechanisms contribute to ETC impairment in activated, pro-inflammatory microglia. A positive feedback loop between iNOS and activated caspase-1 protease was also identified, revealing a new system regulating the degradation of ETC complexes. These findings complement existing knowledge on pro-inflammatory signaling amplification.

Mitochondria-Based Mechanisms and Interventions for Neurotrauma-relevant
Neuroinflammatory Responses

By

Naibo Zhang

Dissertation submitted to the Faculty of the Graduate School of the
University of Maryland, Baltimore in partial fulfillment
of the requirements for the degree of
Doctor of Philosophy
2025

©Copyright 2025 by Naibo Zhang All rights Reserved

Acknowledgements

I would like to thank Graduate Program in Life Sciences and Program (GPILS) in Neuroscience (PiN) for offering me the opportunity and supporting me over these many years. Thank you to the current PiN program directors Dr. Todd Gould and Dr. Thomas Longden, and former directors Dr. MaryKay Lobo, Dr. Brian Mathur and Dr. Donna Calu for their effort to ensure the experience for the students. Thank you to the PiN program Academic Services Specialist Dr. Jennifer McFarland and Dr. Georgia Rogers for your assisting and caring during my study. I appreciate the help from Dr. Renee Cockerham and Dr. Sharron Graves for academic advice and the arrangements for my graduation. Thank you to Elice García-Baca for the help during my course years. Thank you to the Office of International Office (OIS) in the University of Maryland, Baltimore, for your support. When I looked back, I realized this was a long journey that was supposed to be very challenging, without the help from them I couldn't accomplish my study smoothly.

I would like to thank my committee members Dr. Fiskum for his guidance of my research as a true biochemistry professional, and for receiving comprehensive support from all lab members in Fiskum lab as a helpful neighbor. For Dr. Courtney Robertson for her guidance on my pediatric rat traumatic brain injury (TBI) studies, and for her support during multiple National Neurotrauma Society annual conferences. To Dr. Thomas Longden and Dr. Mariusz Karbowski, for their generous support and guidance to improve the rigor and quality of my work, during all these years. To Dr. Marta Lipinski, for her encouragement when I felt discouraging during my course years as a second language speaker, and for her support during my graduation. I would also thank Dr. Junfang Wu, Dr. Mervyn J. Monteiro, Dr. Brian Mathur and Dr. Marta Lipinski for joining my

qualification exam committee. Thanks to Dr. Thomas Blenpied, Dr. David Benavides and Dr. Marta Lipinski as my advisory committee members during my first year.

I would especially like to thank my mentor, Dr. Brian Polster, for his exceptional care and support during my thesis years. Besides his guidance on the study on our common interest in mitochondrial respiration, I thank Brian for allowing me to pursue my interest in TBI and electron transport chain (ETC) complexes degradation mechanisms. I appreciate his patience reviewing my writing from word to word, sentence to sentence, helping me fight with my natural weakness in my writing skills. In Dr. Brian Polster's laboratory, I achieved my initial goal of professionalizing my skills in studying molecular mechanisms and improving my presentation skills. Besides, I proudly inherited his faith in conducting rigorous science. Aside from work, I also learned much from his opinion as we both are serious basketball fans. I will always miss the days we played basketball together after work.

I would thank my parents for their financial support during these inflation years. I understand their torment, and I would like them to expect future success. Thank you to my grandma, Cui, for her emotional support and her unwavering waiting for me to return home. I will eventually make all their efforts worthy. I would like to thank my friends and colleagues I met in Baltimore city. Thanks to Dr. Nagendra Yadava for shadowing me with his mitochondria fundamental knowledge. Thanks to Joseph Sitthixai Vongdeuane and all other students who worked with me, for their effort on generating high quality data. Thanks to Ms. Beth R Horton for being a perfect neighbor who cared and prayed for me, and to her cats Swithen Horton and Macy Horton, for being the world's wisest and warmest cats. Thanks to all the students and scholars on my Saturday basketball team for helping me generate enough dopamine through the end of this journey.

Table of contents

Chapter 1 Introduction.....	1
1.1 Investigating mitochondrial dysfunction in traumatic brain injury	1
1.1.1 <i>Preclinical modeling of traumatic brain injury toward the discovery of improved strategies for long-term management.....</i>	1
1.1.2 <i>TBI-induced mitochondrial deficits and candidates for treatment</i>	2
1.1.3 <i>Evidence for mitochondrial damage in pediatric TBI</i>	9
1.2. Methods for studying mitochondrial respiration after TBI.....	11
1.2.1 <i>Current studies and methods for assessing mitochondrial respiratory function after TBI.....</i>	11
1.2.2 <i>Shortcomings of the Mito Stress Test protocol and the improvement</i>	12
1.3. Investigating the potential of idebenone for treating TBI-induced mitochondrial dysfunction	17
1.3.1 <i>History of idebenone being used as a treatment for neuroinflammation</i>	17
1.3.2 <i>Cytoplasmic reduction of idebenone by NQO1 is the established mechanism of bioactivation</i>	17
1.3.3 <i>The mechanisms of idebenone reduction in pro-inflammatory microglia are unknown</i>	18
1.4. Targeting neuroinflammatory signaling pathways to attenuate loss of ETC complex proteins in pro-inflammatory microglia.....	19
1.4.1 <i>Roles of microglia in neuroinflammation after TBI</i>	19
1.4.2 <i>TLR4 and NLRP3 as targets to prevent the activation-induced loss of ETC subunits</i>	23
1.4.3 <i>Caspase-1 as a target to prevent the activation-induced loss of ETC subunits</i>	24
1.4.4 <i>Inhibition of nitric oxide production as a target to prevent the activation-induced loss of ETC subunits.....</i>	26
Chapter 2 CRABS-ROC, A Respirometry Protocol for Overcoming Substrate Limitations, Reveals Excess Brain Mitochondrial Complex I Capacity.....	30
2.1 Abstract	30
2.2 Introduction	31
2.3 Materials and Methods.....	33
2.3.1. <i>Materials</i>	33
2.3.2. <i>Animals</i>	33
2.3.3. <i>Preparation of primary neuron cultures</i>	33
2.3.4. <i>Preparation of brain homogenate</i>	34
2.3.5. <i>Isolation of mitochondria and synaptosomes</i>	34
2.3.6. <i>Seahorse respirometry – neurons and synaptosomes</i>	35

2.3.7. Seahorse respirometry – homogenate or isolated mitochondria	38
2.3.8. Statistics	38
2.4. Results	39
2.4.1. The uncoupled oxygen consumption rate in the Mito Stress Test is limited by substrate supply	39
2.4.2. Complex I has excess capacity that is obscured in neurons metabolizing glucose	42
2.4.3. CRABS-ROC unmasks a Complex I activity deficit in harlequin mutant mitochondria	45
2.5. Discussion	50
2.6. Conclusions.....	54
Chapter 3 Sex-Specific Acute Impairment of the Mitochondrial Respiratory Chain in a Rat Model of Pediatric Traumatic Brain Injury.....	55
3.1 Abstract	55
3.2 Introduction	55
3.3 Materials and Methods.....	57
3.3.1 Animals and TBI surgery.....	57
3.3.2 Brain homogenate sample collection.....	58
3.3.3 Stock solutions for respirometry	59
3.3.4 Respirometry assay.....	59
3.3.5 Western blots	62
3.3.6 Data Analysis and Statistics	62
3.4 Results.....	63
3.4.1 Detection of male-specific decreases in Complex I- and IV-dependent respiration at 24 hours post-TBI	63
3.4.2 Levels of representative electron transport chain complex subunits are unchanged at acute time points after TBI in males	67
3.5 Discussion.....	69
Chapter 4 Inducible Nitric Oxide Synthase (iNOS)-catalyzed Reduction of the Coenzyme Q10 Analogue Idebenone Restores Mitochondrial Respiration in Pro-inflammatory Microglia.....	73
4.1 Abstract	73
4.2 Significance	74
4.3 Introduction	74
4.4 Results.....	76
4.4.1 Comparison of brain cell idebenone reduction activity.	76
4.4.2 Biochemical enrichment of the LPS/IFN- γ -induced microglial idebenone-reducing enzyme(s).	80

4.4.3 Evidence that iNOS mediates LPS/IFN- γ -induced microglial idebenone-reducing activity.	84
4.4.4. iNOS-dependent rescue of LPS/IFN- γ -mediated respiratory suppression by idebenone in pro-inflammatory microglial cells	87
4.5 Discussion	95
4.6 Materials and Methods	97
4.6.1 Materials.....	97
4.6.2 Preparation and maintenance of cell cultures	97
4.6.3 CRISPR/Cas9 generation of HAPI NOS2 knockout cells.....	98
4.6.4 Pro-inflammatory activation of microglia.....	99
4.6.5 Microplate-based Idebenone Reduction Assay.....	99
4.6.6 Fractionation of HAPI cell extract by size exclusion and NAP(D)H affinity chromatography	100
4.6.7 In-gel activity assays for detection and isolation of idebenone-reducing enzymes	100
4.6.8 Identification of proteins by mass spectrometry	101
4.6.9 Griess Assay	101
4.6.10 Cell-based respirometry	102
4.6.11 Statistical analysis	102
Chapter 5	
Nitric Oxide (NO) Production Prevents the Loss of a Subset of Mitochondrial Electron Transport Chain Subunits During Pro-inflammatory Microglial Activation	103
5.1 Introduction	103
5.2 Materials and Methods	106
5.2.1 Cell culture, pro-inflammatory activation, and sample collection	106
5.2.2 Protein detection by western blot.....	107
5.2.3 Griess assay.....	108
5.2.4 Statistical analysis	108
5.3 Results	109
5.3.1 Pharmacological co-inhibition of TLR4 and caspase-1 may lead to partial rescue of the Complex IV subunit MTCO1	109
5.3.2 Elimination of NO production rescues the Complex II and IV subunits SDHB and MTCO1, respectively, but not the Complex I subunit NDUFB8.....	112
5.3.3 Caspase activity is not required for the loss of ETC complex subunits	115
5.3.4 A caspase-1/iNOS positive feedback loop may contribute to Complex II and IV degradation.....	115
5.4 Discussion	119

Chapter 6 Evaluation of idebenone’s ability to reduce two-week post-injury lesion size following adult mouse TBI.....	121
6.1 Introduction	121
6.2 Materials and methods	122
6.2.1 Reagents.....	122
6.2.2 Animal husbandry.....	123
6.2.3 Controlled cortical impact (CCI).....	123
6.2.4 Intraperitoneal (i.p.) injection	124
6.2.5 Hematoxylin and eosin (H&E) staining	124
6.2.6 Microscopy imaging and quantification of lesion volumes	124
6.3 Results.....	124
6.3.1 CCI with a 1.5 mm depth is optimal for the induction of moderate TBI.....	124
6.3.2 Idebenone failed to decrease the lesion volume at 14 days post-injury.....	125
6.4 Discussion	128
Chapter 7 Discussion	129
References	136

List of Figures

Figure 1.1 Schematic figure showing electron flux through the electron transport chain (ETC) and oxidative phosphorylation under physiological conditions.	4
Figure 1.2 Example traces cartoons illustrating different definitions of respiration states.....	6
Figure 1.3 A schematic figure summarizing chemicals for Seahorse respirometry that are used in this dissertation.	15
Figure 1.4. Schematic diagrams comparing respirometry-based protocols for assessing mitochondrial respiratory dysfunction after brain injury.	16
Figure 1.5 Putative signaling pathways acting upstream of ETC complexes degradation in pro-inflammatory microglia.	22
Figure 2.1 Neither NADH- or TMPD/ascorbate-dependent respiration led to excessive oxygen depletion by primary cortical neurons, but the latter required a correction for chemical oxygen consumption.	37
Figure 2.2 Uncoupled respiration by intact neurons and synaptosomes is limited by substrate availability.	40
Figure 2.3 The antioxidant Trolox does not mimic or occlude pyruvate's enhancement of uncoupled respiration.	41
Figure 2.4 NADH delivery to mitochondria within primary rat cortical neurons reveals excess Complex I capacity.	44
Figure 2.5 Titrations of cytochrome c (cyt c) and alamethicin (alm) for the Complex Respirometry Assay Bypassing Substrate-Restricted Oxygen Consumption (CRABS-ROC) protocol applied to freeze-thawed brain homogenate.	46

Figure 2.6 CRABS-ROC unmasks Complex I deficiency in previously frozen AIF-depleted isolated harlequin (Hq) brain mitochondria.....	48
Figure 3.1 Schematic illustration of the CRABS-ROC protocol used to evaluate mitochondrial electron transport chain function in brain homogenates from the immature rat controlled cortical impact (CCI) TBI model.	61
Figure 3.2 TBI-induced decreases in Complex I- and IV-dependent oxygen consumption rates in male ipsilateral brain homogenates at 24 hours post-injury.....	66
Figure 3.3 Levels of representative electron transport chain complex subunits in uninjured vs. injured hemispheres at 24, 48, and 72 hours post-TBI.	68
Figure 4.1 Idebenone is enzymatically reduced by astrocytes and by pro-inflammatory microglia.	77
Figure 4.2 Idebenone is reduced by recombinant iNOS and <i>NOS2</i> gene deletion attenuates LPS/IFN- γ -induced microglial idebenone-reducing activity.....	82
Figure 4.3 Functional verification of NO release in <i>Nos2</i> KO clones by Griess assay.....	85
Figure 4.4 <i>Nos2</i> gene deletion diminishes the ability of idebenone to restore Complex I-impaired oxygen consumption in pro-inflammatory microglia.	86
Figure 4.5 Chemical oxygen consumption caused by the addition of ascorbate contributes to unreliable OCR.	89
Figure 4.6 <i>Nos2</i> depletion impaired idebenone-stimulated OCR.....	91
Figure 4.7 Recombinant iNOS enables idebenone-mediated bypass of Complex I inhibition in <i>Nos2</i> knockout cells.	93

Figure 5.1 Co-inhibition of TLR4 inhibitor TAK-242 and caspase-1/11 inhibitor VX-765 partially rescued the Complex IV subunit MTCO1 loss in empty vector wildtype HAPI cells while Nos2 KO completely rescued the loss.	111
Figure 5.2 Either pharmacological iNOS inhibition or Nos2 KO rescues ETC complex subunits SDHB and MTCO1.....	114
Figure 5.3 The pan-caspase inhibitor Q-VD-OPh decreases the iNOS enzyme level but fails to prevent the loss of ETC complex subunits.	118
Figure 6.1 Comparisons of lesion size for CCI impact depths of 1.0 mm and 1.5 mm in male and female mice. The dotted area is masking the injured area by the Montage software.	126
Figure 6.2 Effect of idebenone treatment on lesion size in CCI mice at 14 days post-injury.....	127

List of Abbreviations

AA, Antimycin A

AD, Alzheimer's disease

ADP, Adenosine diphosphate

AIF, apoptosis-inducing factor

ANOVA, Analysis of variance

ARE, Antioxidant response element

ATP, Adenosine triphosphate

BCA, bicinchoninic acid

BMDM, Bone marrow-derived macrophage

BSA, Bovine serum albumin,

CoQ, coenzyme Q10

CPTIO, 2-(4-Carboxyphenyl)-4,4,5,5-tetramethylimidazoline-1-oxyl-3-oxide

CRABS-ROC, Complex Respirometry Assay Bypassing Substrate-Restricted Oxygen Consumption

Cyt c, Cytochrome c

DAMP, Damage associated molecular pattern

DCPIP, Dichloroindophenol

DMSO, Dimethylsulfoxide

DNP, Dinitrophenol

DIV, days *in vitro*

ECAR, Extracellular acidification rate

EDTA, Ethylenediaminetetraacetic acid

EGTA, ethylene glycol-bis(β -aminoethyl ether)-N,N,N',N'-tetraacetic acid

ELISA, Enzyme linked immunosorbent assay

EV, empty vector

ETC, Electron transport chain

FBS, Fetal bovine serum
FCCP, Carbonyl cyanide 4-(trifluoromethoxy)phenylhydrazone
GSDMD, gasdermin D
HAPI, Highly aggressively proliferating immortalized
HEPES, 4-(2-hydroxyethyl)-1-piperazineethanesulfonic acid
Hq, harlequin
IFN- γ , Interferon-gamma
IL-10, Interleukin-10
IL-1 β , Interleukin-1 beta
IL-6, Interleukin-6
iNOS, Inducible nitric oxide synthase
KO, Knockout
LPS, Lipopolysaccharide
L/I, LPS/IFN- γ , Lipopolysaccharide + Interferon-gamma
NO, Nitric oxide
Nos2, nitric oxide synthase 2
NOX, NADPH oxidase NQO1,
NAD(P)H:quinone acceptor oxidoreductase 1
Nrf2, nuclear factor erythroid 2-related factor 2
O₂, Oxygen
OCR, Oxygen consumption rate
OLIGO, Oligomycin
ONOO-, Peroxynitrite PD, Parkinson's disease
PDH, pyruvate dehydrogenase
Pier A, Piericidin A
RNS, Reactive nitrogen species
ROS, Reactive oxygen species

TBI, Traumatic brain injury

TCA, Tricarboxylic acid

TMPD, N,N,N',N'-tetramethyl-p-phenylenediamine

TNF- α , Tumor necrosis factor-alpha

TLR-4, Toll-like receptor-4

WT, Wild type

Chapter 1

Introduction

1.1 Investigating mitochondrial dysfunction in traumatic brain injury

1.1.1 Preclinical modeling of traumatic brain injury toward the discovery of improved strategies for long-term management

Traumatic brain injury (TBI) is one of the leading causes of mortality among all central nervous system (CNS) disorders [1]. TBI happens in diverse ways and usually results in complex and persistent conditions involving many cell types, wound healing, and long-term inflammation. Secondary brain injury is caused by persistent inflammation [2], resulting in enlarged lesion size and contributing to cognitive dysfunction. Furthermore, TBI and persistent neuroinflammation increase the lifetime risk of chronic pain [3] and neurodegenerative disorders [4, 5] including Alzheimer's disease [6] and Parkinson's disease. Severe TBI increases the long-term risk of stroke [7].

TBI induces increased amyloid β ($A\beta$) production and Alzheimer's disease-like symptoms [8]. Mild TBI is responsible for a 56% increased risk of Parkinson's disease in United States veterans [9]. Long-term mitochondrial dysfunction is commonly observed in injured brains, disrupting energy production and causing failure to meet the brain's high energy demand[10, 11]. Mitochondrial dysfunction can also contribute to prolonged neuroinflammation by generating excessive reactive oxygen species (ROS) and promoting the activation of pro-inflammatory microglia[10, 12]. The increasingly appreciated exacerbating role of neuroinflammation is redefining TBI as a chronic disorder that may require long-term "management" more so than an acute treatment. Even greater consideration to long-term management may need to be considered

in pediatric/juvenile TBI [13], which will be discussed further in section 1.2. Therapeutic strategies aimed at restoring mitochondrial bioenergetics after TBI during the extended clinical management phase are therefore worthy of pursuit.

Although rodent brains have some distinct TBI and inflammatory responses compared with human brains, rodent TBI models are still commonly used. Just as human TBI is diagnosed and classified into mild, moderate, and severe based on criteria such as the Glasgow Coma Scale (GCS)[14], rodent TBI has also been carefully classified by severity and impact type. Two major categories of animal models are penetrating TBI (open-head TBI) and non-penetrating TBI (closed-head TBI) based on the insult type [15]. One of the most used models is the controlled cortical impact (CCI) penetrating TBI model[16-18], which is programmable for lesion size, depth, velocity, and impact duration to model different severities of human brain injury. CCI is usually a direct focal hit onto the exposed brain surface post-craniotomy, with a known-diameter probe. CCI can be used to model concussions, hemorrhage, edema, and inflammation in a controllable manner.

1.1.2 TBI-induced mitochondrial deficits and candidates for treatment

Mitochondrial bioenergetics deficits caused by TBI result in interrupted neuronal energy supply, accumulation of ROS, mitochondrial DNA (mtDNA) release, and pro-inflammatory microglial activation. These events are all thought to contribute to the overall neuropathology of TBI. Disrupted energy production is usually a central component of the TBI pathology. The electron transport chain (ETC) generates the proton gradient across the mitochondrial inner membrane (MIM) and its function is required for oxidative phosphorylation (OXPHOS; Figure 1.1). Aberrant ETC function can cause bioenergetics failure and ROS accumulation, especially

during a prolonged post-TBI recovery period. Therefore, it is crucial to understand how the ETC is damaged after TBI and develop strategies to restore OXPHOS function. Such strategies may rewire mitochondrial energy supply and reduce the secondary brain damage caused by ETC dysfunction. Mitochondrial dysfunction has been separately studied in both acute (minutes to days) and chronic (weeks to months) periods in animal models. Deficiencies of OXPHOS caused by TBI were evaluated at the resolution of ATP production efficiency and sometimes individual ETC complex-dependent respiration. Many studies have assessed the dysfunction of mitochondrial energy production indirectly by respirometry-based measurements of oxygen consumption rate (OCR).

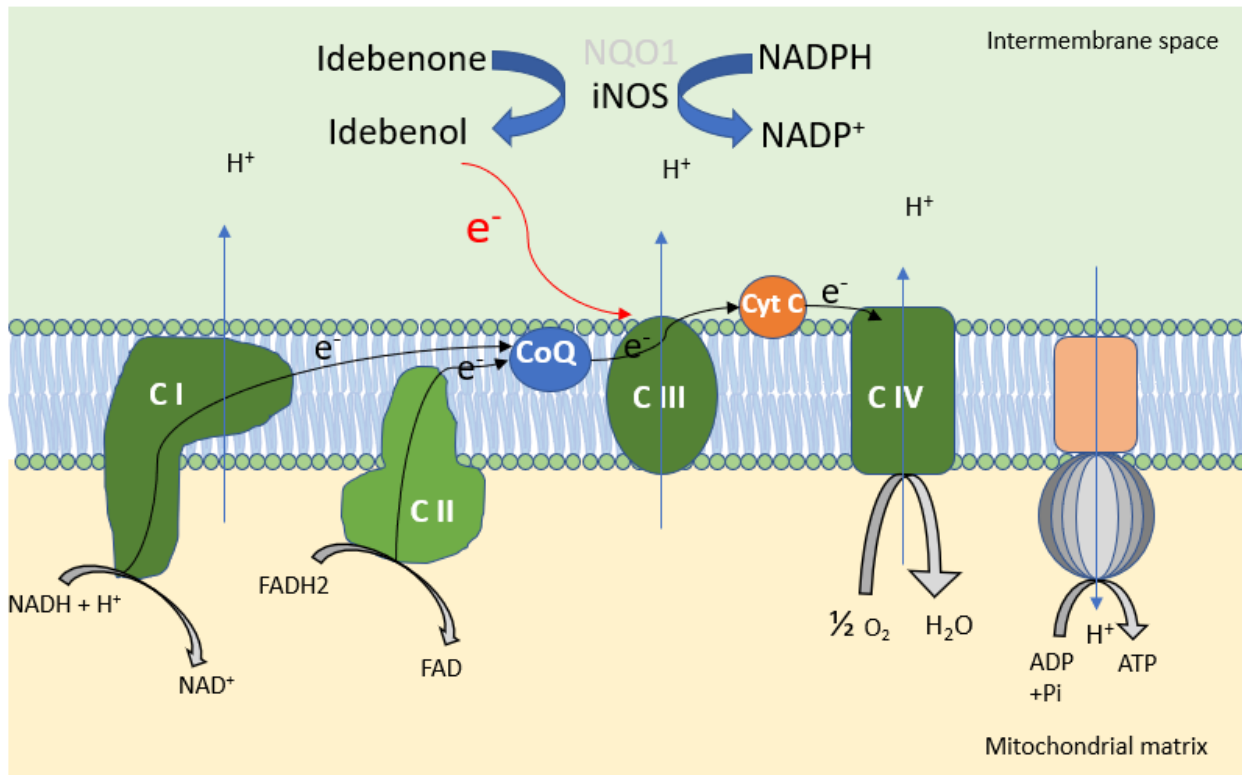
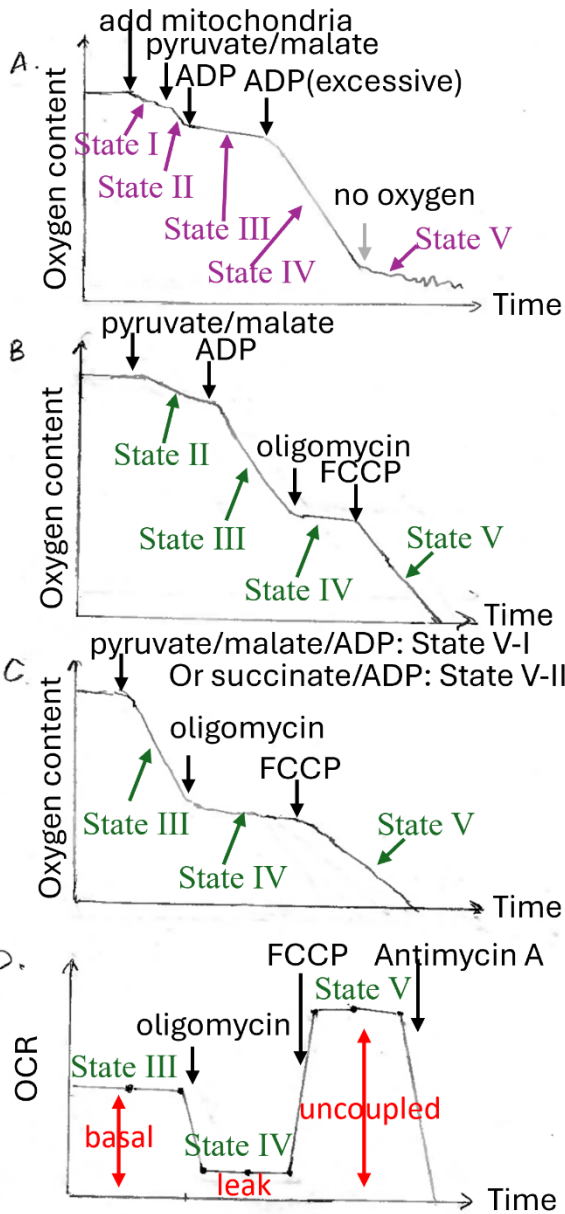


Figure 1.1 Schematic figure showing electron flux through the electron transport chain (ETC) and oxidative phosphorylation under physiological conditions.

CoQ: coenzyme Q, cyt c: cytochrome c, e⁻: electrons. The black arrows show the direction of physiological electron flux. The red arrow shows the supply of electrons provided by the exogenous molecule idebenone. NQO1 is an enzyme expressed by some cell types that is established to reduce idebenone into its bioactive form, idebenol. iNOS is a second enzyme, demonstrated by this dissertation research, that catalyzes idebenone reduction. The blue curved arrows show the redox reactions catalyzed by NQO1 and iNOS, using NADPH as substrate.

Other than the physiological basal OCR and the uncoupled maximal OCR typically evaluated in cells, distinct respiratory states can be induced and measured when using isolated mitochondria. Respiratory States I-V were defined by Chance and Williams in 1955 based on polarographic oxygen electrode measurements [19]. State I respiration is the respiration of isolated mitochondria in the presence of abundant oxygen and inorganic phosphate but no exogenous substrates so that it is usually slow. State II respiration represents slow respiration stimulated by the addition of the Complex I-linked substrates pyruvate and malate when there is no ADP added. State III respiration denotes the highest rate of oxygen consumption stimulated by ADP, which induces phosphorylating respiration driven by the ATP synthase. State IV respiration represents leak-driven respiration which remains after all the ADP added to induce State III respiration has been consumed. The ratio of State III respiration to State IV respiration, which is referred to as Respiratory Control Ratio (RCR), is an important parameter representing the mitochondrial energetic efficiency. The original definition of State V respiration refers to the anaerobic state on the oxygraph after all oxygen is consumed in the system, and the oxygen consumption rate is no longer linear as it was in State IV. However, an alternative definition of State III by Nicholls and Ferguson in their book (David Nicholls and Stuart Ferguson (1992), *Bioenergetics 2*, Academic Press.) represents leak respiration (Figure 1.2B) when oxygen consumption is due to proton leak across the MIM due to the addition of ADP, which is functionally equal to the State IV respiration in Chance and Williams' definition (Figure 1.2A). Alternative definition of State V respiration represents an uncoupled respiration when uncoupler FCCP or DNP is present (Figure 1.2C). It can be further distinguished by Complex I-driven State V respiration and Complex II-driven State V respiration by adding Complex I-and II-specific substrates, respectively [20-22].



Chance and Williams, 1955

Nicholls and Ferguson, 1992

In current Seahorse protocol

Example Seahorse trace in OCR

Figure 1. 2 Example traces cartoons illustrating different definitions of respiration states.

(A) the earliest definition of respiration states first brought up by Chance and Williams in 1955. (B) alternative definitions from the book *Bioenergetics 2*, by Nicholls and Ferguson in 1992. (C) Example traces explaining the modern definition of respiration states measured using Seahorse protocols. State V-I: Complex I-driven State V respiration, an uncoupled respiration driven by the addition of Complex I-specific substrates pyruvate and malate; State V-II: Complex II-driven State V respiration, an uncoupled respiration driven by the addition of Complex II-specific substrate

succinate. **(D)** Example OCR traces adding a reflection of respiration state rates onto modern Seahorse-based OCR traces.

Table 1.1 Studies showing energy production deficiency post-TBI.

model	Affected rates	authors
mouse	RCR, State III, State V-I, State V-II decrease at 1 and 3h post TBI	Gilmer, L.K., et al. 2009
mouse	State III-I (79%), State, State III-II(81%) decrease, at 72h post-TBI	Singh, I.N., et al. 2006
rat	State II-IV, State V-II respiration decrease at day3 but recover incompletely at day5 RCR (declines at day 3 and recovers at day5)	Hill, R.L., et al. 2017
mouse	State III, State V-I, State V-II respiration decrease at day 28 post-TBI (Close-head injury)	Lyons, D.N., et al. 2018

Many studies suggest energy production deficiency after TBI. Actual oxygen consumption, RCR, State III, Complex I-driven State V and Complex II-driven State V respiration were all significantly decreased acutely in the injured cortex at both 1 and 3 h post-trauma [23]. OCR was also decreased at 72 hours after CCI, with State III respiration decreased by 79% or 81% when driven by Complex I or Complex II substrate, respectively [24]. Mitochondrial OCR exhibits partial recovery over time in the rat CCI model. A comprehensive time course study of 9-10 week-old male rats from the earliest three hours post-injury to Day 5 showed significant respiration decreases from three hours to Day 3, and an incomplete recovery of State II-IV respiration and succinate-stimulated respiration at Day 5 [25]. RCR was unaltered until a significant decline at Day 3, followed by a complete recovery at Day 5. However, this study lacked information between Day 3 and Day 5, making the duration of the impairment unclear. More recent studies focused on long-term mitochondrial dysfunction post-TBI. In a mouse closed-head injury TBI model, significant decreases were observed in State III and Complex I-driven and Complex II-driven state V respiration in cortical and hippocampal mitochondria at 28 days post-injury even though in this model, deficits were not seen on Day 3 [20]. I would summarize the data above with some kind of cartoon or table.

Many pharmacological compounds used in preclinical TBI models were reviewed by Thapak and Gomez-Pinilla [15] in 2024. However, only a few of them showed the ability to restore mitochondrial membrane potential or improve energetics, with most targeting inhibition of pro-inflammatory signaling pathways. Among the mitochondria-targeted compounds, cyclosporin A (CsA), which inhibits mitochondrial permeabilization transition pore (mPTP) opening, improved bioenergetics deficits following CCI when administered at 15 minutes post-injury [26]. The mPTP

is a non-selective pore formed on MIM that increases mitochondrial permeability that causes cell necrotic death and neurodegeneration [27].

However, there are no FDA-approved drugs for specifically stimulating mitochondrial ETC function after TBI. Idebenone, a structural analog of ubiquinone (Coenzyme Q) has shown potential for rescuing impaired mitochondrial respiration, and it is approved by the European Medicines Agency (EMA) for the treatment of visual impairment in adolescents and adults with Leber's hereditary optic neuropathy (LHON) [28]. Idebenone and other bioavailable quinone compounds are promising drug candidates for the long-term management of TBI because they can act as both antioxidants and electron donors to reverse respiratory deficiencies. In this dissertation, we tested idebenone for neuroprotection in mouse CCI, as well as for its ability to rescue mitochondrial respiration in our *in vitro* model of microglial activation. The neuroprotective potential of idebenone and its mechanisms of action will be further discussed in 1.3.

1.1.3 Evidence for mitochondrial damage in pediatric TBI

Pediatric/juvenile TBI may involve different injury mechanisms and consequences compared to adult TBI because the brain is still developing. TBI during childhood causes altered neurodevelopment and deficits that extend well into adulthood. Among 2-12 years old children who had experienced moderate to severe TBI, intellectual functional assessment by an IQ test fell to the lower end of the average IQ range at 10 years post-TBI. However, IQ was not significantly different at the 10-year follow up compared with the control group [29]. Reduced cerebral blood flow and decreased brain oxygen metabolism were observed in severely injured children at three months post-TBI [30]. Evidence indicates that pediatric TBI can cause a metabolic crisis leading

to cognitive damage that persists into adulthood. CCI is one of the most widely used preclinical models to experimentally recapitulate TBI damage in juveniles as well as adults. CCI causes significant deficits in hippocampus-dependent cognition at two months post-injury and adult neurogenesis at three months post injury in postnatal day (PND) 5-7 New Zealand white rabbits [31]. The brain development in these rabbits is comparable to the infancy stage in a human and to PND15-20 in rodents. Mechanical damage to the brain causes not only a direct tissue lesion but also subsequent neuroinflammation cascades that can exacerbate the damage. Mitochondrial bioenergetic deficiency and aberrant elevated ROS production are thought to contribute to the neuroinflammation and cell death in the central nervous system (CNS) after TBI. Since the developing juvenile brain exhibits some metabolic differences compared to the mature brain, including with regard to mitochondrial substrate usage [32-34], understanding TBI-induced bioenergetic perturbations in developing brains is crucial to developing treatments that recover brain function.

The focus of mitochondrial studies in pediatric TBI now is very different than 20 years ago when the emphasis was on developmental differences in calcium buffering, brain metabolism, and ROS between immature and mature brains [35], Seahorse-based respirometry has emerged as a new tool to evaluate mitochondrial dysfunction in pediatric TBI. To understand the effects of TBI on the respiratory function of cells in pediatric brains at a more detailed level, it is necessary to investigate respiration rates dependent on individual ETC complexes. This can now be done using a new Seahorse respirometry protocol, the optimization of which is described in Chapter 2.

There are sex differences in mitochondrial respiratory impairments following TBI in adult rodents [21, 22, 36]. Female non-synaptic cortical mitochondria show impaired State III and Complex II-driven State V respiration at 12 hours post CCI, impaired State III, State IV, Complex

I-driven State V and Complex II-driven State V respiration at 24h post CCI, while only male synaptic mitochondria show early impairments in State III, Complex I-driven State V and Complex II-driven State V respiration at 12 hours post-CCI [22]. However, the possibility that sex influences mitochondrial alterations after pediatric TBI is largely unexplored. Physiological progesterone levels are neuroprotective in adult female rats and can preserve mitochondrial bioenergetic function as assessed by measuring the RCR [35]. Additionally, for PND 17-21 rats, pre-treatment with exogenous progesterone protects the RCR of male but not female rats post-TBI [37]. Sex differences in mitochondrial respiratory impairment may be an important factor to consider during the design of bioenergetics-based therapeutics.

1.2. Methods for studying mitochondrial respiration after TBI

1.2.1 Current studies and methods for assessing mitochondrial respiratory function after TBI

The best ways to test for OXPHOS dysfunction in cells or isolated mitochondria are to measure ATP production or oxygen consumption in the presence of energy substrate(s). Clark electrodes and other amperometric sensors measure real-time oxygen consumption directly from biological samples. However, the yield of biological material may be limiting, and the procedure itself is time consuming. Luciferase-based ATP measurements are the most direct way to evaluate net bioenergetic function; however, this method does not distinguish between mitochondria- and glycolysis-derived ATP unless pathway inhibitors are employed. In addition, because steady-state measurements reflect a balance between ATP production and consumption, changes may be difficult to interpret.

Since the technology was first launched in 2006, Seahorse respirometry (Agilent) has been widely used for fast and high-throughput evaluation of mitochondrial ETC function. The employed fluorescent oxygen sensors allow for serial measurements of real-time OCRs in 24 to 96 samples simultaneously, depending on the instrument model. With the use of specific ETC substrates or inhibitors, the Seahorse respirometer is a powerful tool to dissect changes in mitochondrial bioenergetic properties. The Mito Stress Test is a popular protocol for measuring the basal and maximal respiration rates of cells, as well as oxygen consumption linked to ATP synthesis and spare respiratory capacity. The spare respiratory capacity is the difference between the basal and maximal OCR, and it predicts the capacity of the cells' mitochondria to respond to increased energy demand.

1.2.2 Shortcomings of the Mito Stress Test protocol and the improvement

The Mito Stress Test protocol is the most used Seahorse respirometry protocol to study mitochondrial dysfunction in disease models. In the classical protocol, basal respiration rate is measured before oligomycin is added through the Seahorse instrument's first injection port. A schematic figure summarizing common substrates and chemicals that are used in Seahorse respirometry is provided (Figure 1.2). Oligomycin inhibits the ATP synthase to stop mitochondrial ATP production and, in cells, a compensatory increase in glycolysis usually results to meet the energy demand. The difference in OCR before and after oligomycin addition represents the ATP production-associated oxygen consumption. The residual OCR after oligomycin injection is driven by proton leak across the MIM. An uncoupler is added after oligomycin. The protonophore carbonyl cyanide-p-trifluoromethoxyphenylhydrazone (FCCP) is the most widely used uncoupler to disrupt the proton gradient across the MIM. With the loss of protonmotive force, respiratory

control by the ATP synthase is relinquished and the uncoupler-stimulated OCR value is considered the maximal respiration rate.

The energy substrates included in the Seahorse assay medium are typically glucose and pyruvate, which drive ETC activity. Metabolism of these substrates generates electron flux from the reduced forms of nicotinamide adenine dinucleotide (NAD) and flavin adenine dinucleotide (FAD) (Figure 1.1.). NADH is the direct substrate of ETC Complex I and is generated from the tricarboxylic acid (TCA) cycle by dehydrogenase enzymes. Because pyruvate is cell permeable and enters the mitochondrial matrix through a specific transporter, it can be used as an exogenous Complex I-linked substrate. When extra pyruvate is added after FCCP, an OCR increase suggests a restriction in endogenous mitochondrial substrate provision by glycolysis [38] (Example OCR traces Figure 1.3B). In other words, there is a substrate restriction on the maximal respiration rate induced by FCCP when glucose is the only energy substrate provided. Therefore, the FCCP-induced OCR in glucose-metabolizing cells does not represent the full capacity of the ETC. In the classical Mito Stress Test, a combination of the ETC Complex I inhibitor rotenone and Complex III inhibitor antimycin A are injected after FCCP through the third injection port, causing complete inhibition of mitochondria-dependent respiration. Without supraphysiological levels of pyruvate supplementation prior to the injection of ETC inhibitors, the Mito Stress Test fails to yield the maximal ETC-dependent respiration rate because of substrate limitations.

As another way to bypass the endogenous substrate restriction impeding maximal OCR measurement, direct substrates of ETC complexes can be introduced to the mitochondria within cells. Abundant NADH can be supplied to Complex I when the bacterial pore-forming peptide alamethicin is added to permeabilize mitochondrial membranes, instead of adding FCCP uncoupler and pyruvate substrates. Exogenous purified cytochrome *c* also needs to be supplied to the

mitochondria to measure OCR because alamethicin causes the release of the endogenous cytochrome *c*. In this assay, NADH-induced respiration minus the OCR measured following rotenone addition is considered Complex I-dependent respiration, while the Complex II-specific substrate succinate can subsequently be added to induce Complex II-dependent respiration. To assess the full capacity of Complex IV, tetramethylphenylenediamine (TMPD) and ascorbate can then be added, which stimulate electron entry through cytochrome *c*. Thus, this new protocol enables the serial assessment of ETC Complex I-, II-, and IV-dependent respiration. Furthermore, this new protocol can be applied to various sample types, including cultured cells, purified mitochondria, and tissue homogenates. It provides the means to rigorously evaluate the activity of individual ETC complexes under physiologically or pathologically relevant conditions. Identifying specific deficits in individual ETC Complex capacities under pathological conditions, such as TBI and other neurodegenerative disorders, may reveal new strategies to relieve or bypass the ETC impairments.

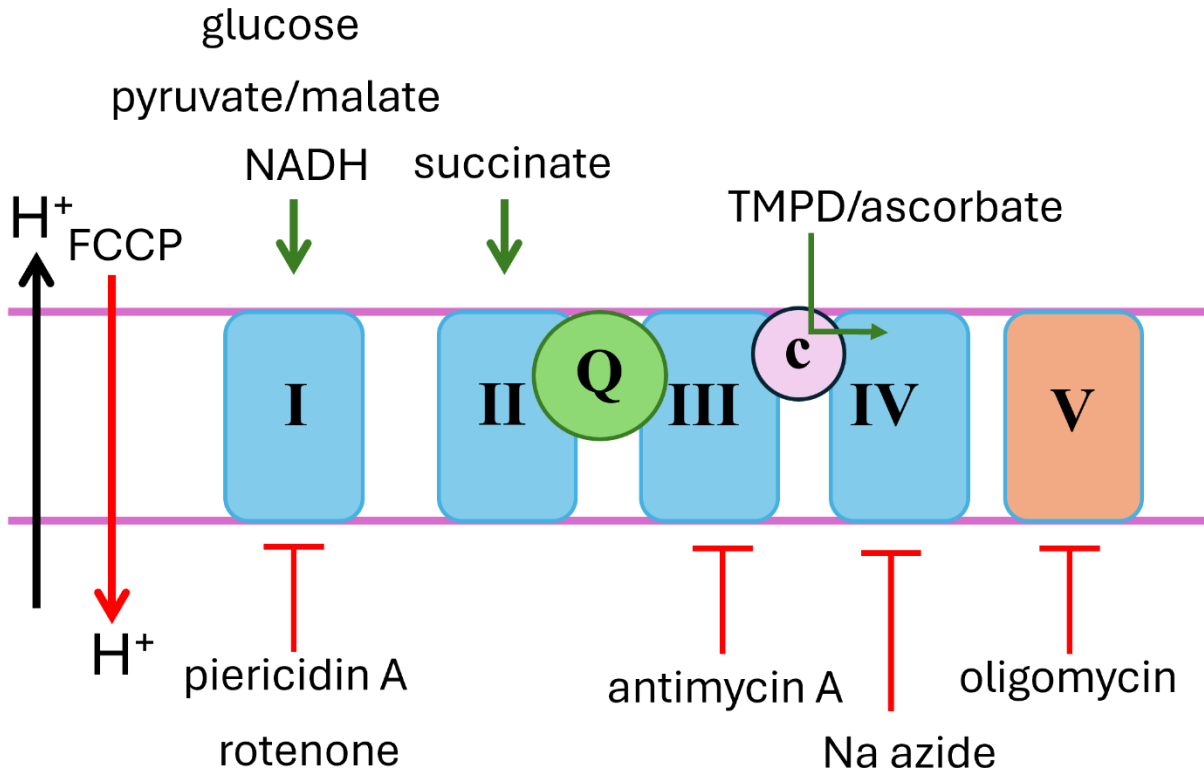


Figure 1.3 A schematic figure summarizing chemicals for Seahorse respirometry that are used in this dissertation.

Red arrow showed FCCP mediating a proton leak into mitochondrial matrix, in reverse of the physiological proton movement direction across the mitochondrial inner membrane. Green arrows show individual ETC complex substrates that stimulate OCR in Seahorse. Red blunted arrow showed inhibitors against each ETC complex.

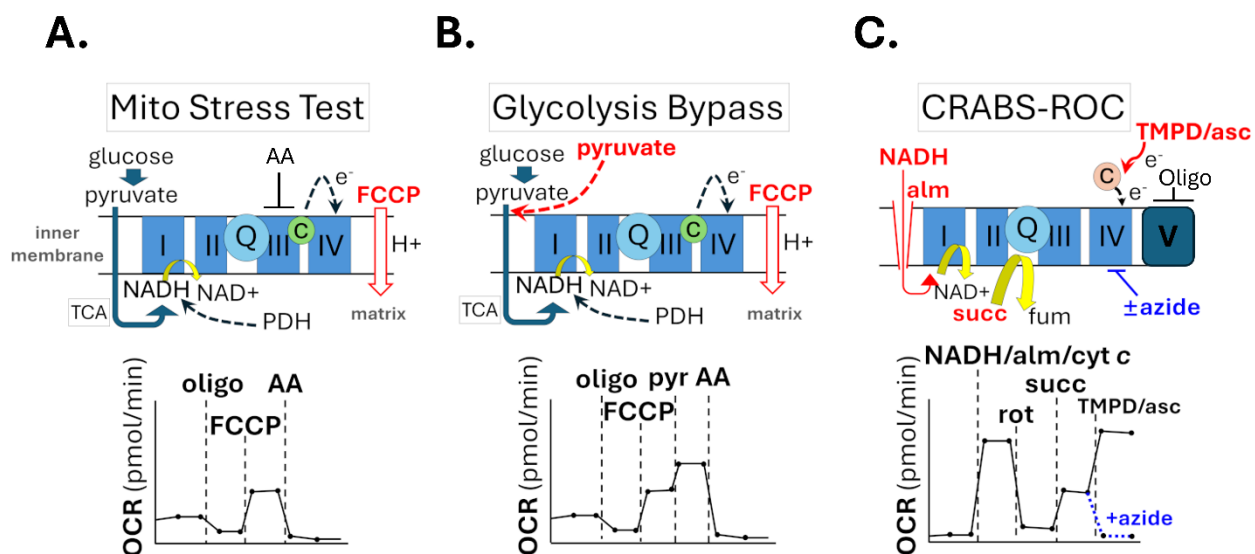


Figure 1.4. Schematic diagrams comparing respirometry-based protocols for assessing mitochondrial respiratory dysfunction after brain injury.

A-C The upper cartoons illustrate substrate supply and electron flux during the respirometry test. Added reagents are shown in red. Lower traces are representative respirometry OCR traces matching each upper cartoon. The abbreviations are as follows: oligo, oligomycin; AA, antimycin A; pyr, sodium pyruvate; alm, alamethicin; cyt *c*, cytochrome *c*; succ, succinate; rot, rotenone; asc, ascorbate. (A) The Mito Stress Test. One of the most popular Seahorse respirometry-based protocols. Addition of FCCP alone shows a modest stimulation of OCR above the basal rate because the provision of endogenous substrates by glycolysis is rate-limiting. (B) Illustration of the endogenous substrate rate restriction by the addition of extra pyruvate after uncoupler. The further increase of uncoupled OCR reveals additional respiratory capacity. (C) The CRABS-ROC protocol for assessing Complex I-, II- and IV-dependent respiratory capacity. The development of this protocol will be described in detail in Chapter 2. The NADH-stimulated OCR reveals additional Complex I capacity because the rate-limiting restrictions of both glycolysis and dehydrogenase enzymes are bypassed.

1.3. Investigating the potential of idebenone for treating TBI-induced mitochondrial dysfunction

1.3.1 History of idebenone being used as a treatment for neuroinflammation

As briefly mentioned earlier, idebenone is a synthetic analog of ubiquinone, also known as Coenzyme Q10 (CoQ10), with the advantage of a shorter side chain conferring better solubility and bioavailability compared with CoQ10. Idebenone showed positive outcomes in a few clinical trials on Alzheimer's diseases [39, 40]; however, some trials reported failure of idebenone to slow cognitive decline [41].

Multiple preclinical studies indicate that idebenone rescues respiration and mitochondrial ATP production in models of rotenone-induced ETC Complex I inhibition [42, 43]. However, idebenone's ability to restore mitochondrial function has not yet been tested in TBI models. A recent mouse TBI study reported that idebenone administered at one- and five-hours post-injury mitigates TBI-induced dysregulation in the expression of ephrin-A signaling genes and alleviates decreases in dopamine receptor-encoding genes *Drd1* and *Drd2* at 24 hours post-TBI [44]. This translational pilot study suggests that idebenone may have neuroprotective potential. We hypothesize that idebenone is neuroprotective through restoring brain mitochondrial respiration and ameliorating pro-inflammatory signaling pathways.

1.3.2 Cytoplasmic reduction of idebenone by NQO1 is the established mechanism of bioactivation

Like ubiquinone, idebenone functions as an ETC Complex III electron donor only in its reduced state. However, the reduced form, idebenol, is poorly soluble in aqueous solution and

therefore lacks bioavailability. Idebenone shares the same quinone moiety with CoQ10, which requires a two-electron reduction to yield the hydroquinone form [45]. The predominantly cytoplasmic enzyme NAD(P)H: quinone oxidoreductase 1 (NQO1) appears to be the major enzyme catalyzing the two-electron reduction of idebenone to its hydroquinone bioactive form in most cells [46] [42]. NQO1 is an inducible enzyme that is regulated by the transcription factor NRF2. Previous studies revealed different bioenergetic responses to idebenone treatment in neural cell types that correlated with the differential expression of NQO1. Primary rat cortical neurons exhibited no NQO1 expression and, accordingly, lacked idebenone-stimulated respiration, while rat cortical astrocytes showed dose-dependent idebenone-stimulated respiration that was dependent on NQO1 activity[47].

1.3.3 The mechanisms of idebenone reduction in pro-inflammatory microglia are unknown

Pro-inflammatory microglia contribute to neuroinflammation after TBI [48]. Mitochondrial dysfunction contributes to pro-inflammatory microglial activation [49, 50]. We hypothesized that idebenone attenuates microglial pro-inflammatory activation by restoring mitochondrial respiration. Former lab members Evan Bordt and Sausan Jaber observed that idebenone can partially restore LPS/IFN- γ -impaired respiration in the activated HAPI microglial cell line [51]. We initially hypothesized that NQO1 reduces idebenone in microglia as was observed in astrocytes [47]. However, although NQO1 enzyme is expressed in microglia, former lab member Sausan Jaber observed that idebenone-driven NADPH oxidation in LPS/IFN- γ activated microglia is NQO1-independent, which is opposite to that in astrocytes[52], suggesting that a different enzyme, other than NQO1, may catalyze the cytoplasmic reduction of idebenone in these cells. To evaluate idebenone's potential to counteract the harmful effects of pro-

inflammatory microglial activation, it is crucial to understand which microglial enzymes contribute to the conversion of idebenone to its reduced form that can act as a Complex III electron donor and antioxidant.

1.4. Targeting neuroinflammatory signaling pathways to attenuate loss of ETC complex proteins in pro-inflammatory microglia

1.4.1 Roles of microglia in neuroinflammation after TBI

Neuroinflammation is a substitute for the term “reactive gliosis” often used in the CNS injury field [53] , and it is preferred here because it better describes the pro-inflammatory role of microglia. Microglia are the main innate immune cell type in the CNS and play key roles in the progression and persistence of neuroinflammation after TBI. Microglia survey the brain to detect damage and disease- or infection-associated processes that disrupt brain homeostasis. Microglia have pattern recognition receptors (PRRs) that detect TBI-induced [54], interferon (IFN) receptors, and receptor for advanced glycation end products (RAGE). Once these receptors are activated, pro-inflammatory signaling cascades including the NLRP3 inflammasome (Figure 1.5) are initiated. Formation of the NLRP3 inflammasome, facilitates the cleavage and activation of caspase-1, which mediates the processing of IL-1 β . Pro-inflammatory microglia release multiple factors that, at high levels, can promote neurotoxicity, including IL-1 β , TNF- α , and nitric oxide (NO). In this way, persistent or excessive microglial activation contributes to secondary brain injury. Microglial mitochondrial bioenergetic dysfunction is implicated in TBI and other neurodegenerative diseases in part through its relationship to immune signaling. Respiratory failure and disrupted metabolism are thought to promote the chronic activation of microglia, contributing to secondary injury after TBI [55, 56].

To study the innate immune signaling pathways relevant to CNS injury, *in vitro* models such as primary isolated microglia, bone marrow-derived macrophages, and immortalized microglial or macrophage cell lines are widely used. Due to difficulty in obtaining primary isolated microglia in sufficient quantities, an immortalized microglia cell line was used in this study. Highly aggressively proliferating immortalized (HAPI) microglial cells were reported to be spontaneously immortalized from postnatal day 3 rat microglia [57]. However, we identified that these cells have a mouse origin based on our sequencing results. We then submitted HAPI cells to the American Type Culture Collection (ATCC) for authentication by short tandem repeat (STR) profiling. The results revealed that HAPI cells have an identical STR profile to the established mouse microglial cell line SIM-A9, supporting their use as a mouse microglial model. In this dissertation, we apply HAPI cells as a rodent microglial model and use lipopolysaccharides (LPS) plus interferon-gamma (IFN- γ) to activate the cells to a pro-inflammatory state. NO release is one of the most common factors seen in activated mouse microglia, myeloid cells such as macrophages, and microglial cell lines. NO release has been used as an important criterion for the characterization of mouse microglial cell lines [58-60]. Besides this reason, the detection of other biomarkers of activated microglia is usually slow and costly, such as expression profiling of activated microglial genes by qPCR and RNA sequencing, ELISA-detection of pro-inflammatory cytokines such as IL-1 β , IL-18 and TNF- α . This is why Griess assay, a fast, colorimetric assay detecting NO release, is widely used for a quick, benchtop characterization of microglial activation. We measure nitric oxide production as a criterion for efficient activation of HAPI cells. Explain more why nitric oxide measurements are used. Sorry if I missed it>

We discussed post-TBI respiratory dysfunction studies in sections 1.3 and 1.4. Most of the studies target the entire brain hemisphere or peri-lesion area in TBI. However, there is a lack of studies specifically focused on microglial respiratory dysfunction post-TBI. It is also unclear whether TBI-induced mitochondrial respiratory dysfunction results in part from structural damage to one or more ETC complexes, including the degradation of specific subunits. We hypothesized that preventing the loss of ETC subunits will rescue mitochondrial respiration in pro-inflammatory microglia. To guide the development of precise treatments, it is crucial to understand the mechanisms of ETC complexes loss. In the studies described in this dissertation, we used pharmacological inhibition of several different pro-inflammatory signaling components to test if TLR4, NLRP3, caspase-1 or iNOS is upstream of ETC degradation.

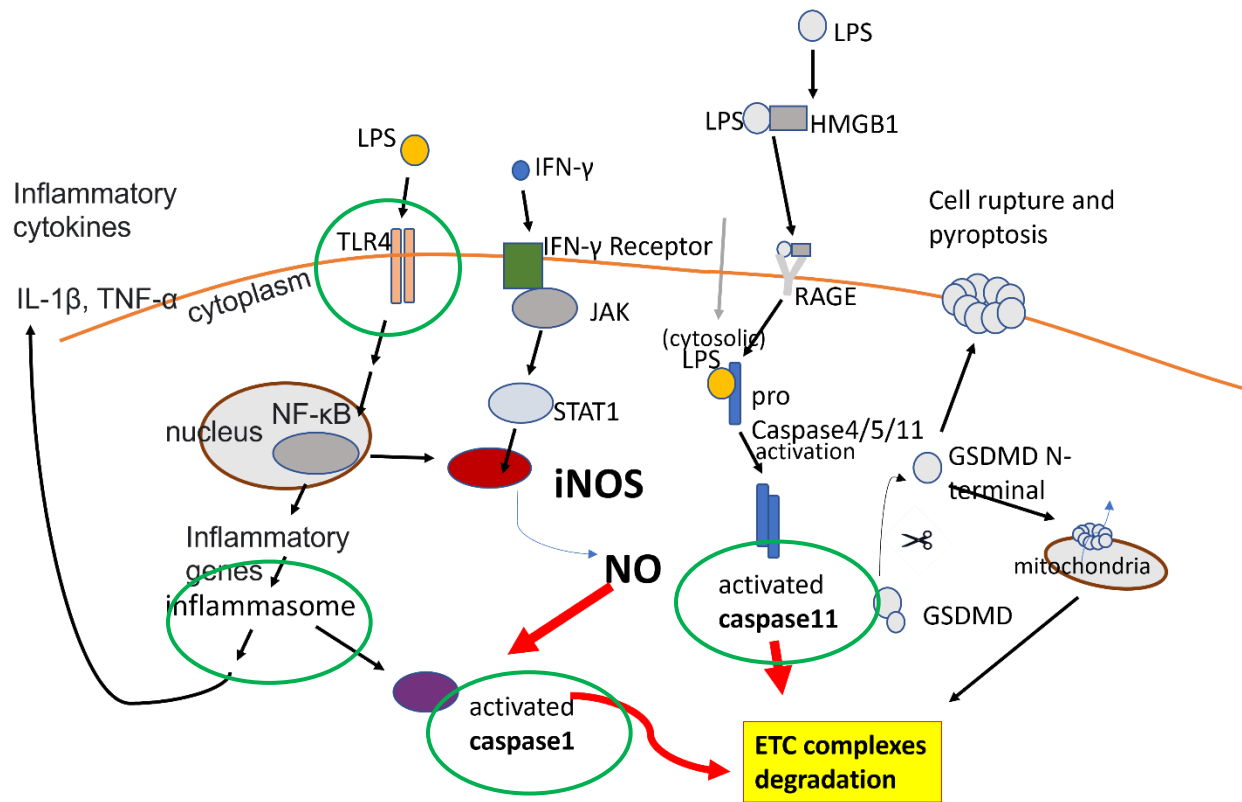


Figure 1.5 Putative signaling pathways acting upstream of ETC complexes degradation in pro-inflammatory microglia.

Red arrows: proposed pathways that are related to ETC complexes degradation: nitric oxide (NO), caspase-1, and caspase-11. Green circles show pharmacologically inhibited targets in this dissertation: TLR4, NLRP3-dependent inflammasomes, and caspase-1/-11. On the right-most side of the diagram, the interrelated GSDMD-mediated pyroptosis signaling pathway is also shown.

1.4.2 TLR4 and NLRP3 as targets to prevent the activation-induced loss of ETC subunits

Toll-like receptor 4 (TLR4) is considered one of the most important and common initiators of innate immune signaling cascades in macrophages and microglia. LPS is the most used TLR4 agonist in preclinical immune studies. To model the role of TLR4 in pro-inflammatory microglia in TBI and other neurodegenerative disorders, in the subsequently described doctoral research HAPI microglial cells were treated with a combination of LPS and IFN- γ (LPS/IFN- γ), which activates microglia to a neurotoxic state [61]. Interrupting TLR4 function seems to be a straightforward therapeutic strategy that can suppress pro-inflammatory signaling from the initiating step. Various TLR4 inhibition strategies have been developed, such as glycolipid-based inhibitors, non-glycolipid-based inhibitors, peptide-based inhibitors, TLR4 competitive antagonists, and TLR4 expression downregulators [62]. Genetic depletion of TLR4 in mice reduces the infarct size after CCI, inhibits IL-1 β and iNOS expression detected by immunohistological staining, increases the basal level of I κ B- α , and inhibits CCI-increased p65 and p-JNK signaling [63]. Another group also reported that the infarct volume is lower in TLR4 knockout (KO) mice compared with wild-type after CCI, and they observed that TLR4 KO decreases pro-inflammatory gene expression while promoting the expression of anti-inflammatory phenotype markers [64].

There are three TLR4 inhibitors that have entered clinical trials. Eritoran (E5564) failed a Phase 3 clinical trial for treating severe sepsis [65] and a trial of E-5531 stopped at Phase 2 due to limited efficacy against septic shock despite having demonstrated the ability to diminish LPS-induced inflammation preclinically [66]. TAK-242 failed in a phase 3 sepsis clinical trial after 28 days of administration due to lack of efficacy [67]. Although TAK-242 has not been tested in any clinical trials for TBI, it is still widely used in preclinical research as a relatively specific TLR4

inhibitor, and we employed it in our studies of ETC alterations during pro-inflammatory microglial activation.

When activated through TLR4 and IFN- γ receptors, microglia undergo multiple signaling cascades to become neurotoxic. The NLRP3-dependent inflammasome, one of the key mediators of neuroinflammation, is induced and assembled [68]. It then mediates the autocleavage of pro-caspase-1 to the active form, facilitating the proteolysis and extracellular secretion of IL-1 β and IL-18. During the formation of the NLRP3-dependent inflammasome, mitochondria play key roles, serving as a “platform” that facilitates ASC and NLRP3 recruitment and assembly through lipid-based interactions [69]. We predict that inhibiting the activity of the NLRP3 inflammasome will protect the mitochondrial ETC complexes from LPS/IFN- γ -induced degradation. MCC950 is a direct NLRP3 protein inhibitor. MCC950 abrogates ASC oligomerization and binds to the NACHT domain of NLRP3 to block ATP hydrolysis, thereby inhibiting NLRP3 inflammasome activation [70]. In this dissertation research, we tested the ability of MCC950 to protect the integrity of the mitochondrial ETC complexes in pro-inflammatory microglia.

1.4.3 Caspase-1 as a target to prevent the activation-induced loss of ETC subunits

The inactive precursor form of caspase-1, pro-caspase-1, resides in the cytoplasm. Caspase-1 can also be secreted extracellularly [71] or translocated into the nucleus [72]. There is no direct evidence for caspase-1 translocation inside mitochondria, however, caspase-1 does interact with mitochondria during NLRP3 inflammasome assembly [69, 73].

Caspase-1 directly interacts with the mitochondria-specific lipid cardiolipin during inflammasome assembly, with the interaction observed during the priming stage of bone marrow-

derived macrophage (BMDM) activation [69]. In that report, a low level of caspase-1 was detected by western blot in the mitochondria-enriched fraction of biochemically fractionated cells. We could find no literature indicating whether caspase-1 specifically interacts with the mitochondrial outer or inner membrane. However, based on the reported mitochondrial localization, we suspect caspase-1 may have mitochondrial roles yet to be discovered, including the possible regulation of ETC complexes.

Previously, caspase-1 has been connected to mitochondrial dysfunction in a few different ways. Caspase-1 inhibits mitophagy in activated BMDMs by cleaving Parkin, which is an important mitophagy regulator [74]. Mitophagy inhibition causes mitochondrial damage to persist and may lead to apoptosis. In addition, activated caspase-1 cleaves gasdermin D (GSDMD). GSDMD N-terminal fragments form pores in the plasma membrane to facilitate pro-inflammatory cytokine release [75]. GSDMD N-terminal fragments also form pores in both mitochondrial membranes, causing mitochondrial DNA release and the induction of pyroptotic cell death [76]. Rapid mitochondrial outer and inner and membrane damage were detected in LPS- and nigericin-treated immortalized Tohoku Hospital Pediatrics-1 (THP-1) macrophage cells during an early stage of pyroptosis [76]. Caspase-1 can also cleave the BH3-domain-only cytosolic protein BID to induce a GSDMD-independent apoptotic form of cell death [77]. Once cleaved, BID activates the BCL-2 family pro-apoptotic proteins BAX and BAK, which cause mitochondrial outer membrane permeabilization through pore formation. The production of truncated BID (tBID) is inhibited in DNA- or ATP-stimulated Casp1^{-/-}Casp11^{-/-} BMDMs [74].

As mentioned earlier, in the cytoplasm, activated caspase-1 cleaves pro-IL-1 β and pro-IL-18 to their active, secreted forms. However, whether caspase-1 contributes to pro-inflammatory signaling by cleaving any substrates in the mitochondria remains unknown. We tested whether

caspase-1 cleaves ETC subunits in pro-inflammatory microglia, contributing to the mitochondrial respiratory dysfunction observed after LPS/IFN- γ stimulation. Belnacasan, also known as VX-765, is a selective caspase-1 sub-family inhibitor that inhibits both caspase-1 and caspase-11 activities. Multiple clinical trials and preclinical studies support VX-765's efficacy in diseases with an inflammatory component, such as Alzheimer's disease, epilepsy, diabetes, arthritis, and psoriasis. The benefits are thought to stem in part from the attenuation of IL-1 β production achieved through caspase-1 inhibition. Episodic and spatial memory impairment in the J20 Alzheimer's disease mouse model was reversed by VX-765 treatment and reoccurred after a stop in treatment [78]. A few other preclinical studies suggest that VX-765 is neuroprotective and can reverse cognitive impairments. For example, in a mouse model of TBI, VX-765 alleviated the production of pro-inflammatory cytokines such as IL-1 β , IL-18, IFN- γ while promoting increases in IL-10 and TGF- β [79]. The authors also observed a reduction in lesion size that correlated with VX-765's ability to ameliorate neuroinflammation.

1.4.4 Inhibition of nitric oxide production as a target to prevent the activation-induced loss of ETC subunits

Nitric oxide (NO) is an important neurotransmitter in physiological conditions, mediating neuronal communication and synaptic plasticity. Physiological NO is also a key regulator of brain blood flow, orchestrating nutrients and oxygen supply to support brain functions.

NO is generated by the nitric oxide synthase (NOS) family of enzymes, which includes three isoforms: nNOS, eNOS and iNOS. Neuronal NOS (nNOS) is a specific NOS type which is usually expressed in neuronal cells to produce NO as a neurotransmitter, while endothelial NOS

(eNOS) is expressed in vascular endothelial cells to regulate blood flow. NO generated by endothelial NOS (eNOS) reduces vascular permeability and increases blood flow through vasodilation. Relevant to injury-induced immune responses, vasodilation can also restrict the migration of innate immune cells and leukocytes [80]. Inducible nitric oxide synthase (iNOS) can be found in many immune cell types such as macrophages, microglia, and neutrophils [81]. As the name implies, iNOS is an induced enzyme which is only expressed under infections or inflammatory conditions through exposure to specific stimuli. These include lipopolysaccharide (LPS) and/or pro-inflammatory cytokines such as IFN- γ , IL-1 β , or TNF- α . Compared with physiological NO produced by eNOS or nNOS, NO produced by macrophage or microglial iNOS is released at much higher levels and acts as a pro-inflammatory factor, amplifying neuroinflammation in TBI and other neurodegenerative diseases.

NO's direct effects on mitochondria were carefully investigated at the beginning of the 21st century by biochemical methods using exogenous addition of NO or its highly reactive peroxynitrite derivative (ONOO⁻). For example, it was found that NO inhibits Complex I activity through its peroxynitrite species form and metabolizing intermediates [82]. Some in-depth studies concluded that there are respiratory deficiencies at the level of multiple individual ETC complexes. This was revealed by using Complex I- or Complex II-specific substrates—pyruvate/malate or succinate, respectively—on permeabilized cells or purified mitochondria. When individual substrate-induced oxygen consumption was measured from digitonin-permeabilized L1210 mouse lymphocytic leukemia cells following saturated bubbling of NO into the O₂-free culture medium, Complex I- and Complex II-linked oxygen consumption were decreased to 16% and 44% of control, respectively [83]. Studies of ETC respiratory impairments by inducing endogenously produced micromolar level of NO in LPS/IFN- γ -stimulated microglia and macrophages are even

more relevant to our study. In 2001, Moss and Bates detected significant decreases in Complex I and IV respiratory activities as well as in the ATP level in the LPS/IFN- γ -treated mouse macrophage cell line J744.A1 and the microglial cell lines N11 and BV2 [84]. In 2002, Chenais et al. reported 45% inhibition of Complex I activity and 59% inhibition of Complex II activity in LPS/IFN- γ -treated BV2 cells but did not observe attenuation of Complex IV activity [85]. Both studies on BV2 microglial cells used the NOS inhibitor L-NMMA to show that the respiratory impairments were NO-dependent. The intact Complex IV respiration in the later report is possibly due to the lower concentrations of LPS/IFN- γ (50 ng/ml LPS and 20U/mL IFN- γ vs. 10 μ g/ml LPS and 50U/mL IFN- γ) and shorter treatment time (16 hours, as opposed to 20 hours). Overall, these studies suggest that endogenous NO in stimulated microglial cells impairs the activity of multiple ETC complexes.

To ameliorate the amplification of neuroinflammation by NO, methods such as inhibiting iNOS expression or eliminating NO production seem to have potential. Genetic ablation and pharmacological inhibition of iNOS should provide good evidence of NO involvement. *Nos2* KO macrophages are a useful cellular model to study NO's role in immunometabolism, as macrophages, like microglia express TLR4 and IFN- γ receptor, and the two cell types respond to LPS/IFN- γ stimulation in similar ways. Studies using *Nos2* KO mouse macrophages suggest that NO is a crucial factor responsible for TCA cycle alterations, citrate accumulation, and the loss of ETC complex subunits [86]. 1400W, is an NO production inhibitor that does not affect the expression level of iNOS enzyme. In a rat fluid percussion TBI model, 1400W administered through a bolus at 18 hours post-TBI and via an osmotic pump infusion between 18-72 hours post-TBI reduced the brain lesion volume by 64% at 72 hours post-injury [87]. In this dissertation, newly created *Nos2* KO HAPI cells were used to elucidate the contribution of the iNOS enzyme

to microglial cytoplasmic idebenone reduction, and the role of NO in LPS/IFN- γ -triggered degradation of microglial ETC complexes. The pharmacological inhibitor 1400W was used to help specifically implicate NO production by iNOS as crucial in the ETC degradation process vs. other potential consequences of genetically removing the enzyme.

Chapter 2

CRABS-ROC, A Respirometry Protocol for Overcoming Substrate Limitations, Reveals

Excess Brain Mitochondrial Complex I Capacity

2.1 Abstract

Mitochondrial bioenergetic competency in cells is frequently assessed by the Mito Stress Test protocol, which includes uncoupler addition for evaluating respiratory capacity. The uncoupled oxygen consumption rate (OCR) is usually defined as maximal respiration, with little consideration of whether the measured rate is restricted by substrate supply. In this study, we show that the uncoupled OCR is substrate-limited in rat primary cortical neurons and isolated mouse forebrain synaptosomes. We use a different respirometry protocol we name CRABS-ROC (Complex Respirometry Assay Bypassing Substrate-Restricted Oxygen Consumption) that enables evaluation of individual electron transport chain (ETC) complex capacities using saturating levels of substrates to bypass this restriction. Optimization of the cytochrome *c* concentration was critical for ETC complex capacity assessment. Applying CRABS-ROC to primary cortical neurons reveals >2-fold excess Complex I capacity beyond the uncoupled OCR of cells metabolizing glucose and pyruvate. Furthermore, we demonstrate that CRABS-ROC can expose a Complex I deficit in isolated harlequin mutant brain mitochondria that display wild-type levels of Complex I-substrate-linked respiration despite having about half the normal level of Complex I. Thus, CRABS-ROC should be broadly useful for studies on mitochondrial function because it can both reveal excess ETC capacity and unmask ETC alterations that may be missed by the most widely used methods.

2.2 Introduction

The energy storage molecule ATP is essential for brain function. Mitochondria couple electron transport to ATP generation through a series of membrane-embedded proton pumping complexes that produce an electrochemical gradient with potential energy [88]. Oxygen is the final electron acceptor in this oxidative phosphorylation process that uses the proton-motive force of the gradient to drive ADP to ATP phosphorylation. As cellular respiration consists primarily of mitochondrial oxygen consumption, measurement of oxygen consumption rate (OCR) is a convenient way to evaluate the bioenergetic competency of mitochondria within cells. However, in healthy cells OCR is dictated by proton gradient utilization by the ATP synthase, which in turn is driven by the ADP/ATP ratio or “energy demand” [88]. Therefore, to assess the bioenergetic capabilities of the mitochondrial network in cells, it is necessary to either increase energy demand or remove this restriction.

Chemical uncouplers like carbonyl cyanide 4-(trifluoromethoxy)phenylhydrazone (FCCP) and 2,4-dinitrophenol are widely used as part of the Mito Stress Test to evaluate mitochondrial capacity because they accomplish the latter goal and are not cell-type specific [38, 89]. Uncouplers dissociate electron transport from ADP phosphorylation, which increases OCR by removing ATP synthase control [88]. Thus, the OCR in uncoupler-treated cells is usually considered as maximal respiration, reflecting the mitochondrial “respiratory capacity,” while the difference between uncoupler-stimulated OCR and basal OCR is thought to indicate the “spare” or “reserve” respiratory capacity of the cell [38, 89].

A drawback of this method for assessing mitochondrial capability, however, is that the uncoupled respiration rate depends not only on the intrinsic capacity of the mitochondrial electron transport chain (ETC) components, which includes the ETC protein complexes, but also on the

rate of electron entry from NADH and FADH₂. While the redox center FAD/FADH₂ is covalently bound to several enzymes that converge to feed electrons to coenzyme Q, NADH, the immediate substrate of Complex I (NADH:ubiquinone oxidoreductase; EC 7.1.1.2), is provided primarily by dehydrogenase enzymes of the tricarboxylic acid (TCA) cycle [88]. Pyruvate, the glycolysis end-product that enters the TCA cycle as acetyl-CoA, is cell permeable and can be added with uncoupler to bypass the glycolysis rate restriction of OCR [38, 89]. Nevertheless, the activity level of one or more NADH-yielding dehydrogenase enzymes may still be a rate-limiting factor for measuring the true capacity of Complex I, the main site of ETC electron entry. Consistent with this possibility, evidence suggests that pyruvate dehydrogenase (PDH; EC 1.2.4.1), which is regulated by post-translational modifications that include phosphorylation and lipoylation, exerts control over mitochondrial respiration rate in many cell types [90].

To help overcome the limitation of evaluating mitochondrial bioenergetic competency using uncouplers, in this study we employ a simple respirometry protocol we name CRABS-ROC (Complex Respirometry Assay Bypassing Substrate-Restricted Oxygen Consumption) that enables direct interrogation of the capacity of individual complexes within the ETC in parallel to classical cellular respiratory capacity measurements that are influenced by substrate restrictions. We show that in addition to cells, the protocol is readily applied to isolated mitochondria or tissue homogenate, requiring only high nanogram to low microgram amounts of protein, respectively. By applying CRABS-ROC to harlequin (Hq) mutant mouse mitochondria that show ~50% respiratory chain Complex I deficiency [91-94] due to insufficiency of the mitochondrial import protein apoptosis-inducing factor (AIF) [95-98], we demonstrate that substrate supply limits the respiration of brain mitochondria, which have excess Complex I capacity to support oxygen consumption.

2.3 Materials and Methods

2.3.1. Materials

Saponin (catalogue #S7900), alamethicin (catalogue #A4665), cytochrome *c* (catalogue #C2506), NADH (catalogue #10128023001) and pyruvate (catalogue #P2256) were from Sigma-Aldrich (St. Louis, MO). The bicinchoninic acid (BCA) assay was purchased from Thermo Fisher (Waltham, MA). Seahorse XF24 and XFe96 FluxPaks were acquired from Agilent Technologies (Santa Clara, CA) or Seahorse Bioscience (North Billerica, MA). Other reagents were obtained from Sigma-Aldrich unless noted otherwise. NADH and pyruvate were prepared fresh from powder immediately prior to experiments.

2.3.2. Animals

Male harlequin (Hq) mutant mice (strain name B6CBACa $A^{w-J}/A-Aifm1^{Hq/J}$) and age-matched male wild-type (WT) controls on the same background were acquired from the Jackson Laboratory (Bar Harbor, ME). Mice were kept on a 12-hour light/dark cycle, fed *ad libitum*, and housed according to standard animal care protocols. Embryonic Day 18 Sprague-Dawley rats from Charles River (Wilmington, MA) were used for the preparation of mixed-sex primary rat cortical neuron cultures. Postnatal day 18 male rats were used for the preparation of brain homogenates. All protocols were approved by the Institutional Animal Care and Use Committee (IACUC) and were in accordance with the *International Guiding Principles for Biomedical Research Involving Animals*, as issued by the Council for the International Organizations of Medical Sciences.

2.3.3. Preparation of primary neuron cultures

E18 rat cortices were dissociated using trypsin to prepare primary rat cortical neurons as

previously described [99, 100]. Cells were plated in V7-PS or V28-PS microplates (Agilent Technologies) at a density of 80,000-100,000 cells/well (0.32 cm²) in Neurobasal medium (100 µl) containing B27 supplement (2%), fetal bovine serum (10%), L-glutaMAX (0.5 mM), streptomycin (100 µg/ml), and penicillin (100 IU/ml). Medium was replaced with 0.5 ml of the same medium but lacking fetal bovine serum at two hours post-plating. Cytosine arabinofuranoside (5 µM) was added on days *in vitro* (DIV) 4 to inhibit glial proliferation. Without removing any medium, fresh Neurobasal medium (0.2 ml) containing supplements was added to each well on DIV 6. Neurons were maintained at 37°C in a humidified atmosphere of 95% air/5% CO₂ and used for experiments at 6-15 DIV.

2.3.4. Preparation of brain homogenate

Following euthanasia, the brain was rapidly removed, and frontal and occipital brain tissue was dissected with a razor blade on an acrylic brain matrix previously cooled in ice. Using sharp scissors, the tissue was then rapidly minced in MS+EGTA buffer consisting of 225 mM mannitol, 75 mM sucrose, 1 mM ethylene glycol-bis(β-aminoethyl ether)-N,N,N',N'-tetraacetic acid (EGTA), 1 mg/ml fatty acid-free bovine serum albumin (BSA), and 5 mM HEPES, pH 7.4. The minced tissue was then washed with MS+EGTA buffer and homogenized in the same buffer using a glass Dounce homogenizer with six strokes of pestle A (loose-fitting), followed by six strokes of pestle B (tight-fitting). The homogenized sample was centrifuged at 1000×g for 10 minutes at 4 °C to remove nuclei and unbroken cells and then stored at -80 °C until used for OCR measurements.

2.3.5. Isolation of mitochondria and synaptosomes

A Percoll™ density gradient was used to isolate non-synaptosomal brain mitochondria

from 2-3 Hq male mice and from 2-3 male WT littermates in parallel as previously described [101]. Mouse forebrain synaptosomes were isolated from male C57BL6/J mice as described [93]. Mitochondrial and synaptosomal protein concentrations were determined by the Bio-Rad (Hercules, CA) Bradford method or by the BCA method (Thermo Fisher). Mitochondria and synaptosomes were stored on ice and used for OCR measurements on the day of isolation and then frozen at -80° C. Following thawing on a later date, the same mitochondria were used for OCR measurements by the CRABS-ROC protocol.

2.3.6. Seahorse respirometry – neurons and synaptosomes

Neuronal [102] and synaptosomal [103] OCR measurements were made using a Seahorse XF24 Extracellular Flux Analyzer (Agilent Technologies) as previously described [47]. Artificial cerebrospinal fluid (aCSF) assay medium consisted of 120 mM NaCl, 3.5 mM KCl, 1.3 mM CaCl₂, 0.4 mM KH₂PO₄, 1 mM MgCl₂, and 5 mM HEPES, pH 7.4. Glucose was additionally present at 15 mM and fatty acid-free BSA at 4 mg/ml to model the extracellular protein concentration unless indicated otherwise. Cells or synaptosomes were incubated in aCSF assay medium for one hour prior to measurements in a CO₂-free incubator at 37°C. For some experiments, cells were incubated in aCSF for 45 minutes prior to this step in a 95% air/5% CO₂ incubator at 37°C, followed by an additional media change to fresh aCSF.

For the experiments in which the permeabilizing agents saponin and alamethicin were employed, the aCSF contained an increased concentration of HEPES (20 mM) because greater buffer capacity was required. For those experiments, the neurons were plated on V28-PS plates, which have a higher measurement volume (28 ml) than standard V7-PS plates (7 ml). Avoiding complete oxygen depletion during OCR measurements is critical for accurate OCR determination.

The greater volume of the transiently closed measurement chamber established in V28-PS plates successfully prevented excessive oxygen depletion due to the high OCR of NADH-stimulated respiration (Figure 2.1). Figure 2.1 also demonstrates the background correction that was applied to account for chemical oxygen consumption upon *N,N,N',N'*-tetramethyl p-phenylenediamine (TMPD) plus ascorbate injection whenever that injection combination was used.

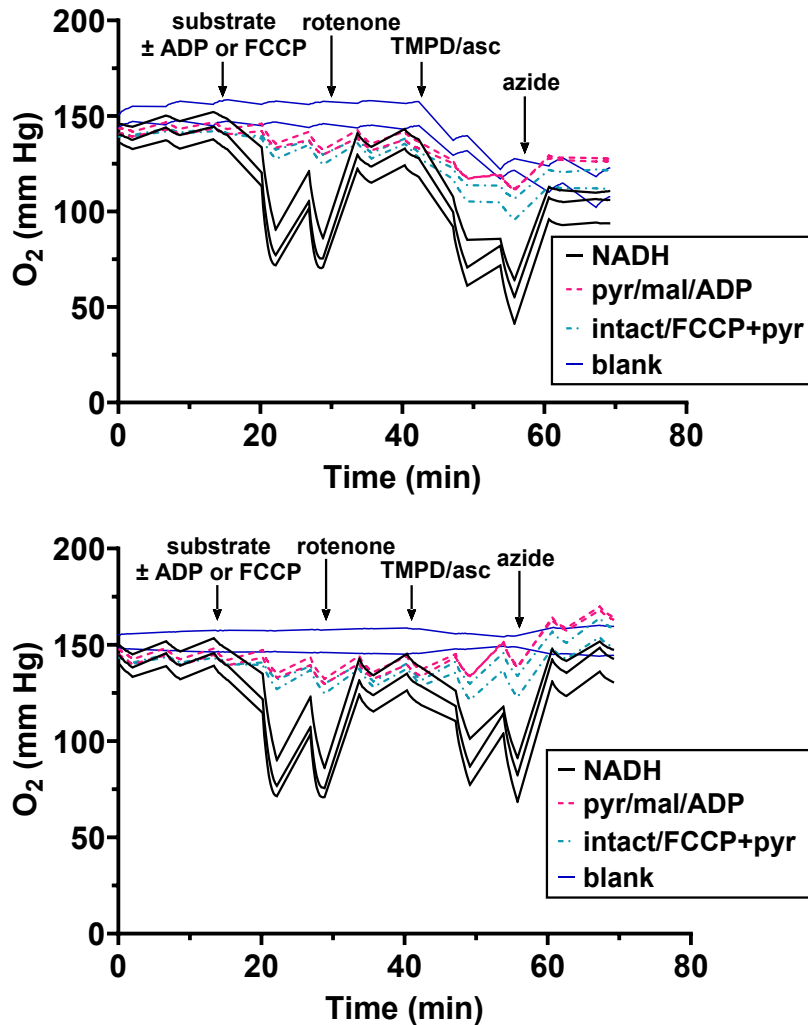


Figure 2.1 Neither NADH- or TMPD/ascorbate-dependent respiration led to excessive oxygen depletion by primary cortical neurons, but the latter required a correction for chemical oxygen consumption.

(A) Oxygen level changes without background correction are shown for the experiment depicted in Figure 2.4 and the full drug injection details can be found in the Figure 2.4 legend. Also shown here are two wells lacking cells (“blank”) to which 0.1 mM TMPD and 10 mM ascorbate were added when indicated. (B) The oxygen level changes depicted in A are shown following background correction to the two blank wells.

2.3.7. Seahorse respirometry – homogenate or isolated mitochondria

Brain homogenate and isolated brain mitochondria were diluted in MAS assay medium to concentrations of 0.4 mg/ml and 0.02 mg/ml, respectively. The MAS medium consisted of 220 mM mannitol, 70 mM sucrose, 5 mM KH_2PO_4 , 5 mM MgCl_2 , 1 mM EGTA, and 2 mM HEPES, pH 7.4. Twenty ml of the diluted suspensions were added to XFe96 plates (Agilent Technologies) for final amounts of 8 mg brain homogenate and 0.4 mg brain mitochondria, respectively, while four wells on each plate received 20 ml of MAS medium to be used as a temperature control. The XFe96 plates were centrifuged at $2,000\times g$ for 5 minutes at 4 °C without braking to adhere mitochondria to the bottom of the wells, and then 160 μl of MAS assay medium was added to each well. OCR was measured using a Seahorse XFe96 Extracellular Flux Analyzer (Agilent Technologies) as previously described [104].

2.3.8. Statistics

OCR were compared by paired *t* test for two groups and by two-way ANOVA with repeated measures for more than two groups using GraphPad Prism version 10.4.1 (GraphPad, Boston, MA). Parametric tests were employed because the Shapiro-Wilk normality test was passed. Following the ANOVA, the Šídák post hoc test was used for pairwise comparisons. $P < 0.05$ was considered significant. Power analyses were not done because this was not a planned study; the experiments were originally done as part of other studies and repurposed for this thesis. For example, in the case of WT and harlequin isolated mitochondria, we used all remaining frozen samples from a previously published study [93].

2.4. Results

2.4.1. *The uncoupled oxygen consumption rate in the Mito Stress Test is limited by substrate supply*

Mitochondrial respiratory capacity is usually assessed following uncoupler addition as a component of the widely used Mito Stress Test protocol [38, 105]. The protocol also includes the prior addition of the ATP synthase inhibitor oligomycin to estimate mitochondrial coupling. Although literature has demonstrated that supraphysiological pyruvate concentrations can enhance glycolysis-supported mitochondrial OCR [106, 107], pyruvate is usually absent or present at ≤ 1 mM when the Mito Stress Test protocol is employed. We applied the Mito Stress Test protocol to primary rat cortical neurons metabolizing a physiological concentration of glucose (3 mM), which supplies the glycolysis end product pyruvate to mitochondria, and then added an excess, supraphysiological amount of pyruvate (10 mM) [107] to determine whether maximal respiration had been obtained upon addition of the uncoupler FCCP. Significantly greater OCR was obtained after pyruvate addition compared to the uncoupled OCR of neurons metabolizing only physiological glucose (Figure 2.2A, B). Pyruvate has antioxidant activity [108, 109]. However, the antioxidant Trolox (50 mM) failed to mimic or occlude pyruvate's enhancement of uncoupled respiration (Figure 2.4), supporting the interpretation that pyruvate acts as a substrate rather than as an antioxidant in this context.

Most bioenergetics studies are done in the presence of supraphysiological glucose concentrations. To determine if the substrate limitation is overcome at a typical supraphysiological glucose concentration, we repeated the experiment using neurons incubated with 15 mM glucose and obtained the same results (Figure 2.2A, B). Together, these results suggest that mitochondrial substrate supply downstream of physiological glucose utilization is rate-limiting in neurons.

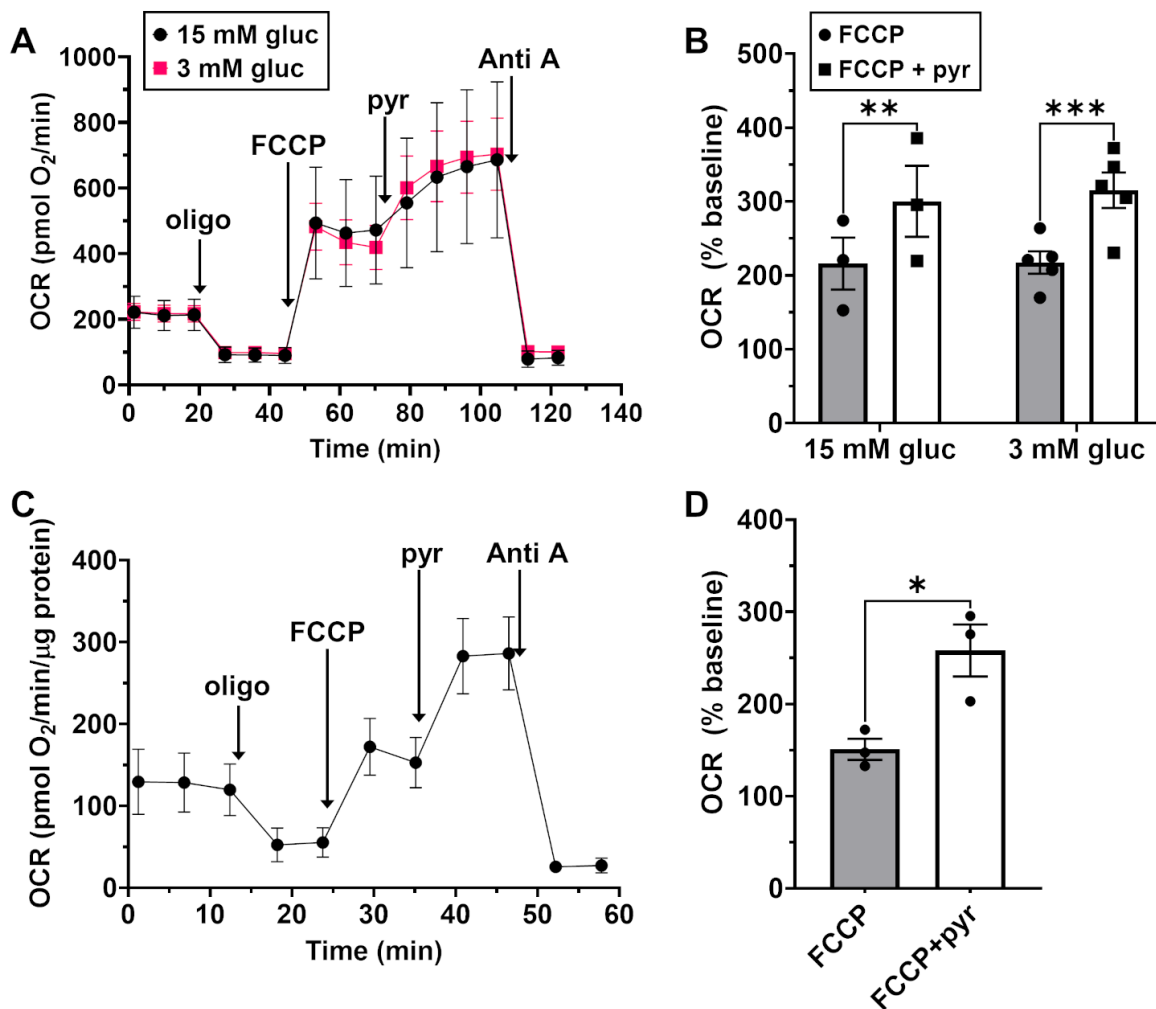


Figure 2. 2 Uncoupled respiration by intact neurons and synaptosomes is limited by substrate availability.

(A) The oxygen consumption rate (OCR) of primary cortical neurons at baseline and following the sequential addition of oligomycin (oligo, 0.5 $\mu\text{g/ml}$), FCCCP (3 μM), pyruvate (pyr, 10 mM), and antimycin A (Anti A, 1 μM). The results are mean \pm SEM from biological replicates. The glucose (gluc) concentration was 3 mM ($n=5$) or 15 mM ($n=3$), as indicated. (B) The maximal OCR following the FCCCP and pyr additions (mean \pm SEM). $*p<0.01$; $***p<0.001$. (C) The OCR of forebrain synaptosomes at baseline and following the sequential addition of oligo (2 $\mu\text{g/ml}$), FCCCP (4 μM), pyr (10 mM), and Anti A (10 μM). The results are mean \pm SEM from $n=3$ biological replicates. (D) The maximal OCR following the FCCCP and pyr additions (mean \pm SEM). $*p<0.05$.

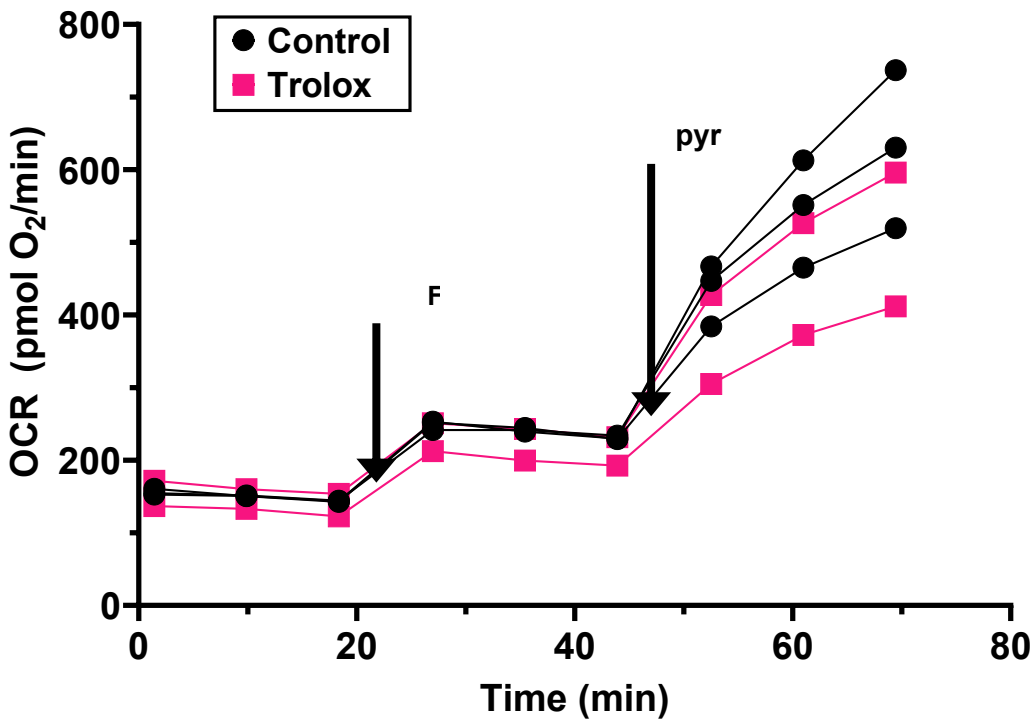


Figure 2. 3 The antioxidant Trolox does not mimic or occlude pyruvate’s enhancement of uncoupled respiration.

The oxygen consumption rate (OCR) of primary cortical neurons at baseline and following the sequential addition of FCCP (0.2 mM) and pyruvate (10 mM) is shown in the absence or presence of 50 mM Trolox (2-3 technical replicates each). The NMDA receptor antagonist MK801 (10 mM), the AMPA receptor antagonist CNQX (10 mM), and the calcium channel blocker nifedipine (1 mM) were present in all wells, making it additionally unlikely that pyruvate was stimulating OCR by increasing neuronal activity. A reduced FCCP concentration was used for this experiment compared to others because BSA was not included in the assay medium.

The mitochondrial reliance of cells cultured in glucose is thought to be low, whereas synaptic function is thought to be highly dependent on mitochondrial ATP supply. Therefore, we acutely isolated pre-synaptic terminals (“synaptosomes”) from mouse forebrain to further investigate substrate limitations when employing the Mito Stress Test. Pyruvate addition led to a significant stimulation of the uncoupled OCR of synaptosomes metabolizing glucose, very similar to the enhancement observed in cells (Figure 2.2C, D). Previously, we showed that pyruvate also enhances the uncoupled respiration measured in mouse organotypic hippocampal slices, which consist of multiple brain cell types in their native architecture [110]. Therefore, the results from a variety of neural models suggest that mitochondrial substrate supply is rate-limiting when measuring mitochondrial respiratory capacity using uncoupler in the Mito Stress Test.

2.4.2. Complex I has excess capacity that is obscured in neurons metabolizing glucose

NADH, not pyruvate, is the direct Complex I substrate. Therefore, it is possible that the provision of NADH was still rate-limiting in measuring respiratory capacity with the uncoupler/pyruvate combination. However, NADH is not cell permeable and, thus, cannot be readily incorporated into the Mito Stress Test protocol. Previously, we optimized Seahorse cell-based respirometry for measuring respiration by permeabilized cells [102]. The assay uses saponin to deliver a defined ETC substrate combination to mitochondria by selectively permeabilizing the plasma membrane. Subsequently, we showed that Complex I-III-IV linked activity could be measured using Seahorse respirometry by additionally adding the bacterial pore forming peptide alamethicin to transport the Complex I substrate NADH across the mitochondrial inner membrane [111]. This assay required the provision of exogenous cytochrome *c* to replace the endogenous cytochrome *c* released by alamethicin.

To evaluate whether primary rat neurons have excess Complex I capacity, we employed the permeabilized cell assay and a Complex I-III-IV linked activity assay in parallel while also comparing OCR to intact neurons treated with FCCP and an overabundance of the cell permeable Complex I substrate pyruvate (Figure 2.4). Exogenous pyruvate was included to bypass the rate-limiting provision of endogenous pyruvate by glycolysis. The three different compound injection protocols were done simultaneously on a single plate. Whereas the ADP-stimulated respiration of permeabilized cells provided with the Complex I-linked substrates pyruvate and malate was similar to that measured in intact cells treated with FCCP plus pyruvate (Figure 2.4), a >2-fold higher OCR was measured when alamethicin was used to deliver the immediate Complex I substrate NADH (Figure 2.4). These results revealed that neuronal Complex I capacity is obscured when tricarboxylic acid (TCA) cycle dehydrogenase substrates drive respiration.

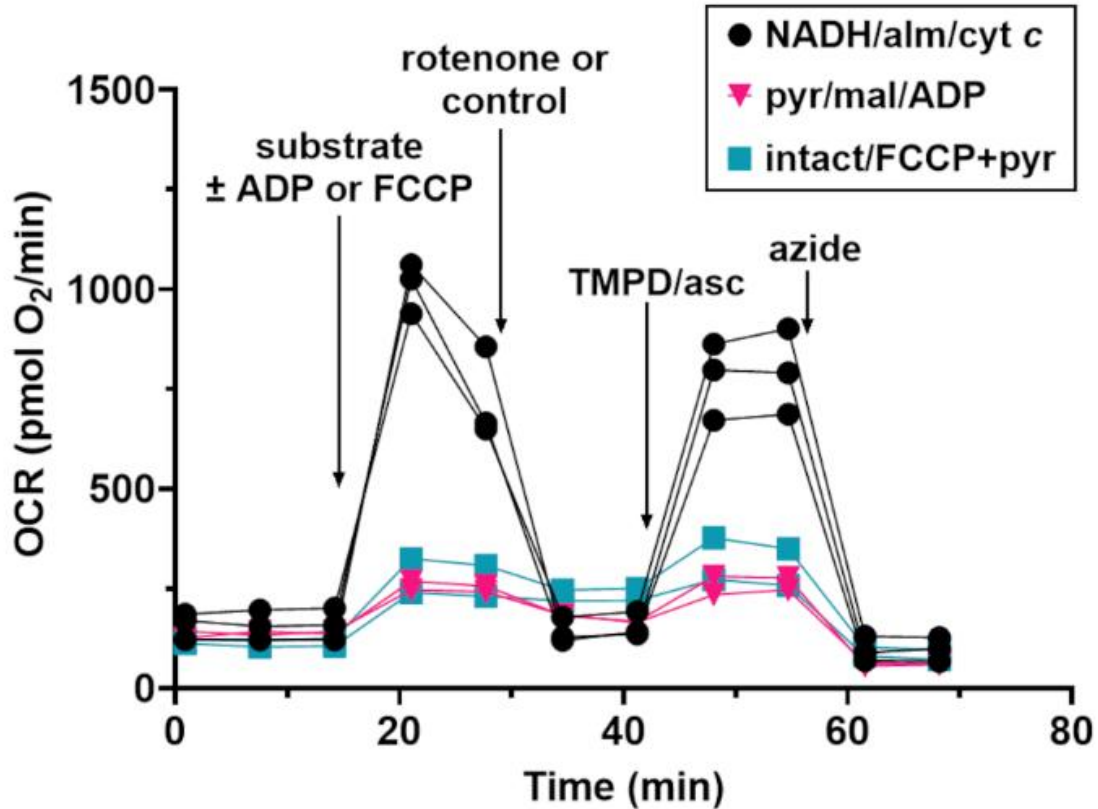


Figure 2.4 NADH delivery to mitochondria within primary rat cortical neurons reveals excess Complex I capacity.

Intact neurons (squares), plasma-membrane-permeabilized neurons (triangles), and mitochondrial-membrane-permeabilized neurons (circles) were compared. Three baseline O₂ consumption rate (OCR) measurements were made and then one of the following three cocktails was injected as indicated: 0.5 mM NADH + 40 µg/ml alamethicin + 100 µM cytochrome *c* (“NADH/alm/cyt *c*”), 5 mM pyruvate + 5 mM malate + 1 mM ADP (“pyr/mal/ADP”), or 3 µM FCCP + 10 mM pyruvate (“intact/FCCP+pyr”). Saponin (sap, 3 µg/ml) plus EGTA (5 mM) and K₂PHO₄ (3.6 mM) were additionally present in the “NADH/alm/cyt *c*” and “pyr/mal/ADP” injections. Rotenone (1 µM) or control, TMPD (0.1 mM) + ascorbate (asc, 10 mM), and sodium azide (5 mM) were then sequentially injected as indicated. Only the NADH/alm/cyt *c* group received rotenone; the other groups received an aCSF control injection. The results are technical replicates of one experiment and are representative of two (pyr/mal/ADP group) to three (other groups) biological replicates.

2.4.3. CRABS-ROC unmasks a Complex I activity deficit in harlequin mutant mitochondria

Next, we sought to apply the Complex I-III-IV-linked activity assay to a model of genetic Complex I deficiency, the harlequin mouse, while also incorporating measurement of Complex II activity. We named this modified assay protocol “CRABS-ROC” to reflect its ability to bypass endogenous substrate-restricted oxygen consumption by providing the respective Complex I and II substrates NADH and succinate in excess. Harlequin mice harboring a mutation in the gene encoding AIF [112], a component of the mitochondrial disulfide relay protein import pathway [95-98], have about a 2-fold reduction in assembled Complex I [91-94]. Unexpectedly, we [93] and others [92] found that despite this Complex I deficiency, isolated harlequin mouse brain mitochondria show a wild-type ADP-stimulated respiration level when oxidizing the Complex I-linked substrates glutamate and malate. This finding suggests that even in isolated mitochondria, the full Complex I capacity may be obscured when Complex I-linked TCA cycle dehydrogenase substrates are used.

CRABS-ROC can be applied to frozen tissue samples [104, 113], giving us the opportunity to re-evaluate Complex I activity in the stored isolated brain mitochondria samples from our prior study. As the cytochrome *c* and alamethicin concentrations in the Respirometry In Frozen Samples (RIFS) protocol [104, 113] differ from those we optimized for neurons in cell culture under different experimental conditions [111], we first re-titrated cytochrome *c* and alamethicin using RIFS on freeze-thawed rat brain homogenate. We found that concentrations of 100 mM cytochrome *c* (Figure 2.5A) and 40 mg/ml alamethicin (Figure 2.5B) yielded maximal respiration whereas the previously employed concentrations of 8 mM [104] or 10 mM [113] cytochrome *c* (Figure 2.5A) and 10 mg/ml alamethicin (not shown) [104, 113] were suboptimal.

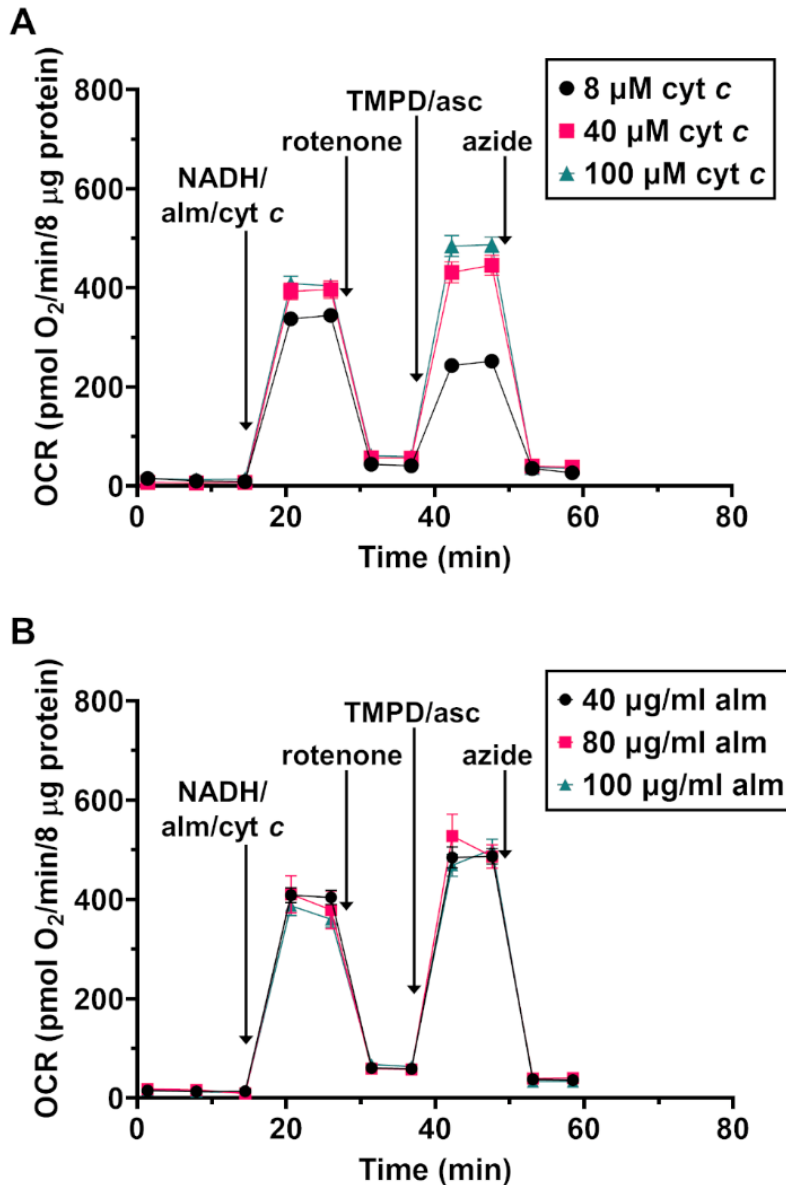


Figure 2. 5 Titrations of cytochrome c (cyt c) and alamethicin (alm) for the Complex Respirometry Assay Bypassing Substrate-Restricted Oxygen Consumption (CRABS-ROC) protocol applied to freeze-thawed brain homogenate.

(A) Oxygen consumption rate (OCR) measurements from brain homogenate. NADH (1 mM) was added with the pore-forming peptide alm (40 μg/ml) and cyt *c* to initiate Complex I dependent respiration, followed by the Complex I inhibitor rotenone (2 μM), the Complex IV substrate TMPD (0.4 mM) with ascorbate (asc, 2 mM), and the Complex IV inhibitor sodium azide (50 mM). The cyt *c* concentration was varied as shown. The results are mean ± SEM, *n*=6-8 technical replicates per group. (B) OCR measurements from brain homogenate. The same additions were made as in A, but the cyt *c* concentration was 100 μM and the alm concentration was varied as shown. The results are mean ± SEM, *n*=8 technical replicates per group.

Next, WT and Hq mitochondria, which displayed equivalent ADP-stimulated respiration when oxidizing the Complex I-linked substrates malate and glutamate (Figure 2.6A), were subjected to an optimized CRABS-ROC protocol consisting of the sequential additions of NADH, rotenone, succinate, and combined TMPD/ascorbate. By including some wells in which sodium azide was injected together with TMPD/ascorbate, this protocol allows for the measurement of Complex I, Complex II, and Complex IV activities in individual samples (Figure 2.6B). We observed trends toward decreased Complex I-dependent respiration (Figure 2.6C) and increased Complex II-dependent respiration (Figure 2.6D). As expected, there was no difference in Complex IV-dependent respiration in Hq mitochondria compared to WT (Figure 2.6E). Because Complex IV activity was clearly unchanged, we expressed the activities of the other complexes as a ratio of the Complex IV activity, which reduced the data variability through internal normalization. Following normalization, the Complex I-dependent OCR measured upon NADH addition was significantly lower in Hq mitochondria compared to WT (Figure 2.6F). The CRABS-ROC protocol also revealed a strong trend ($p=0.06$) toward increased Complex II-dependent OCR in Hq mitochondria (Figure 2.6G). Furthermore, the ratio of Complex I to Complex II-dependent OCR was significantly decreased by over two-fold (Figure 2.6H). Thus, CRABS-ROC unmasked a Complex I activity deficit that multiple studies [92, 93] failed to reveal by conventional respirometry using Complex I-linked substrates. It also revealed a likely adaptive increase in Complex II activity.

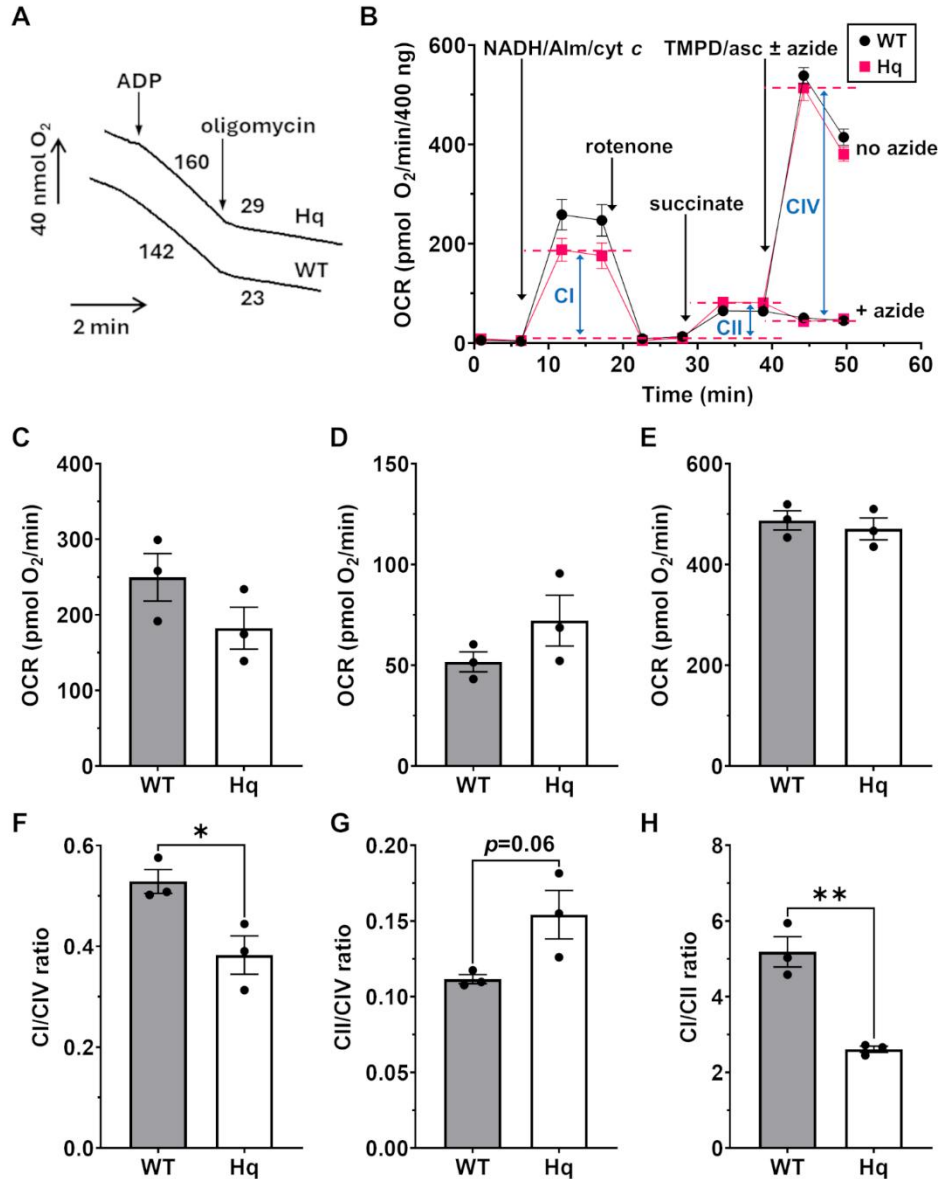


Figure 2.6 CRABS-ROC unmasks Complex I deficiency in previously frozen AIF-depleted isolated harlequin (Hq) brain mitochondria.

(A) Reprinted with permission from Fig. 2.1C of [93]. ADP (1 mM)-stimulated oxygen consumption was measured using a Clark-type oxygen electrode at 30°C for wild-type (WT) and Hq brain mitochondria (0.25 mg/ml) incubated in a potassium chloride-based assay medium. Oligomycin (3 µg/ml) was then added. Oxygen consumption rates (OCR) are shown in nmol O₂/min/mg mitochondrial protein; additional experimental details can be found in [93]. The addition of FCCP after oligomycin failed to yield higher OCR than the ADP-stimulated rates (data not shown). (B) OCR measurements from WT and Hq brain mitochondria. NADH (1 mM) was added with the pore-forming peptide alamethicin (alm, 40 µg/ml) and cytochrome *c* (cyt *c*, 100 mM), followed by rotenone (2 µM), succinate (5 mM), and TMPD (0.4 mM) plus ascorbate (asc, 2 mM). Sodium azide (50 mM) was added with TMPD/asc when indicated. The OCR subtractions used to calculate Complex I-dependent (I), Complex II-dependent (II), and Complex IV-dependent (IV) OCR are shown graphically for the Hq trace and were done in the

same way for the WT trace, with calculations using the first data point following each injection. The results are mean \pm SEM from $n=3$ biological replicates. **(C)** Complex I-dependent OCR. **(D)** Complex II-dependent OCR. **(E)** Complex IV-dependent OCR. **(F)** The ratio of Complex I-dependent to Complex IV-dependent OCR. **(G)** The ratio of Complex II-dependent to Complex IV-dependent OCR. **(H)** The ratio of Complex I-dependent to Complex II-dependent OCR. The results in C-H are mean \pm SEM, $n=3$. * $p<0.05$; ** $p<0.01$

2.5. Discussion

Over the past two decades, mitochondrial bioenergetics research has expanded rapidly, largely driven by the introduction of the Seahorse Extracellular Flux Analyzer. This technology popularized the Mito Stress Test, a respirometry injection protocol that became the standard protocol in bioenergetics studies [38, 105]. However, in many—if not most—studies this was the only protocol employed, and potential limitations related to substrate availability were often overlooked.

Our experiments employing exogenous pyruvate demonstrate that the Mito Stress Test significantly underestimates respiratory capacity in neurons due to insufficient mitochondrial substrate provision by glycolysis and other endogenous metabolic pathways. This limitation may also extend to other cell types. Using a complementary respirometry protocol we named CRABS-ROC, we demonstrated that substrate availability not only underestimates respiratory capacity, but it also masks the capacity of Complex I in both intact cells and isolated mitochondria. This suggests that even when glycolysis is not rate-limiting, as is the case when an exogenous mitochondrial substrate such as pyruvate is provided, maximal respiration is still constrained by the rate at which TCA cycle dehydrogenases supply NADH to the ETC—a process that is tightly regulated by enzymes such as PDH [90].

Importantly, the CRABS-ROC protocol was able to uncover a Complex I activity deficit in harlequin mutant mitochondria that went undetected by a conventional respirometry protocol [92, 93] and also by a spectrophotometry-based Complex I assay [92], despite an approximately 50% reduction in most Complex I proteins. Previous studies required titration with Complex I inhibitors to functionally demonstrate the deficiency in harlequin mitochondria [92, 93]. This highlights the enhanced sensitivity of CRABS-ROC in detecting subtle bioenergetic impairments

that may be present in many disease models. The existence of excess Complex I capacity likely explains why both harlequin mutant mice and *Ndufa1*^{S55A} mutant mice—each exhibiting ~50% Complex I deficiency—maintain a relatively normal lifespan [112, 114], with female *Ndufa1* mice even showing a modest lifespan extension relative to WT controls [114].

Alamethicin-based respirometry protocols similar to CRABS-ROC were previously employed for measuring ETC complex activities within freeze-thawed brain homogenate or isolated mitochondria [104, 113]. These studies showed that ETC complex activities are not compromised by freezing, and the ability to use frozen samples for ETC measurements was cited as a main advantage.

In this study, we highlighted the utility of a further optimized protocol, CRABS-ROC, for investigating mitochondrial bioenergetic function under conditions that bypass endogenous substrate limitations. Importantly, we demonstrated that the protocol can be applied not only to tissue homogenates and isolated mitochondria, but also to cells in parallel to intact or permeabilized cell systems (Figure 2.4). These simultaneous measurements enable direct comparisons of mitochondrial bioenergetic properties among conditions where glycolysis- or TCA cycle-mediated substrate restrictions are either present or removed.

Spectrophotometry-based individual and linked ETC complex activity assays have been used for decades [115]. However, many of these ETC activity assays rely on the donation of electrons to an artificial electron acceptor and some employ exogenous benzoquinone, including a Complex I assay that failed to detect the Complex I deficit in Hq brain mitochondria [92]. In contrast, the CRABS-ROC protocol relies on endogenous inner membrane ubiquinone as well as oxygen consumption by Complex IV, facilitating comparison of ETC activities to physiologically relevant intact cells. When evaluating Complex I activity by CRABS-ROC with a side-by-side

intact cell comparison and OCR as the common readout, the large excess of neuronal Complex I capacity could be readily detected and appreciated. Notably, CRABS-ROC's high sensitivity enabled easy investigation in a specific primary cell population, cortical neurons, whereas spectrophotometric ETC complex activity assays have mostly been applied to brain homogenate or isolated brain mitochondria that are derived from a mixture of neurons and glia.

Our CRABS-ROC protocol employed a 100 mM cytochrome *c* concentration, whereas previous related protocols used a ≥ 10 -fold lower concentration (i.e., 8 mM [104] or 10 mM [113]). We wondered how these cytochrome *c* concentrations compare to the physiological cytochrome *c* concentration in brain mitochondria. We failed to find studies directly estimating the concentration of cytochrome *c* in the intermembrane space. However, alamethicin releases essentially all of the cytochrome *c* from isolated brain mitochondria through swelling-induced outer membrane rupture and this amount was reported as 9.5 ng cytochrome *c*/mg of mitochondrial protein (equivalent to 0.76 nmol/mg) [116]. Based on a mitochondrial intermembrane space volume of ~ 1 ml/mg mitochondrial protein [117], the physiological cytochrome *c* concentration within brain mitochondria is ~ 760 nM; it may approach 2 mM based on another intermembrane space volume estimate [118]. These numbers indicate that the higher cytochrome *c* concentration we optimized by titration is closer to the physiological concentration than those used by other alamethicin-based respirometry protocols.

Our cytochrome *c* titration revealed that the cytochrome *c* concentration influences not only absolute, but also relative ETC complex activities. We found that Complex IV-dependent OCR exceeds Complex I-dependent OCR in both brain homogenate and isolated brain mitochondria, whereas previous studies reported the opposite [113] or that they are similar [104]. Because NADH-dependent respiration also depends on Complex IV activity in the Complex I-III-

IV linked activity assay, the Complex I-dependent OCR should not exceed the Complex IV-dependent OCR unless the concentration of TMPD/ascorbate or cytochrome *c* is rate-limiting. We found that lowering the CRABS-ROC cytochrome *c* concentration further below the physiological level, from 100 μ M to 8 μ M, disproportionally decreased Complex IV-dependent respiration (Figure 2.5), causing Complex I-dependent OCR to exceed Complex IV-dependent OCR as reported by [113] even though the OCR of both was reduced. This finding illustrates that the measured ratios of ETC complex activities can change if cytochrome *c* is rate-limiting. Future studies might directly compare ETC complex activity rates and ratios measured by CRABS-ROC under optimized conditions to those measured by classical assays. It is notable that CRABS-ROC detected a difference in Complex I activity (Figure 2.6) that could also be detected by Complex I inhibitor titration [92, 93] but was missed by a spectrophotometry-based Complex I assay [92].

The existence of excess Complex I capacity has important implications for disease biology. Loss of Complex I function is implicated in the pathogenesis of Parkinson's disease [119-121], a late-onset neurodegenerative disorder primarily affecting the elderly [122]. Exposure to environmental toxins that inhibit Complex I are linked to the sporadic form of Parkinson's disease [123-125]. Our finding that neurons possess substantial excess Complex I capacity may help explain in part the disease's typically late onset and slow progression, as a threshold of cumulative toxin exposure may be required prior to the manifestation of clinical symptoms.

While the CRABS-ROC protocol offers enhanced sensitivity for detecting mitochondrial respiratory deficits, it has several limitations. To facilitate Complex I substrate delivery, the protocol compromises the integrity of the inner mitochondrial membrane. As a result, it is unsuitable for studies investigating the influence of mitochondrial structural dynamics, such as fusion, fission, or membrane lipid alterations, on the ETC complexes. Additionally, CRABS-ROC

relies on the addition of exogenous substrates and cytochrome *c*—an intermembrane space ETC component—at concentrations that differ from physiological levels. Consequently, the protocol is better suited for assessing maximal ETC enzyme capacities rather than physiological ETC activity. Therefore, CRABS-ROC should not be viewed as a replacement for the Mito Stress Test, but rather as a complementary approach that can be run in parallel with assays involving intact or plasma-membrane-permeabilized cells. Finally, it is important to note that although the CRABS-ROC protocol was optimized for our samples (rat neurons, rat brain homogenate, and mouse isolated brain mitochondria), the reagent concentrations employed may not be universally optimal. Protocol optimization should be independently verified before use, with reagent concentrations adjusted as necessary.

2.6. Conclusions

Our study highlights the limitations of the widely used Mito Stress Test protocol in accurately assessing mitochondrial bioenergetic capacity due to substrate constraints. To address this, we introduced the CRABS-ROC protocol—a complementary approach that assesses the capacity of individual respiratory chain components and enables detection of hidden ETC deficits. Our findings emphasize the importance of considering substrate availability in bioenergetics research, especially when investigating mitochondrial dysfunction in disease models where the impairments may be subtle. This approach could also have translational applications in understanding functional aspects of human Complex I deficiencies.

Chapter3

Sex-Specific Acute Impairment of the Mitochondrial Respiratory Chain in a Rat Model of Pediatric Traumatic Brain Injury

3.1 Abstract

Pediatric traumatic brain injury (TBI) causes mitochondrial bioenergetic impairment affecting brain metabolism and development. Whether there are intrinsic sex-based differences in how the mitochondrial electron transport chain (ETC) complexes of the immature brain are affected in the acute period following TBI is unknown. To address this gap, we applied the Seahorse respirometry-based protocol CRABS-ROC to measure the activity of individual ETC complexes in brain homogenates of 17-day old male or female rats at 24 hours post-TBI in the controlled cortical impact TBI model. There were no differences in the Complex I-, II-, or IV-dependent oxygen consumption rates (OCRs) between the ipsilateral and contralateral hemispheres in females. However, the Complex I- and Complex IV-dependent OCRs were significantly reduced in injured male brain tissue relative to the contralateral, non-impacted side. Nevertheless, males showed no changes in representative subunits of each ETC complex detected by western blot at 24, 48, or 72 hours post-TBI, suggesting that the male-specific ETC deficiencies following TBI are not a result of ETC complex protein degradation. In summary, TBI acutely impaired the Complex I and IV activities of immature male rats whereas females were spared. Further work is needed to elucidate the underlying mechanisms.

3.2 Introduction

Traumatic brain injury (TBI) is a leading cause of morbidity and mortality in children and adolescents, with long-term consequences for cognitive, behavioral, and neurological development

[126, 127]. Illustrating the chronic nature of injury-associated disease, elevated global cognitive deficits were observed at 10 years post-TBI among severely injured children 2-12 years old, with the severity and age of injury determining the extent of processing speed impairments [29]. In animal studies, pediatric TBI caused young adulthood deficits in hippocampal neurogenesis and cognitive function [31].

Mitochondrial bioenergetic deficits are a hallmark of pediatric TBI, with evidence from both human and animal studies indicating post-TBI oxidative phosphorylation impairment, reduced ATP production, and increased reliance on glycolysis [30, 128-131]. Large animal (swine) models of pediatric TBI revealed evidence for decreased Complex I-driven respiration and increased Complex II-driven respiration at 24 hours post-injury [128-130]. The TBI-induced respiratory impairment was greater following focal TBI than after a diffuse, rotational brain injury [128, 129], and acute mitochondrial respiratory deficits following immature rat focal TBI were also reported [37, 128, 130, 132]. In humans, reduced cerebral blood flow and decreased brain oxygen metabolism were observed in severely injured children even at three months post-TBI [30].

There has been some study of sex differences in mitochondrial bioenergetic function in adult brain injury models, including TBI, but with differences mostly attributed to sex hormones [21, 133, 134]. There is one report of sex-dependent mitochondrial functional differences in a juvenile closed-head TBI model [135], with females showing greater oxygen consumption rates (OCRs), but respiration was measured at a chronic, three week timepoint. Whether there are sex-dependent TBI-induced mitochondrial alterations in the pre-pubescent brain during the acute post-injury period is unknown, as most immature animal studies used only one sex. Therefore, the goal of this study was to test for sex-specific mitochondrial electron transport chain (ETC) deficits at an acute, 24-hour time point in a pediatric rat TBI model.

Recently, we described the Seahorse respirometry protocol CRABS-ROC (Complex Respirometry Assay Bypassing Substrate-Restricted Oxygen Consumption) that can measure Complex I, II, and IV activities in low microgram amounts of brain homogenate [136]. An advantage of this protocol is that it can reveal subtle differences in Complex I function that may be missed by evaluating respiration in the presence of classical Complex I-linked substrates—e.g., pyruvate and malate—when the supply of NADH from tricarboxylic acid cycle dehydrogenase enzymes may be rate-limiting. A second advantage is that mitochondrial isolation is unnecessary since brain homogenate is used, avoiding inaccuracies due to the incomplete recovery of mitochondria during the isolation procedure [137]. Therefore, we applied the CRABS-ROC protocol to test for sex-specific functional ETC deficits caused by pediatric TBI. Western blot analysis of representative ETC complex proteins was performed at 24-72 hours post-injury to evaluate whether functional differences coincide with alterations at the protein level. The results demonstrate that there are intrinsic sex differences in the mitochondrial resilience to TBI, revealing male-specific Complex I and IV vulnerabilities that are likely post-translational in nature.

3.3 Materials and Methods

3.3.1 Animals and TBI surgery

All animal procedures were conducted in accordance with the Guide for Care and Use of Laboratory Animals of the NIH and were approved by the Institutional Animal Care and Use Committee (IACUC) at Johns Hopkins University. Controlled cortical impact was conducted on 17-day-old male and female Sprague–Dawley rats to the left brain hemispheres under 2% isoflurane inhalant anesthesia, followed by midline scalp incision and left parietal craniotomy [37, 132]. Impact was performed with a 3 mm metal impactor tip at a depth of 1.5 mm, a duration of

50 msec, and a velocity of 5.5 ± 0.4 m/s as described [37]. The skull flap was then replaced to seal the craniotomy and the skin was sutured. Rats were awakened from anesthesia and were returned to their original cages with their littermates and mother. Sample sizes of $n=11$ males and $n=11$ females were used for the TBI-respirometry experiments, with the uninjured brain hemisphere serving as the internal control. A sample size of $n=4$ males was used for each of the 24-hour, 48-hour, and 72-hour post-TBI time points (12 males total). Four naïve animals were used to support the use of contralateral samples as appropriate controls.

3.3.2 Brain homogenate sample collection

Rats were euthanized and whole brains were dissected 24 hours after CCI (Figure 3.1A). Uninjured frontal and occipital brain tissue was removed using a razor blade. Peri-contusional cortex was then separated in the injured, ipsilateral (left) side. The equivalent area in the uninjured, contralateral (right) side was also dissected. The tissue from each hemisphere was separately homogenized in 5 mL of MS+EGTA buffer using a 7 mL glass homogenizer by delivering six strokes with pestle size A (loose-fitting), followed by six strokes with pestle size B (tight-fitting). The MS+EGTA buffer consisted of 225 mM mannitol, 75 mM sucrose, 1 mM ethylene glycol-bis(β -aminoethyl ether)-N,N,N',N'-tetraacetic acid (EGTA), 1 mg/ml fatty acid-free bovine serum albumin (BSA), and 5 mM HEPES, pH 7.4. Nuclei and unbroken cells were removed from the homogenized samples by centrifugation at $1000\times g$ for 10 min at 4°C and the supernatants were stored at -80°C.

3.3.3 Stock solutions for respirometry

Alamethicin was dissolved at 40 mg/mL in ethanol. Horse heart cytochrome *c* (catalogue# C2506, MilliporeSigma, St. Louis, MO) was prepared at 100 mg/mL in MAS buffer. Rotenone was dissolved at 2 mM in DMSO. Succinate was prepared at 1 M in water. TMPD was dissolved at 500 mM in ethanol and 0.1 mg/mL ascorbate was added to this TMPD stock solution to prevent auto-oxidation. A separate ascorbate stock solution was dissolved in MAS buffer at 1M. All these reagents were obtained from MilliporeSigma and the prepared stock solutions were stored at -20°C.

NADH (catalogue #10128023001, MilliporeSigma) powder was stored in a 4°C desiccator and, for every experiment, freshly dissolved in MAS buffer immediately prior to use. Sodium azide (MilliporeSigma) was also prepared freshly from powder for each experiment.

3.3.4 Respirometry assay

Twelve samples with 6-8 technical replications per sample were run on each XFe96 Seahorse Analyzer cell culture microplate (Agilent Technologies; Santa Clara, CA) (Figure 3.1B). Tissue homogenates samples were thawed on ice, followed by a Pierce bicinchoninic acid (BCA) assay from Thermo Fisher Scientific (Waltham, MA) to determine protein concentrations. Four µg of homogenate protein per well, diluted in 20 µL of MAS buffer, were added to XFe96 microplates. The MAS assay buffer consisted of 220 mM mannitol, 70 mM sucrose, 5 mM KH₂PO₄, 5 mM MgCl₂, 1 mM EGTA, and 2 mM HEPES, pH 7.4.

The microplates were centrifuged at 2000×g (without braking) for 5-10 min at 4°C to sediment and attach biological material. Additional MAS buffer (160 µL) was gently added to the side wall of each well to bring the starting assay volume to 180 µL. Reagents dissolved in MAS buffer were loaded into pre-hydrated Seahorse xFe96 cartridges as follows: Port A - Complex I

substrate NADH, alamethicin, cytochrome *c*; port B – Complex I inhibitor rotenone; port C - Complex II substrate succinate; port D – Complex IV substrate TMPD and ascorbate. In three of the 6-8 technical replicates per sample, the Complex IV inhibitor sodium azide was added together with the TMPD and ascorbate (Figure 3.1C). Oxygen consumption rate measurements were acquired using an XFe96 Extracellular Flux Analyzer (Agilent Technologies). Ipsilateral and contralateral samples from individual animals were always loaded on the same XFe96 plate and every plate contained samples from both males and females, as well as at least one reference sample from a naïve animal.

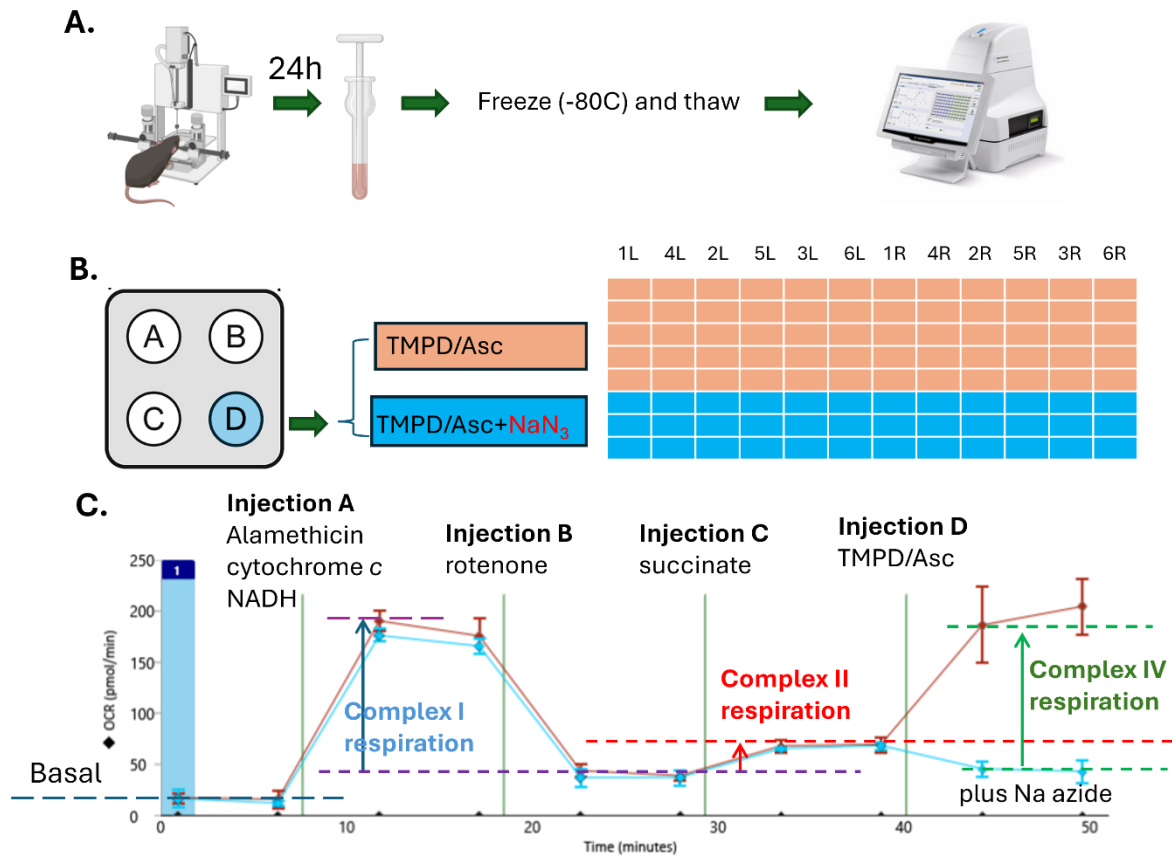


Figure 3.1 Schematic illustration of the CRABS-ROC protocol used to evaluate mitochondrial electron transport chain function in brain homogenates from the immature rat controlled cortical impact (CCI) TBI model.

(A) CCI to respirometry experimental flowchart. (B) Example sample loading template showing the different D port injections used to calculate Complex IV activity. Each column had 6-8 technical replications for each hemisphere sample (with a few wells serving as blank controls), L: left/ipsilateral; R: right/contralateral. (C) Sample Seahorse respirometry data traces illustrating how Complex I, II, and IV activities were calculated.

3.3.5 Western blots

Brain hemisphere lysates from separate cohorts of male rats were collected for western blots. Halt protease and phosphatase cocktail (Thermo Fisher Scientific) was added into ice-cold RIPA lysis buffer (Thermo Fisher Scientific) before use. Rat hemispheres were lysed in RIPA buffer at 50-100 μL per 2 mm^3 of tissue, followed by 6W sonication on ice for 10 seconds per sample. Samples were left on ice for an additional 10 minutes and then centrifuged at 1,7000 $\times g$ for 20 minutes at 4°C. Supernatants were collected as protein samples and were stored at -80°C. Protein samples were then thawed on ice before use.

Fifty μg of total protein were loaded after preheating samples to 50°C for 10 minutes in Laemmli buffer containing sodium dodecyl sulfate. Samples were run on Invitrogen NuPAGE 4%-20% gradient mini acrylamide gels. Electrophoresis was done at 200V for 20 minutes. Proteins were then transferred to PVDF membranes using the Bio-Rad semi-dry transfer system. LiCOR Revert 700 total protein stain was done for normalization of protein loading. Rodent OXPPOS antibody cocktail (RRID:AB_2629281, Abcam; Waltham, MA) was diluted in blocking buffer (2.5% bovine serum albumin + 2.5% non-fat milk in TBS-T) at 1:1000 for immunodetection. Rhodamine-conjugated tubulin antibody (RRID:AB_2884950, Bio-Rad; Hercules, CA) was co-diluted at 1:25,000. Fluorescent secondary antibodies from LI-COR Biosciences (Lincoln, NE) were used at 1:20,000. The protein bands were visualized using a LI-COR Odyssey Fc Imager and the protein levels were quantified by densitometry using Image Studio 6.0 software (LI-COR Biosciences).

3.3.6 Data Analysis and Statistics

OCR data analysis and statistics were performed using Agilent Wave Analyzer software and GraphPad Prism 10.4.1 software (San Diego, CA), respectively. Complex I-dependent

respiration = NADH-induced OCR - rotenone-inhibited OCR; Complex II-dependent respiration = succinate-induced OCR - rotenone-inhibited OCR; Complex IV-dependent respiration = OCR difference between TMPD/ascorbate-induced OCR and OCR following TMPD/ascorbate plus sodium azide addition. Both OCRs and protein levels were analyzed by within-subjects two-way ANOVA with brain hemisphere (ipsilateral vs. contralateral) and sex as factors. The Šidák *post hoc* test was used for pairwise comparisons and $p < 0.05$ was considered significant.

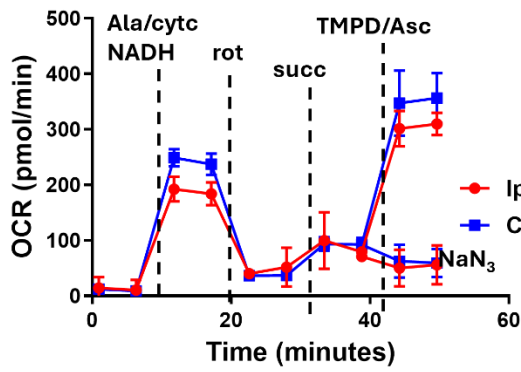
3.4 Results

3.4.1 Detection of male-specific decreases in Complex I- and IV-dependent respiration at 24 hours post-TBI

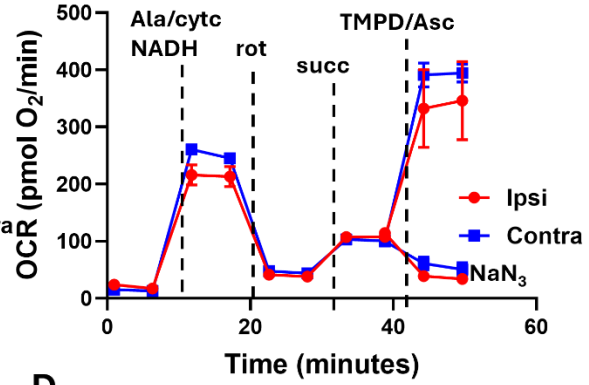
Oxygen consumption by mitochondria within ipsilateral and contralateral brain homogenates was measured by Seahorse respirometry at 24 hours post-CCI brain injury (Figure 3.1). After three baseline measurements, NADH was added together with the pore-forming peptide alamethicin and the electron carrier cytochrome *c* to induce primarily Complex I-dependent respiration. This was followed by addition of the Complex I inhibitor rotenone and the OCR difference before and after rotenone administration was taken to represent the Complex I-dependent OCR. The Complex II substrate succinate was then added to induce Complex II-dependent OCR. Finally, N,N,N',N'-tetramethyl-para-phenylene-diamine (TMPD), a Complex IV electron donor that passes electrons to cytochrome *c*, was co-added with ascorbate, which reduces TMPD. In three of the eight technical replications, the Complex IV inhibitor sodium azide was included with the TMPD mixture. The difference between the TMPD/ascorbate-stimulated OCR and the azide insensitive OCR was taken to represent Complex IV-dependent OCR.

We observed a significant decrease of Complex I- and IV-dependent OCRs (Figures 3.2C and 3.2E, respectively) in ipsilateral hemispheres compared to contralateral hemispheres in males but not females. Complex II-dependent OCR did not change significantly between ipsilateral and contralateral brain homogenates in either sex (Figure 3.2D). We also calculated the ipsilateral/contralateral ratio for the OCRs dependent on each complex. The ratio decreased for Complex IV activity in males (Fig. 3.2H), while a significant difference in Complex I (Figure 3.2F) or II (Figure 3.2G) activity was not detected.

A. representative male OCR traces

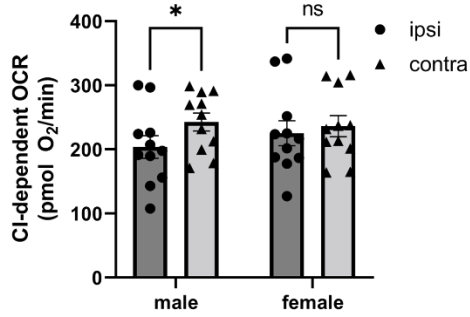


B. representative female OCR traces

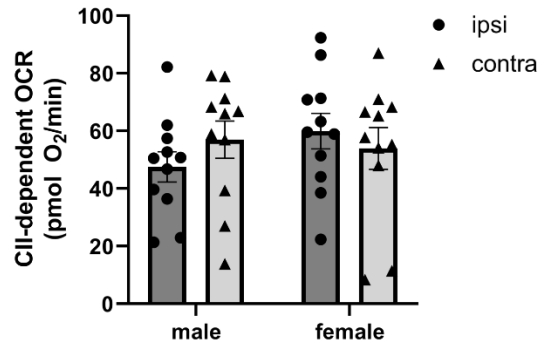


C.

Complex I-dependent OCR

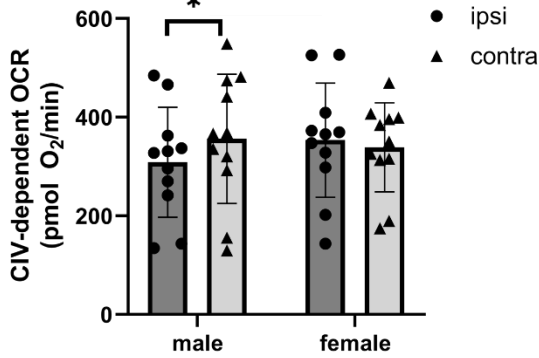


Complex II-dependent OCR



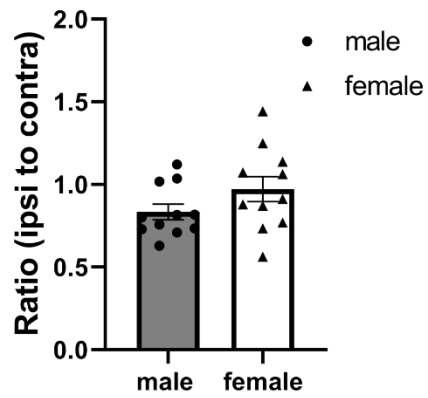
E.

Complex IV-dependent OCR

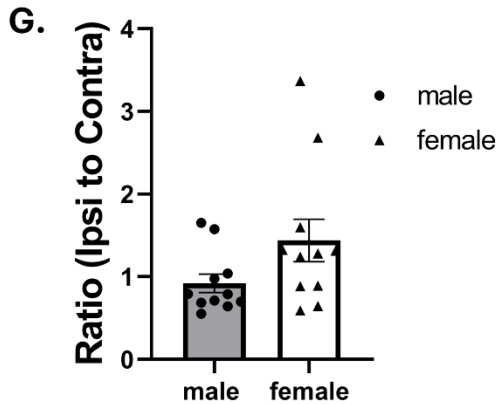


F.

Complex I



Complex II



Complex IV

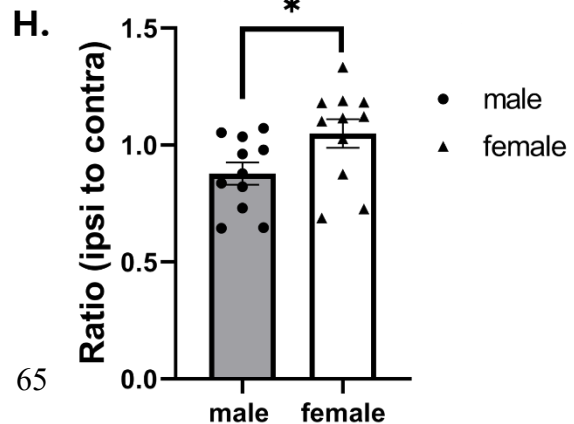


Figure 3.2 TBI-induced decreases in Complex I- and IV-dependent oxygen consumption rates in male ipsilateral brain homogenates at 24 hours post-injury.

A and B. Representative XFe96 respirometry traces (mean \pm SD, n=8 wells) from a male (**A**) and female (**B**) subjected to TBI. **C-E.** Complex I- (**C**), II- (**D**), and IV (**E**)-dependent respiration in male and female rat brain homogenates. ipsi: ipsilateral or injured hemisphere; contra: contralateral or uninjured hemisphere. OCR were analyzed by within-subjects two-way ANOVA (repeated measures) with Šidák *post hoc* analysis for multiple comparisons among groups. Data are mean \pm SEM, n=11. * p <0.05. **F-H.** Ipsilateral to contralateral OCR ratio in Complex I- (**F**), II- (**G**), and IV (**H**)-dependent respiration. OCR ratios were analyzed by Student's t-test. Data are mean \pm SEM, n=11. * p <0.05.

3.4.2 Levels of representative electron transport chain complex subunits are unchanged at acute time points after TBI in males

Since we observed decreased Complex I- and IV-dependent respiration in male ipsilateral brain homogenates, we asked whether this respiration deficiency could be caused by protein instability of the affected ETC complexes after TBI. Upon performing western blots using the OXPHOS cocktail of ETC antibodies, we failed to observe significant changes in the protein level of any of the representative ETC complex subunits at 24, 48, or 72 hours post-injury, suggesting an alternative mechanism for the male-specific post-TBI Complex I and IV deficits.

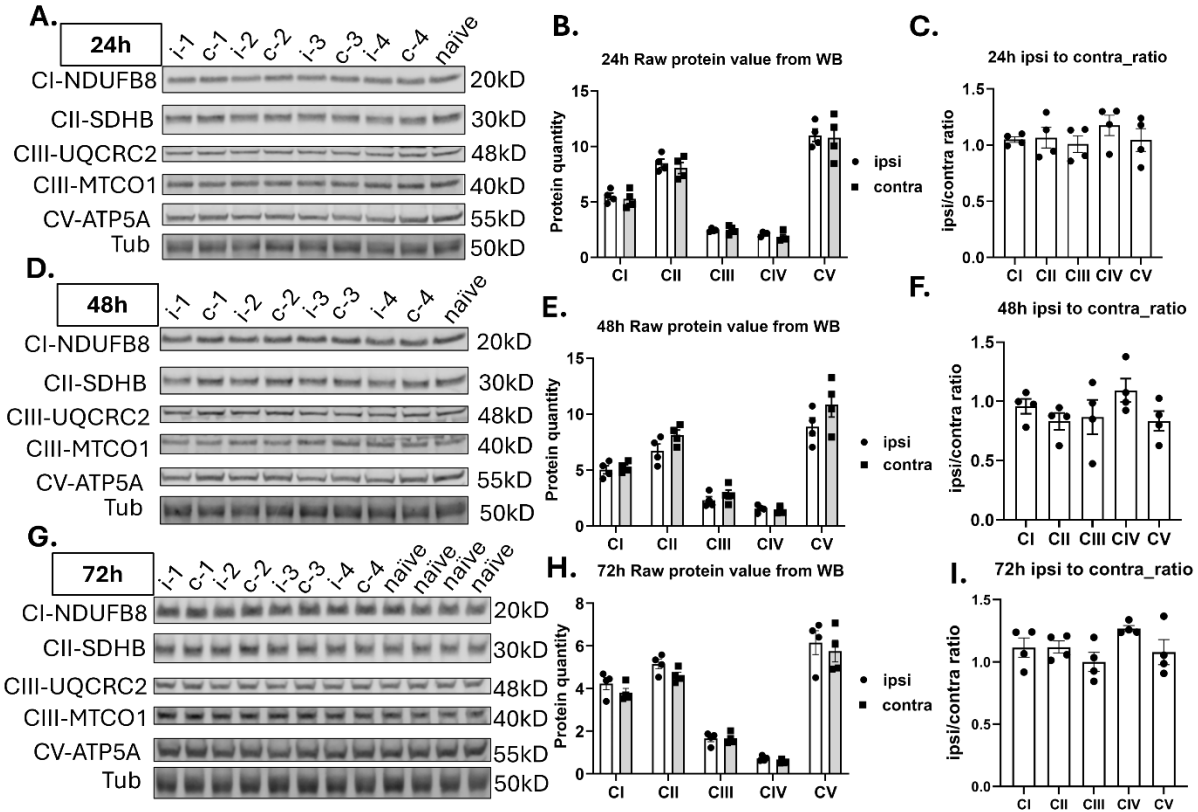


Figure 3.3 Levels of representative electron transport chain complex subunits in uninjured vs. injured hemispheres at 24, 48, and 72 hours post-TBI.

Western Blot examination of ETC complex subunits with rodent OXPHOS antibody cocktail (Abcam) at the indicated post-injury time points. i: left/ipsilateral/injured hemisphere; c: right/contralateral/uninjured hemisphere. Subjects are all males. **(A), (D), and (G).** western blot images for 24h, 48h, and 72h post-TBI, respectively. **(B), (E), and (H).** western blot quantifications, normalized to tubulin, for 24h, 48h, and 72h post-TBI, respectively. **(C), (F), and (I).** ipsilateral to contralateral ratio for 24h, 48h, and 72h post-TBI, respectively. Protein levels of ipsilateral and contralateral TBI brains were analyzed by within-subjects two-way ANOVA (repeated measures) with Šidák *post hoc* analysis for multiple comparisons among groups. Ipsilateral to contralateral ratios were analyzed by ordinary on-way ANOVA, Data are mean \pm SEM, $n=4$.

3.5 Discussion

Both acute and sub-acute changes to mitochondrial bioenergetic function have been reported in pediatric TBI animal models [37, 128-130, 132, 135]. However, there has been little investigation of sex differences, particularly during the early response to TBI. In this study, we observed ETC Complex I- and IV-dependent respiration deficiencies in the PND17 rat pediatric TBI model at 24 hours post-injury that were only seen in males. Despite these functional differences, there were no changes to the protein levels of representative ETC complex subunits from Complexes I-IV, including NDUFB8 (Complex I subunit) and MT-COI (Complex IV subunit), at 24-72 hours post-injury. A significant TBI-associated decrease in the ATP synthase subunit ATP5A was observed in the ipsilateral brain tissue relative to the contralateral side, however the deficit was minor (~10%) and observed only at 48 hours post-injury.

There have been a few previous studies of mitochondrial dysfunction in pediatric TBI animal models, with most employing isolated mitochondria. In a three-week post-injury study of isolated mitochondria, females showed a TBI-induced increase in Complex I-linked OCR that was attributed to elevated proton leak, whereas in that same PND30 rat juvenile TBI model, male Complex I-dependent OCR was about two-fold lower compared to females and unchanged following TBI [135]. We failed to see the large respiration difference between males and females that was documented in this study. However, our study was done in substantially younger animals and used brain homogenates rather than isolated mitochondria.

Developmental changes may contribute to the varying mitochondrial susceptibility to TBI observed in previous studies because brain mitochondria undergo changes in protein levels and ETC activities during the early postnatal day period [138-140]. A pediatric TBI study of PND9-10 female rats observed a small deficit in the Complex I substrate-linked, ADP-stimulated respiration

of ipsilateral brain mitochondria at 24 hours post-injury [130], whereas a later study done with PND17-21 rats detected no impairment [37]. Although this later finding is concordant with the lack of female ETC deficiencies observed in our PND17 rat TBI study, that same study also failed to observe a TBI-induced change in the Complex I-linked OCR of ipsilateral mitochondria from males at 24 hours post-injury, in contrast to the Complex I activity deficit we observed. In the prior study, OCR was measured using isolated brain mitochondria incubated with the Complex I-linked substrates pyruvate and malate—a condition where tricarboxylic acid cycle dehydrogenase activities are rate-limiting for Complex I activity—whereas in our study we evaluated Complex I capacity in brain homogenates by providing the direct Complex I substrate NADH. Additionally, mitochondrial isolation fails to recover a substantial fraction of the mitochondria present within brain homogenate [137], which may also contribute to different findings with brain homogenates compared with isolated mitochondria.

Although we observed significantly lower Complex I and IV capacities in peri-contusional brain homogenate relative to the contralateral hemisphere, the deficits were relatively small (~10-15%). Nevertheless, a proton nuclear magnetic resonance spectroscopy study of PND16-17 male rats reported a TBI-induced increase in the brain lactate to creatine ratio at 24 hours post-injury, reflective of decreased oxidative metabolism and/or increased glycolysis [131]. This finding in a comparable CCI model suggests that the mitochondrial ETC deficits we observed in PND17 brain-injured males are relevant to the *in vivo* brain situation.

After examining the representative ETC complex subunit protein levels, we did not observe any TBI-induced protein declines at 24, 48, or 72 hours post-injury. Since we only detected the protein level of one subunit within each ETC complex, we cannot exclude the possibility that the

Complex I and Complex IV deficits detected at 24 hours post-injury were caused by protein level changes to other subunits. However, there are several alternative possibilities.

Complexes I and IV are closely related based on evidence that defective Complex IV destabilizes Complex I in mammalian cells [141] and *C.elegans* [142]. As the balance of individual and super-assembled complexes within the ETC is essential for maintaining proper mitochondrial respiratory function, it is possible that the TBI-induced Complex I and IV capacity decreases are due to a disruption in supercomplex assembly or stability. The protein level of the Complex I subunit NDUFB8 is often evaluated as a proxy for the assembled complex because it is essential for NADH dehydrogenase function. However, NDUFAF2, a key protein that coordinates the association between mitochondrial DNA-derived and nuclear DNA-derived Complex I subunits, would be a good candidate to evaluate in future studies.

Oxidative post-translational modifications (PTM), including reversible and irreversible cysteine modifications, tyrosine nitration, carbonylation, and tryptophan oxidation can decrease the activity of ETC complexes with Complex I being particularly susceptible [143]. These redox PTMs may be caused by TBI-induced increases in the generation of reactive oxygen and nitrogen species. While redox PTM-induced Complex I activity decreases were observed in aging and neurodegenerative diseases [144], our findings raise the possibility that there is a connection between TBI-induced Complex I respiratory deficiency and oxidative PTMs at an acute post-injury time point.

This chapter highlighted the sex-related differences in mitochondrial ETC complex I- and IV-dependent respiration in injured immature rat brains. We observed the differences at PND17, prior to when sex hormones induce secondary sexual characteristics. Sex differences in mitochondrial respiratory function were reported at acute post-injury time points in adult TBI [22];

however, here we uncovered that the immature brain also exhibits TBI-induced ETC deficits that are both acute and sex-specific . These findings may encourage the consideration of sex as a factor in the investigation and design of new therapies for pediatric TBI patients.

Chapter 4

Inducible Nitric Oxide Synthase (iNOS)-catalyzed Reduction of the Coenzyme Q10 Analogue Idebenone Restores Mitochondrial Respiration in Pro-inflammatory Microglia

4.1 Abstract

The mitochondrial electron transport chain is non-linear, with multiple entry points. The Coenzyme Q10 (CoQ10) analogue idebenone, used to treat the mitochondrial Complex I eye disease Leber Hereditary Optic Neuropathy (LHON) [145], bypasses Complex I by feeding electrons to Complex III. Supporting repurposing idebenone for additional disorders, Complex I dysfunction has emerged as a drug target in persistent microglia-mediated brain inflammation that contributes to multiple neurodegenerative diseases. However, idebenone's pro-drug-like behavior, requiring reduction by the enzyme NAD(P)H:quinone oxidoreductase 1 (NQO1) that exhibits cell-type specific brain expression, is thought to be an obstacle for expanded clinical use. Among unstimulated primary rat cortical neurons, astrocytes, and microglia, we found only NQO1-expressing astrocytes displayed a robust ability to reduce idebenone. However, pro-inflammatory activation markedly enhanced the ability of microglia to reduce idebenone, which was unexpectedly NQO1 inhibitor-insensitive. Biochemical purification strategies identified inducible nitric oxide synthase (iNOS) as a novel idebenone-reducing enzyme. iNOS knockout diminished the ability of idebenone to stimulate mitochondrial respiration in activated microglia while recombinant iNOS delivery reconstituted the ability of idebenone to bypass impaired Complex I. Our results identify the inflammatory enzyme iNOS as a novel branch point for mitochondrial electron transport chain entry through Complex III and show that iNOS activity can be redirected by the clinical drug idebenone to restore mitochondrial respiration in pro-inflammatory microglia.

4.2 Significance

Prior evidence indicates that mitochondria within some cells can use cytoplasmic NAD(P)H as an electron source when the clinically safe CoQ10-like molecule idebenone is supplied. To fuel mitochondria through Complex III, the pro-drug idebenone was thought to require chemical reduction catalyzed by NQO1, an enzyme not expressed by most brain cell types. Our results establish iNOS as another enzyme that, through idebenone reduction, can co-opt cytoplasmic NADPH to support mitochondrial bioenergetic function. We show that the microglial expression of iNOS—the very enzyme driving mitochondrial dysfunction during pro-inflammatory activation—can be exploited by idebenone to recover mitochondrial oxygen consumption by bypassing sites of nitric oxide-mediated electron transport chain damage.

4.3 Introduction

Electron transport by the respiratory chain allows mitochondria to produce ATP by oxidative phosphorylation [88]. Ubiquinone, commonly called Coenzyme Q (CoQ), is a lipophilic electron carrier with antioxidant properties [146]. Enzymatic cycling between the oxidized and reduced forms is critical both for its ability to act as antioxidant and to support mitochondrial ATP production. Despite possessing these two activities crucial for cell survival, CoQ's poor bioavailability limits its therapeutic potential. The synthetic short-chain CoQ analogue idebenone was developed as a neurotherapeutic drug candidate designed to overcome the poor bioavailability of CoQ [147]. In animal models, idebenone was shown to cross the blood-brain barrier [148, 149] and enhance *ex vivo* mitochondrial oxygen consumption [150]. Oral idebenone is approved in many countries to treat Leber Hereditary Optic Neuropathy (LHON), a disease caused by

mitochondrial Complex I mutations [145, 151]. However, idebenone has not fared well in clinical trials for other neurodegenerative disorders [152].

Evidence suggests that idebenone behaves as a prodrug requiring conversion to idebenol, the non-bioavailable, reduced form of the drug that is believed to mediate its beneficial actions [152]. Idebenol, like ubiquinol, can suppress lipid peroxidation and transfer electrons to Complex III of the mitochondrial respiratory chain [42, 153, 154]. Studies indicate that enzymatic reduction of idebenone is catalyzed by NAD(P)H:quinone oxidoreductase 1 (NQO1) in cells [42, 47, 155]. NQO1 expression level in the target cell population is therefore expected to dictate the usefulness of idebenone for treating a given disease.

Microglia, the innate immune cells of the brain, have become an attractive drug target in several neurodegenerative and psychiatric disorders [156]. A highly pro-inflammatory state of microglia is induced by the Toll-like Receptor 4 (TLR4) agonist lipopolysaccharide (LPS) combined with the cytokine interferon- γ (IFN- γ). This reactive state is associated with a suppression of mitochondrial metabolism and the ability to promote neurotoxicity *in vitro* or *in situ* [157-159]. Our prior work demonstrated that whereas cortical astrocytes can use idebenone as an electron donor to bypass Complex I inhibition, cortical neurons, which do not express NQO1, lack the ability [47]. Whether microglia can enzymatically reduce idebenone has yet to be assessed. Because pro-inflammatory LPS stimulation is reported to upregulate NQO1 via the nuclear factor E2-related factor 2 (Nrf2) transcription factor [160], we hypothesized that LPS/IFN- γ -treated microglia would exhibit an NQO1-dependent enhancement in the ability to reduce idebenone, facilitating its ability to bypass mitochondrial Complex I.

To test this hypothesis and further elucidate the relative capabilities of brain cells for idebenone prodrug conversion, we used a biochemical quinone reduction assay to quantitatively

compare the abilities of neurons, astrocytes, and microglia to reduce idebenone. We found that cortical neurons did not reduce idebenone, consistent with their lack of NQO1 expression [47], while microglia only showed a high rate of idebenone reduction approaching that of astrocytes when stimulated to the pro-inflammatory state. Subsequent experiments revealed that inducible nitric oxide synthase (iNOS) was a main enzyme contributing to the enhanced idebenone reduction in LPS/IFN- γ -stimulated microglia, promoting Complex III-dependent stimulation of mitochondrial oxygen consumption.

4.4 Results

4.4.1 Comparison of brain cell idebenone reduction activity.

The bioenergetic and antioxidant benefits of idebenone are thought to depend on the ability of cells to catalytically generate its reduced form [152]. Neurons and astrocytes differ in how their mitochondria respond to idebenone treatment [47], while little is known about how the drug acts in microglia. To quantitatively compare cellular idebenone-reducing ability, we measured the NADPH oxidation rate in concentrated cellular extract upon idebenone addition (Figure 4.1A). Extracts were concentrated using a 50 kDa cut-off filter, which significantly enhanced activity per mg protein relative to unconcentrated extract. The <50 kDa flow-through fraction exhibited little ability to oxidize NADPH in the presence of idebenone, indicating that idebenone reducing enzymes were successfully captured and concentrated by the filter.

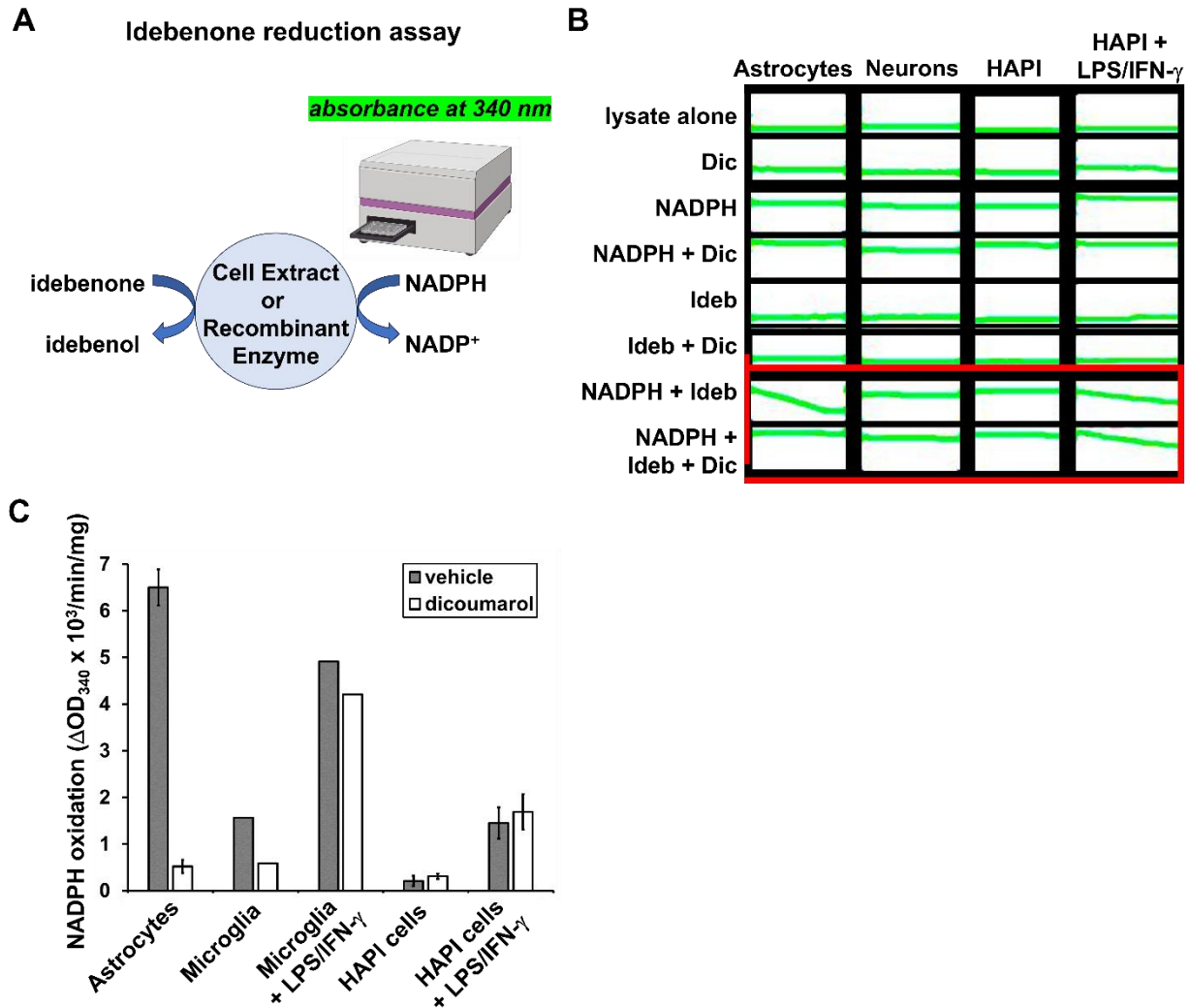


Figure 4.1 Idebenone is enzymatically reduced by astrocytes and by pro-inflammatory microglia.

(A) Schematic representation of the NADPH-oxidation based idebenone reduction assay. (B) NADPH oxidation rate was quantified by measuring decrease in absorbance at 340 nm (DOD_{340}) in the presence of NADPH (200 μ M) and idebenone (Ideb, 200 μ M), with or without the co-presence of the NQO1 inhibitor dicoumarol (Dic, 20 μ M). Representative traces of DOD_{340} over time for the indicated cell types, including all control conditions. (C) Idebenone-dependent NADPH oxidation rates, calculated by subtracting the DOD_{340} measured under the same experimental conditions in the absence of idebenone. Mean \pm SEM from $n=3$ astrocyte or $n=9$ HAPI cell extracts are shown in C, while the data from primary microglia extract is from a single

experiment. No activity was observed in primary cortical neuron extracts, with the traces in *B* representative of two independent experiments.

Rat cortical astrocytes exhibited the highest rate of idebenone reduction per mg protein among the tested cell types (Figures 4.1 *B* and *C*). Astrocyte idebenone-reducing activity was almost completely abolished by the NQO1 inhibitor dicoumarol, congruent with the many studies suggesting an NQO1 requirement for idebenone reduction in cells (e.g., [42, 47, 155]). Primary rat microglia showed little idebenone-reducing activity relative to astrocytes (Fig. 4.1 *B* and *C*), with possible dicoumarol sensitivity of the modest activity. Neurons lacked detectable activity (Figure 4.1*B*), consistent with their inability to use idebenone as an exogenous electron donor [47]. Thus, despite evidence that succinate dehydrogenase and glycerol-3-phosphate dehydrogenase can reduce idebenone in isolated mitochondria or sub-mitochondrial particles [161-164], our cell extract-based idebenone reduction assay recapitulated the NQO1 dependence seen in cells. In addition, the cell type differences in activity correlated with the reported NQO1 expression pattern in the healthy brain [165].

Next, we evaluated the idebenone-reducing ability of microglia stimulated to a pro-inflammatory state. Microglia exposed to LPS/IFN- γ for 18 hours showed a significant ~4-fold increase in NADPH-dependent idebenone reduction (Figure 4.1*C*). Surprisingly, this activity was not sensitive to dicoumarol, suggesting that an enzyme other than NQO1 is responsible for this activity. The number of primary microglia necessary for the quinone reduction assay was prohibitive for further characterization. Therefore, subsequent experiments were performed with the HAPI microglial cell line [57], which also exhibited dicoumarol-insensitive LPS/IFN- γ -stimulated idebenone-reducing activity (Figure 4.1) and could be generated in the abundance needed for biochemical fractionation.

4.4.2 Biochemical enrichment of the LPS/IFN- γ -induced microglial idebenone-reducing enzyme(s).

LPS primes microglia for pro-inflammatory activation by inducing the transcription of several pro-inflammatory mediators [157]. IFN- γ activates LPS-primed microglia to a neurotoxic state through the IFN- γ receptor [159]. We tested LPS and IFN- γ individually and found that the combined treatment was necessary to robustly stimulate dicoumarol-insensitive idebenone-reducing activity (data not shown). Furthermore, we were able to detect robust activity after 10 h, but not after 6 h, of LPS/IFN- γ -stimulation, supporting the possibility that an induced rather than existing enzyme mediates this novel activity. As a first step toward identifying the responsible enzyme, we enriched for NAD(P)H binding proteins in the >50 kDa fractions of non-stimulated and LPS/IFN- γ -treated cells using Cibacron blue affinity chromatography [166]. A total of 683 proteins were identified by mass spectrometry. Overall, these proteins were enriched for NAD(P)H-dependent dehydrogenase enzymes. However, multiple dehydrogenase enzymes were uniquely detected or elevated in the LPS/IFN- γ sample compared with the control sample, necessitating additional purification strategies to identify the idebenone-reducing enzyme(s).

To narrow down the number of candidate enzymes, we used a parallel biochemical enrichment approach based on an in-gel activity assay. Cellular extracts prepared from non-stimulated or LPS/IFN- γ -treated HAPI microglia cells were subjected to native polyacrylamide gel electrophoresis in the presence of the blue dye 2,6-dichloroindophenol (DCPIP). Upon NADPH and idebenone addition, three colorless bands appeared within the gel that were specific to the LPS/IFN- γ -treated sample, indicating the presence of enzyme(s) capable of reducing DCPIP to its colorless product (Figure 4.2A). The upper and lower bands were excised and the proteins within these bands were extracted, digested, and identified by mass spectrometry. The middle band

could not be excised cleanly because of its proximity to the other two. A total of 342 proteins were identified in the higher molecular weight band while 586 proteins were identified in the lower molecular weight band. The NADPH-binding proteins fatty acid synthase (Fasn), isocitrate dehydrogenase 1 (Idh1), thioredoxin reductase 1 (Txnrd1), and inducible nitric oxide synthase (iNOS) were present in both excised colorless bands and, also, present in the affinity chromatography-enriched LPS/IFN- γ -treated sample.

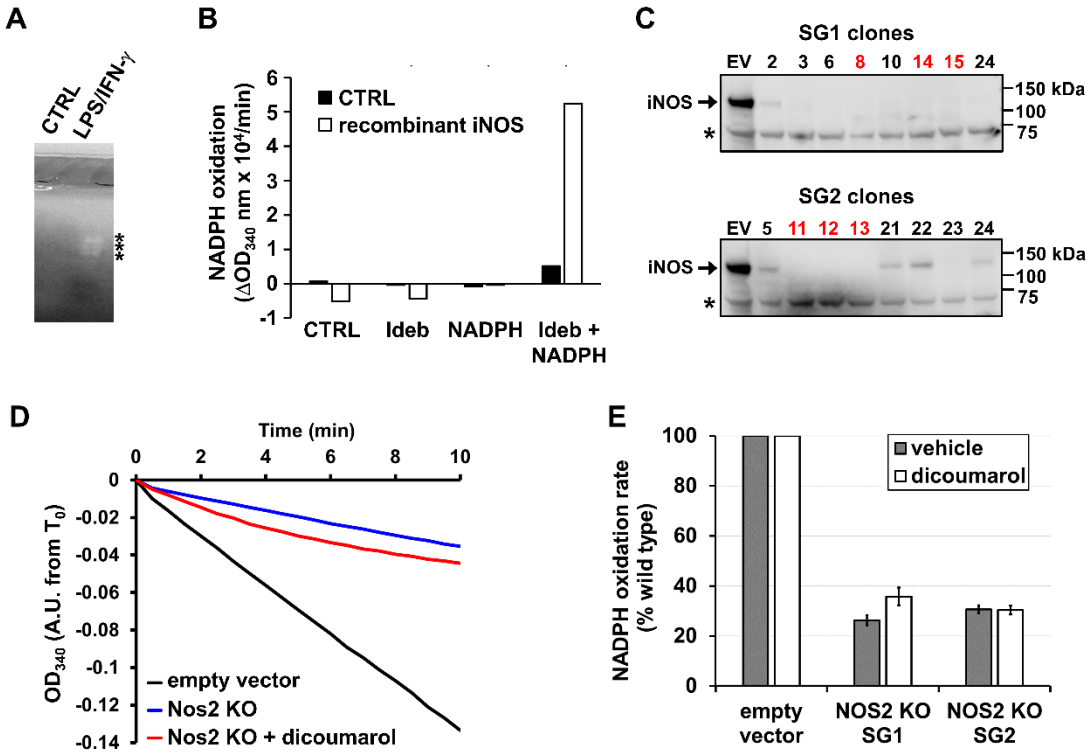


Figure 4.2 Idebenone is reduced by recombinant iNOS and *NOS2* gene deletion attenuates LPS/IFN- γ -induced microglial idebenone-reducing activity.

(A) In-gel activity assay of HAPI cell extract from LPS/IFN- γ -stimulated or non-treated control (CTRL) cells. Cell extract proteins were separated by polyacrylamide gel electrophoresis under non-denaturing conditions in the presence of the blue redox dye DCPIP (shown in grayscale). Idebenone and NADPH addition resulted in the appearance of three colorless bands (asterisks). (B) Idebenone-dependent NADPH oxidation by recombinant iNOS. Decrease in 340 nm absorbance (OD_{340}) was measured over 10 minutes in the presence or absence of 200 μM NADPH, 200 μM idebenone, and 1 U/ml of recombinant iNOS. (C) *NOS2* was eliminated by CRISPR-Cas9 gene editing using small guide RNA SG1 or SG2. Western blots demonstrating the absence of LPS/IFN- γ -induced iNOS expression in several single-cell clones derived from HAPI SG1 or SG2 knockout (KO) pools. The SG1 clones 8, 14, and 15 and the SG2 clones 11, 12, and 13 (red font) were

selected for the subsequent assays. iNOS was not detectable in wild-type HAPI empty vector (EV) cells in the absence of the 18-hour LPS/IFN- γ stimulation (data not shown). (**D**) Representative raw idebenone-dependent NADPH oxidation measurements (means of three technical replicates) by cell extracts, as monitored by decrease in absorbance at 340 nm [OD₃₄₀, shown in arbitrary units (A.U.) from time 0 (T₀)]. Cell extracts were from empty vector (EV) HAPI cells or from *NOS2* KO SG2 clone 13, incubated in the absence and presence of dicoumarol (20 μ M). All cells were treated with LPS (10 ng/ml) and IFN- γ (10 ng/ml) for 18 hours prior to harvest. (**E**) Idebenone-dependent NADPH oxidation rates by *NOS2* KO SG1 or SG2 cell extract, expressed as a percentage of EV wild type control. Data are mean \pm SEM from the 3 different SG1 or SG2 *NOS2* KO clones selected in *C* (highlighted in red), run in triplicate, with empty vector controls run in parallel.

Among these enzymes, inducible nitric oxide synthase (iNOS) encoded by the *Nos2* gene is well-established to be an LPS/IFN- γ -inducible enzyme. In addition, an iNOS-idebenone interaction is predicted by molecular modeling [167]. We therefore tested the hypothesis that iNOS is responsible for the distinct microglial idebenone-reducing activity that appears after LPS/IFN- γ stimulation.

4.4.3 Evidence that iNOS mediates LPS/IFN- γ -induced microglial idebenone-reducing activity.

We tested whether iNOS can directly reduce idebenone by incubating recombinant iNOS with idebenone in the presence of NADPH. Consistent with the hypothesis that iNOS can directly reduce idebenone to idebenol, we observed an idebenone-dependent reduction in NADPH absorbance when all three components were present, but no change in absorbance when the enzyme was incubated with idebenone or NADPH alone (Figure 4.2B).

Next, we sought to determine the extent to which iNOS is responsible for the idebenone-reducing activity of pro-inflammatory cells by eliminating the enzyme via CRISPR-Cas9-mediated genetic deletion. CRISPR-Cas9 HAPI *Nos2* knockout (KO) cells were created using two distinct small guide RNAs, SG1 and SG2. Several single-cell complete KO clones from each KO pool were isolated and validated by immunoblot (Figure 4.2C), functional assay (Figure 4.3), and next generation sequencing. *Nos2* KO abolished ~70% of LPS/IFN- γ -stimulated idebenone-reducing activity (Figure 4.2 D and E). The residual activity in *Nos2* SG1 and SG2 KO clones was dicoumarol-insensitive, suggesting that LPS/IFN- γ -stimulated HAPI microglial cells express one or more enzymes other than iNOS and NQO1 with modest idebenone-reducing capability.

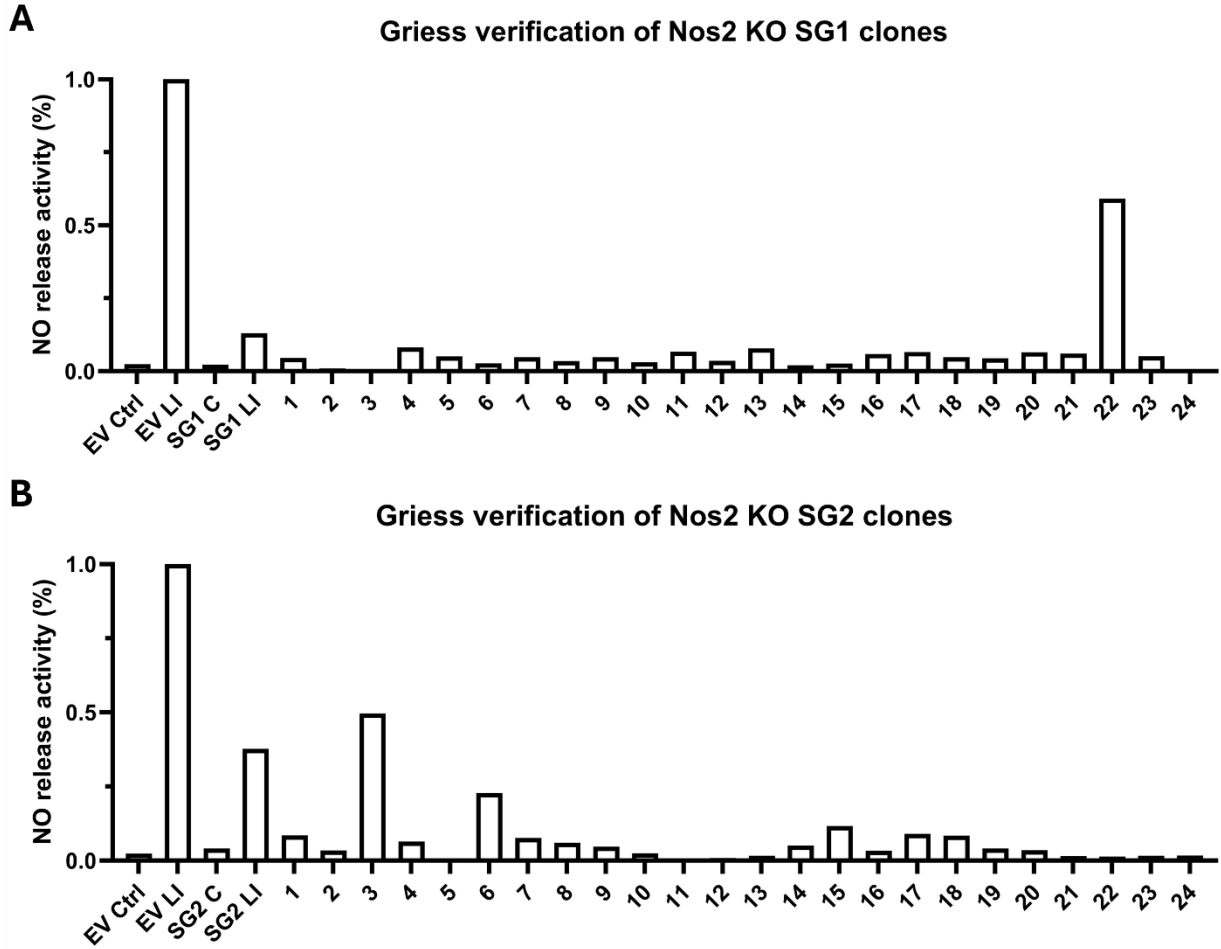


Figure 4.3 Functional verification of NO release in Nos2 KO clones by Griess assay.

(A) NO release activity percentage of Nos2 KO cells constructed with SG1 guide RNA. SG1 C, Non-activated control of SG1 pool; SG1 LI, LPS/IFN- γ -activated SG1 pool. 1-24, individual clones. (B) NO release activity percentage of Nos2 KO cells constructed with SG2 guide RNA. SG2 C, Non-activated control of SG2 pool; SG2 LI, LPS/IFN- γ -activated SG2 pool. 1-24, individual clones. All data are mean of two technical replications.

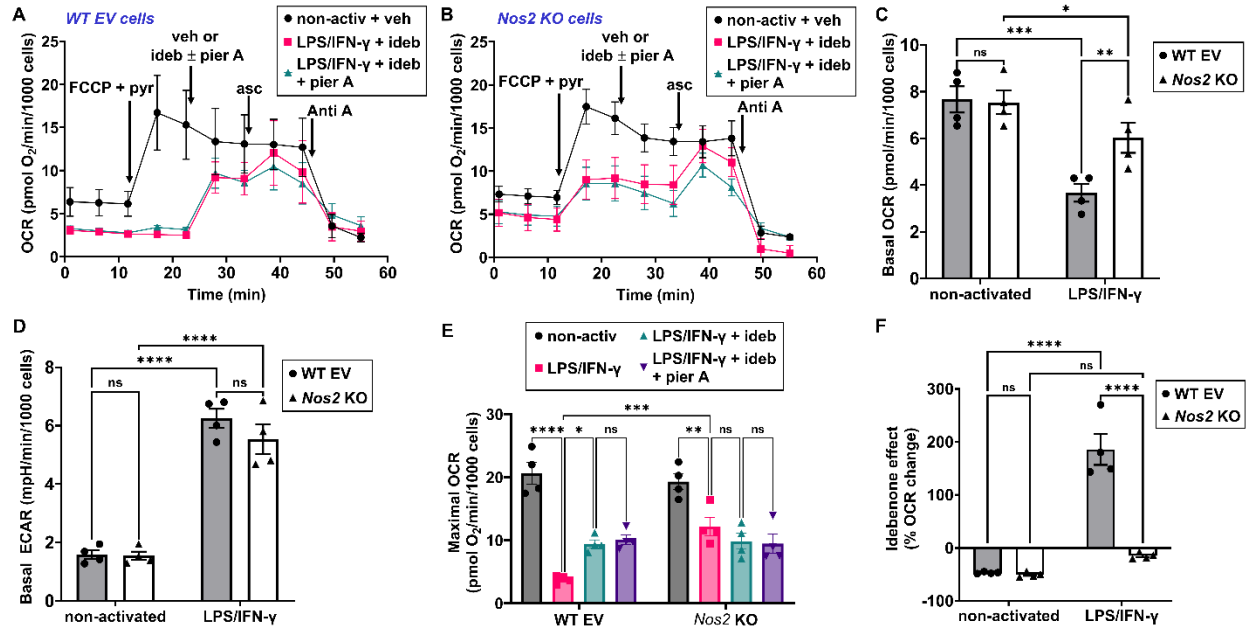


Figure 4.4 *Nos2* gene deletion diminishes the ability of idebenone to restore Complex I-impaired oxygen consumption in pro-inflammatory microglia.

(A-B) Representative oxygen consumption rate (OCR) measurements from wild-type (WT) empty vector control (A) or *Nos2* KO SG2 clone 13 (B) HAPI cells that were pre-treated with LPS (10 ng/ml) and IFN- γ (10 ng/ml) for 9 hours and then sequentially exposed to FCCCP (4 μ M) plus pyruvate (10 mM), vehicle or idebenone (40 μ M) \pm piericidin A (1 μ M), ascorbate (10 mM), and antimycin A (1 μ M) as indicated (arrows). (C-D) Quantification of basal OCR (C) and basal ECAR (D) in LPS/IFN- γ -activated and non-activated wild type and *Nos2* KO cells. n=4, mean \pm SEM, two-way ANOVA with repeated measures and Šidák's *post hoc* comparison. *p<0.05, **p<0.01, ***p<0.001, ****p<0.0001. (E) Quantification and comparison of idebenone-induced maximal OCR. n=4, mean \pm SEM, one-way ANOVA with Dunett's multiple comparison. *p<0.05, **p<0.01, ***p<0.001, ****p<0.0001. (F) Percentage OCR changes of idebenone-stimulated OCR. n=4, mean \pm SEM, one-way ANOVA with Dunett's multiple comparison. ****p<0.0001.

4.4.4. *iNOS-dependent rescue of LPS/IFN- γ -mediated respiratory suppression by idebenone in pro-inflammatory microglial cells*

Measurement of idebenone-initiated NADPH oxidation rate does not distinguish between two-electron reduction to idebenol, which can act as a mitochondrial Complex III electron donor, and one-electron reduction to a semiquinone, which can generate superoxide. Therefore, we sought to evaluate the effects of idebenone on microglial respiration. LPS/IFN- γ -induced pro-inflammatory microglial activation causes suppression of mitochondrial respiration that is associated with iNOS induction [158, 168]. We hypothesized that idebenone would rescue LPS/IFN- γ -induced mitochondrial respiratory impairment by iNOS-dependent transfer of electrons to Complex III.

First, it was necessary to determine how the absence of iNOS affects the activation-associated respiratory suppression phenotype. HAPI wild-type (WT) empty vector (EV) control cells and *Nos2* KO cells were treated with LPS/IFN- γ for 12 hours to induce the expression of iNOS in cells with the WT gene, and then the oxygen consumption rate (OCR) of each cell line was measured and compared with the non-activated control condition. Non-activated WT EV and *Nos2* KO cells displayed a comparable basal OCR (Figure 4.4 A-C). Each cell type exhibited a decreased OCR (Figure 4.4 A-C) and an increased glycolysis-associated extracellular acidification rate (ECAR; (Figure 4.4D)) after 12 hours of LPS/IFN- γ stimulation. However, the OCR in LPS/IFN- γ -treated cells was significantly preserved in *Nos2* KO cells compared with the activated WT EV control (Figure 4.4C). LPS/IFN- γ also significantly decreased the mitochondrial respiratory capacity, defined as the OCR measured in the presence of the uncoupler FCCP plus excess substrate, in both cell types, although *Nos2* KO mitigated the extent of respiratory capacity loss (Figure 4.4E). These findings resemble the ability of *Nos2* KO to partially inhibit the

metabolic shift from oxidative phosphorylation to glycolysis in LPS/IFN- γ -stimulated macrophages [169-171].

Next, we evaluated the ability of idebenone to restore LPS/IFN- γ -impaired respiratory capacity in each cell type. The addition of idebenone after FCCP stimulated OCR in WT EV cells, partially rescuing the LPS/IFN- γ -induced respiratory capacity loss (Figure 4.4 *A, E, F*). Idebenone-stimulated OCR was insensitive to the Complex I inhibitor piericidin A but was inhibited by the Complex III inhibitor antimycin A, consistent with the ability of idebenol to bypass Complex I inhibition by transfer of electrons to Complex III. In contrast to the results in WT EV cells, idebenone failed to stimulate OCR in *Nos2* KO cells (Figure 4.4 *B, E, F*). One explanation for idebenone's inability to rescue respiration in *Nos2* KO cells is that there is insufficient production of bioactive idebenol in the absence of iNOS-catalyzed idebenone reduction. However, an alternative explanation is that the idebenone-sensitive portion of respiratory capacity loss was already rescued by *Nos2* ablation, while the remaining respiratory impairment occurs downstream of Complex III, thereby showing idebenone insensitivity. If the first explanation is correct and inadequate idebenone reduction explains the failure of *Nos2* KO cells to increase OCR in response to its addition, then we predicted that ascorbate would stimulate respiration in *Nos2* KO cells by chemically reducing idebenone. The Seahorse Wave software (Agilent) showed increased OCR in both WT EV and *Nos2* KO cells when ascorbate was added after idebenone (Figure 4.4 *A* and *B*). However, we found that the reaction of idebenone with ascorbate led to chemical oxygen consumption that completely depleted oxygen in the media, resulting in unreliable OCR readings (Figure 4.5). Therefore, a different experiment to distinguish between the two alternative hypotheses to explain idebenone's lack of OCR stimulation in *Nos2* KO cells was needed.

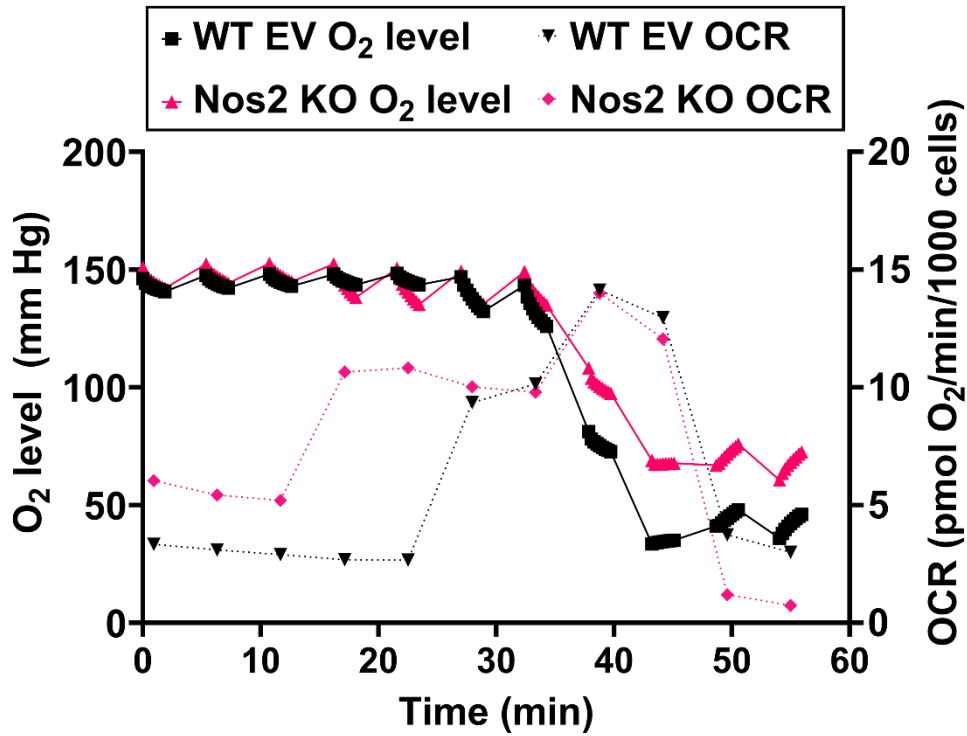


Figure 4.5 Chemical oxygen consumption caused by the addition of ascorbate contributes to unreliable OCR.

Left y-axis: oxygen level. Solid lines show real-time oxygen level with a dramatic drop after adding ascorbate. Right y-axis: OCR. Dashed lines showed the OCR of corresponding representative wells.

The protection of LPS/IFN- γ -induced respiratory inhibition afforded by *Nos2* KO hindered our ability to quantitatively compare idebenone's ability to stimulate OCR in the two cell lines. To directly evaluate the ability of idebenone in each cell line to bypass Complex I by feeding electrons to Complex III, we first added the Complex I inhibitor piericidin A. Piericidin A inhibited OCR to the same low level in EV control and KO cells (Figure 4.6 A). Idebenone stimulated respiration to a significantly greater extent in EV control cells compared with the *Nos2* KO cells using two different KO cell clones (Figure 4.6 A and B). Idebenone's stimulation of OCR was Complex III-dependent, as determined by the subsequent addition of the Complex III inhibitor antimycin A (Figure 4.6A).

To exclude the possibility that the reduced OCR stimulation in *Nos2* KO cells was due to lower Complex IV capacity, the exogenous Complex IV electron donor TMPD in combination with the reducing agent ascorbate was added in place of idebenone. TMPD feeds electrons to cytochrome *c* downstream of Complex III, which are subsequently passed to Complex IV. TMPD stimulated OCR to the same level in EV control cell and *Nos2* KO cells (Figure 4.6C), suggesting that the impaired idebenone response in *Nos2* KO cells is not due to diminished Complex IV capacity. This result is consistent with the hypothesis that *Nos2* KO are deficient in the utilization of idebenone as a Complex III substrate.

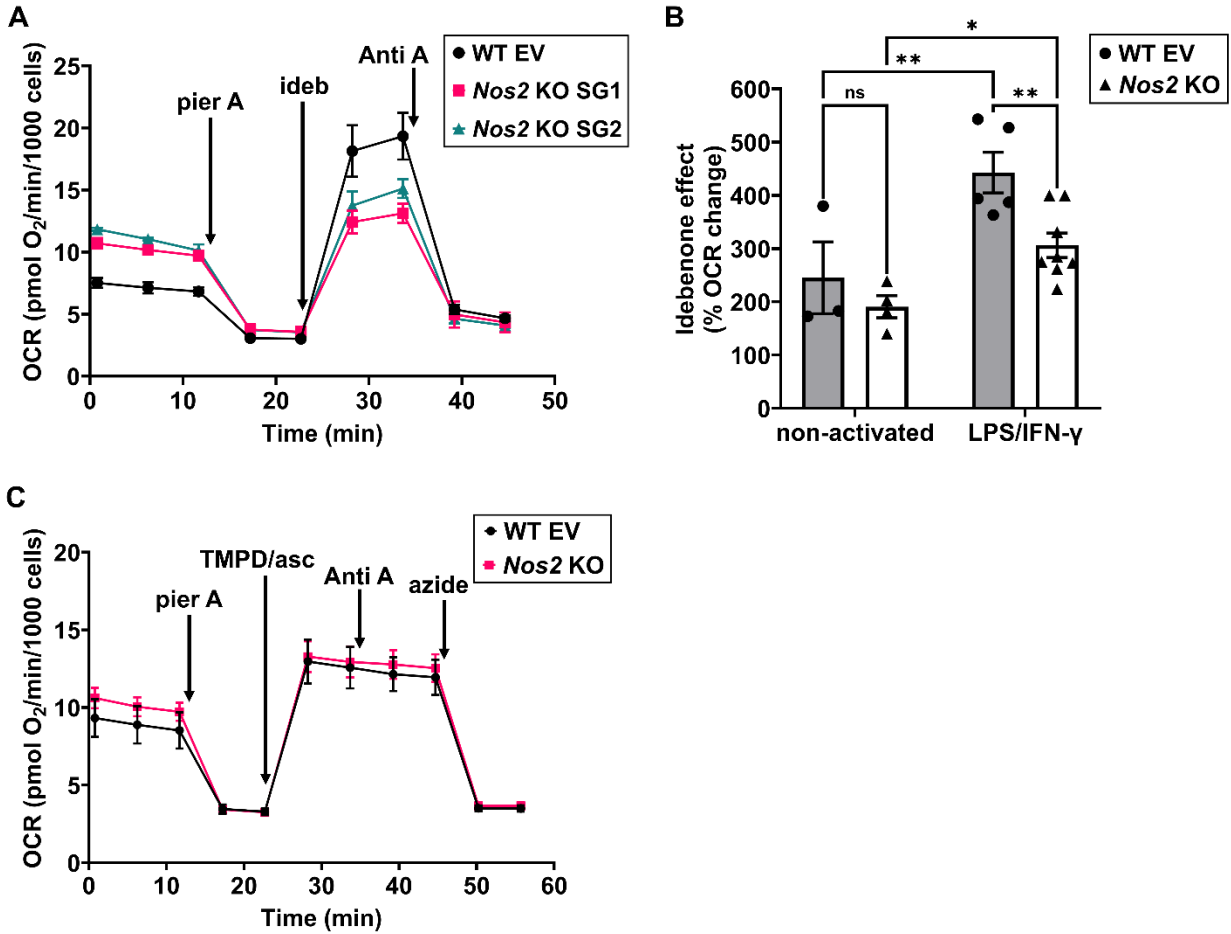


Figure 4.6 Nos2 depletion impaired idebenone-stimulated OCR.

WT EV, wild type empty vector. (A) Idebenone-stimulated, Complex I-independent, Complex III-dependent OCR decreases in both *Nos2* KO lines generated with different guide RNA. The representative traces are mean \pm SD from 6 technical replicates and the data are representative of 3-5 independent experiments (WT EV, n=5, *Nos2* KO SG1, n=3, *Nos2* KO SG2, n=5). (B) Quantification of idebenone-stimulated OCR. The results of the two *Nos2* KO clones were combined. Two-way ANOVA, multiple comparisons with uncorrected Fisher's LSD. Non-activated, n=3-4. LPS/IFN- γ -activated, n=5-8. * p<0.05, ** p<0.01, ns, not significant. (C) OCR traces showing that the impaired idebenone-stimulated, Complex I-independent, Complex III-dependent OCR did not result from a difference in Complex IV-dependent respiration. Trace data are mean \pm SD and are representative of 3-5 independent experiments (WT EV, n=3, *Nos2* KO, n=5).

To show that iNOS is not only required for idebenone to maximally stimulate respiration but is also sufficient to promote idebenone-supported mitochondrial respiration, we added recombinant iNOS, NADPH substrate, and idebenone to permeabilized *Nos2* KO cells that were either non-activated (Figure 4.7 *A* and *C*) or pre-stimulated with LPS/IFN- γ (Figure 4.7 *B* and *D*). Results showed that iNOS, like the known idebenone-reducing enzyme NQO1, supported idebenone-mediated Complex III-dependent respiration in the presence of the Complex I inhibitor piericidin A in both non-activated and LPS/IFN- γ cells.

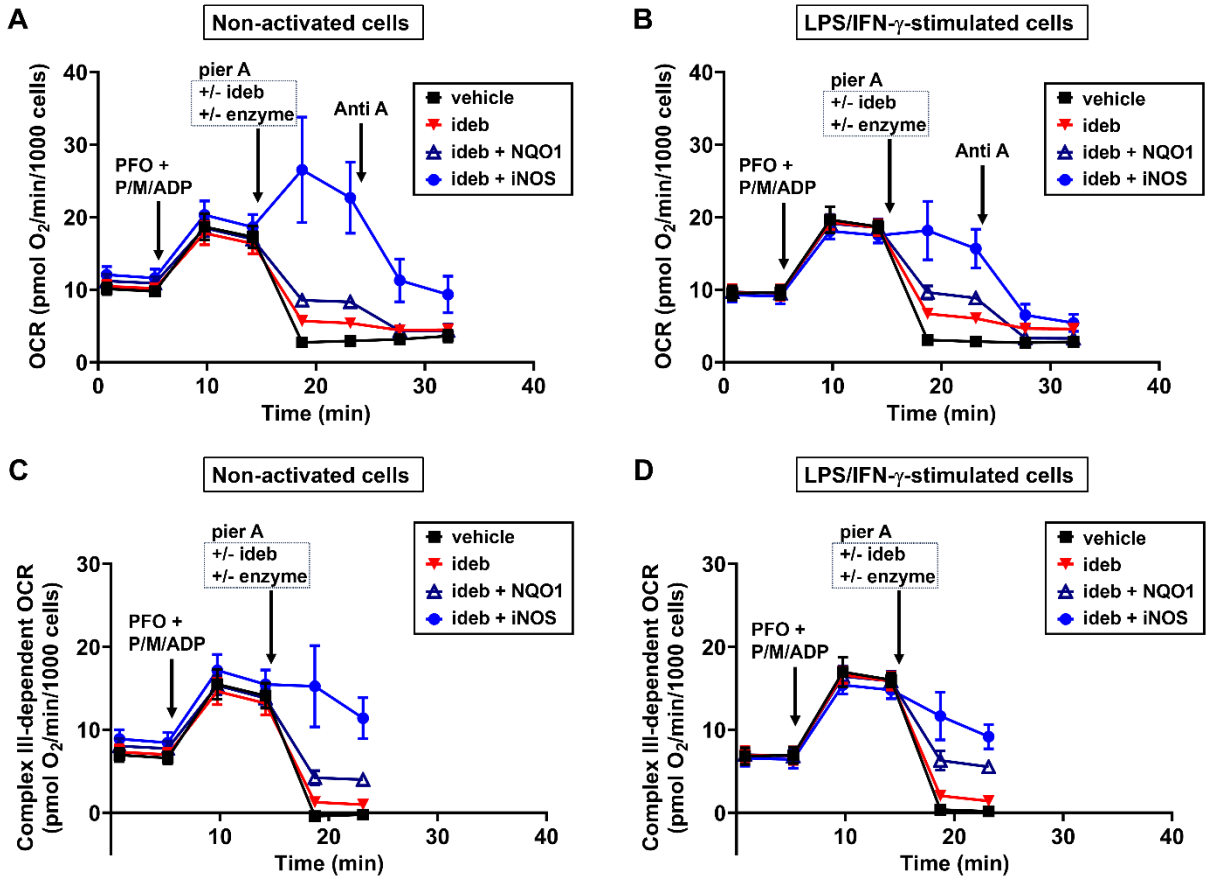


Figure 4.7 Recombinant iNOS enables idebenone-mediated bypass of Complex I inhibition in *Nos2* knockout cells.

(*A* and *B*) Oxygen consumption rate (OCR) measurements from *Nos2* KO SG2 clone 13 cells that were either not activated (*A*) or pre-treated with LPS (10 ng/ml) and IFN- γ (10 ng/ml) for 9-11 hours (*B*). Complex I-linked respiration was stimulated at the first arrow by permeabilizing the cells with perfringolysin O (PFO, 0.5 nM) in the presence of pyruvate (P, 5 mM), malate (M, 5, mM), and ADP (1 mM), and then the Complex I inhibitor piericidin A was added \pm idebenone with or without the indicated enzymes (second arrow). Antimycin A (Anti A) was added at the third arrow to inhibit Complex III. (*C*) Complex III-dependent OCR measurements from the non-activated cells shown in *A*. The mean of the Anti A-insensitive OCR in the vehicle control group was subtracted from the first four measurements while the Anti-A-insensitive OCR of the individual group was subtracted from the last two measurements. (*D*) Complex III-dependent OCR measurements from the LPS/IFN- γ -activated cells shown in *B*, determined using the same

calculation method as in *C*. The traces in *A-D* are mean \pm SD of 3-8 individual wells per group and are representative of three independent experiments.

Collectively, these results support the hypothesis that a two-electron reduction of idebenone by iNOS promotes transfer of electrons to Complex III in LPS/IFN- γ -stimulated microglia, bypassing Complex I inhibition. However, because respiratory stimulation by idebenone was only diminished but not abolished in *Nos2* KO cells, the results indicate the presence of additional, unidentified enzymes catalyzing the conversion of idebenone to idebenol in activated microglia.

4.5 Discussion

Complex I-independent but Complex III-dependent respiration stimulation is seen in rat primary cortical astrocytes [47]. We observed an idebenone-associated respiration rescue that is also insensitive to Complex I inhibitor piericidin A but sensitive to Complex III inhibitor antimycin A in LPS/IFN- γ -activated microglial cells, as evidence of idebenone being an electron donor to rescue impaired respiration, via Complex III, but bypassing the impaired Complex I. Like ubiquinone, the two-electron reduction of idebenone to idebenol is required prior to function as an electron donor. The reduction of idebenone is catalyzed by NQO1 in rat cortical astrocytes and NQO1 inhibitor dicoumarol abolishes the respiratory rescue. Due to the poor expression of NQO1 in rat cortical neurons, idebenone exhibits a dose-dependent respiratory inhibition, presumably by the production of reactive semi-quinone due to insufficient reduction of idebenone, while recombinant NQO1 reverses the inhibition of idebenone. The observation of idebenone-stimulated respiration in activated microglial cells suggests alternative enzymes are involved in catalyzing the two-electron reduction of idebenone. Neuronal NOS is one of several enzymes that through enzymatic quinone reduction, participates in the bioactivation of the chemotherapeutic drug mitomycin C to an alkylating agent [172]. Through the usage of a redox indicator *in situ*, we

identified iNOS as one of the induced enzymes that catalyzes the reduction of idebenone, in activated HAPI microglial cells.

The NADPH-oxidation method we used to identify the reduction of idebenone is highly comparative to the classical NADPH diaphorase histochemistry methods which detects the NO-producing neurons as a popular diagnostic and pathological criteria in many preclinical biochemistry studies in late 20th century. The dicoumarol-insensitive neuronal NADPH diaphorase was characterized in rat striatum as an alternative enzyme from DT-diaphorase (NQO1) in 1989 [173] and later in 1991, it was further characterized as a NOS enzyme [174]. Quinone-structured staining reagent LY883583 was later used to detect NQO enzymes in the brain [175]. Quinone is known to inhibit nNOS activity of NO synthesis by competitively inhibiting NADPH and non-competitively inhibiting L-arginine[176]. All these studies using quinone substrates to detect quinone-reducing enzymes in reverse suggest NQO1 and NOS enzymes reduce quinone.

Nitric oxide can directly react with ubiquinol [177], suggesting that it can also react with its short-chain analogue idebenol. The [NADPH] reduction rate observed in the presence of recombinant iNOS, NADPH, and idebenone is very likely independent of a direct idebenol-NO reaction, however, as iNOS is not expected to produce NO in the absence of its substrate, L-arginine. Furthermore, although L-arginine may be present in cell extracts, the iNOS inhibitor 1400W failed to suppress the idebenone-induced NADPH oxidation rate, suggesting that iNOS can catalyze idebenone reduction by a mechanism that is independent of its ability to generate NO.

In this study, we identified iNOS as a major contributor for idebenone reduction in pro-inflammatory microglia. However, the residual one quarter of NADPH oxidization activity in Nos2 KO HAPI cells, regardless of the presence of dicoumarol (Figure 4.2D), suggested the existence of additional enzymes, other than iNOS and NQO1, catalyzing the cytoplasmic reduction

of idebenone. Enzymes other than NQO1, including succinate dehydrogenase[178] and glycerol 3-phosphate dehydrogenase, were reported to catalyze idebenone reduction.

Finally, the therapeutic potential of idebenone for its capability of restoring mitochondrial respiration enhances the importance of our work. Pharmacologically inhibiting NO production restores mitochondrial respiration and thus improves the repolarization of M1(pro-inflammatory) macrophages to M2 (anti-inflammatory) macrophages[171]. Idebenone could be a strategy to repolarize microglia from pro-inflammatory activation via improving mitochondrial respiratory impairments.

4.6 Materials and Methods

4.6.1 Materials

All reagents were purchased from Sigma-Aldrich (St. Louis, MO) unless otherwise indicated.

4.6.2 Preparation and maintenance of cell cultures

All procedures were approved by the University of Maryland Institutional Animal Care and Use Committee and were compliant with the NIH Guide for the Care and Use of Laboratory Animals. Primary rat cortical astrocytes and microglia were prepared from postnatal day 1 Sprague Dawley rat pups as described [179, 180]. The purity of the astrocyte and microglia cultures produced by these methods are $\geq 93\%$ [180, 181] and $\geq 90\%$ [179], respectively. Primary rat cortical neurons were prepared from Sprague Dawley rat embryos on embryonic day 18 as previously described [99, 100, 107]. To enrich for neurons, cytosine β -d-arabinofuranoside, which inhibits glial proliferation, was added after 4 days *in vitro* (DIV). Neurons exhibit less than 5% glial

contamination when prepared by this method [107]. Microglia, astrocytes, and neurons were cultured for at least 7, 18, or 11 DIV, respectively, prior to experiments. The cultured medium for microglia was Dulbecco's Modified Eagle's Medium (DMEM)/F12 supplemented with penicillin (100 IU/ml) plus streptomycin (100 µg/ml) solution (Gemini Bio-Products, Broderick, CA) and 10% FBS. Astrocytes were cultured in Eagle's Minimal Essential Medium (EMEM, Quality Biological, Gaithersburg, MD) containing 10% FBS, 1% non-essential amino acids (NEAA, Lonza, Walkerville, MD), and 50 µg/ml gentamicin. Neurons were cultured in Neurobasal Medium (Thermo Fisher, Waltham, MA) supplemented with 1x Gem21 (Gemini Bio-Products), 1x Glutamax (Thermo Fisher), and penicillin (100 IU/ml) plus streptomycin (100 µg/ml). For all three primary cell culture preparations, the dissociated cells were pooled from one litter of animals that included both males and females.

HAPI mouse microglial cells (RRID: CVCL_0F62) were generously provided by James Connor (Penn State University). Although originally misidentified as rat rather than mouse cells ([57], https://web.expasy.org/cellosaurus/CVCL_0F62), proteomic characterization [182] and functional studies over nearly two decades, e.g. [57, 183, 184], have validated them as a microglial cell model. The cells were cultured in DMEM containing 10% FBS and penicillin (100 IU/ml) plus streptomycin (100 µg/ml). All cells were maintained at 37°C in a humidified atmosphere consisting of 95% air and 5% CO₂.

4.6.3 CRISPR/Cas9 generation of HAPI NOS2 knockout cells

Two different guide RNAs delivered by lentivirus were used to create NOS2 knockout (KO) HAPI cell pools SG1 and SG2 by CRISPR/Cas9 gene editing. NOS2 KO single cell clones

were isolated from each pool and then validated by measurement of nitric oxide release, immunoblot, and next-generation sequencing.

4.6.4 Pro-inflammatory activation of microglia

Primary rat or HAPI microglia were treated with a combination of 5, 10, or 100 ng/mL lipopolysaccharide (LPS; Sigma-Aldrich, cat# L2654), as indicated, and 10 ng/mL recombinant interferon- γ (IFN- γ ; R&D Systems, Minneapolis, MN, cat# 485-MI-100) for 18 hours to induce a pro-inflammatory state.

4.6.5 Microplate-based Idebenone Reduction Assay

Idebenone-reducing activity was evaluated indirectly by measuring the idebenone-dependent oxidation of NADPH in fresh cell extracts, with or without concentration by molecular weight cut-off (MWCO) filter or following addition of recombinant mouse iNOS enzyme (Sigma-Aldrich). Cells were washed twice with PBS and then scraped into a 25 mM Tris-HCl pH 7.4 hypotonic lysis solution containing 1:200 protease inhibitor cocktail (Sigma-Aldrich). Cell extracts were sonicated twice for 15 seconds on ice, then centrifuged at 17,000g for 20 minutes at 4°C. When indicated, supernatants were concentrated by centrifuging again at 14,000g for 20 minutes at 4°C using 50 kilodalton (kDa) MWCO Amicon Ultra-0.5 Centrifugal Filter Units (Sigma-Aldrich). MWCO concentration increased assay sensitivity, facilitating its use for primary cells difficult to obtain in high abundance, without altering the relative results. The sample fraction retained by the 50 kDa cut-off filter was collected for the assay and protein concentration was estimated using a Nanodrop 1000 (Thermo Fisher Scientific) or by the Pierce micro bicinchoninic acid (BCA) assay [185]. Idebenone-dependent oxidation of NADPH was detected by measuring

NADPH absorbance at 340 nm over a 10-20 min time course in the presence or absence of 0.2 $\mu\text{g}/\mu\text{l}$ sample protein, 200 μM NADPH, and 200 μM idebenone. Enzyme inhibitors (e.g. dicoumarol) or vehicle control were also added when indicated. Assays were run in 96-well microplates using either a Varioskan Lux (Thermo Fisher Scientific) or FLUOstar OPTIMA (BMG LABTECH, Inc., Cary, NC) multimodal plate reader.

4.6.6 Fractionation of HAPI cell extract by size exclusion and NAP(D)H affinity chromatography

4.6.7 In-gel activity assays for detection and isolation of idebenone-reducing enzymes

MWCO-concentrated cell extracts of HAPI microglia cells were collected as described above after treatment with 100 ng/mL LPS and 10 ng/mL IFN- γ for 18 hours. Precast Tris-Glycine WedgeWell gels (Invitrogen) were used for this assay. As for native polyacrylamide gel electrophoresis (PAGE), the anode buffer was composed of a 1x solution of Novex Tris-Glycine Native Running Buffer. The cathode buffer was made from running buffer with the addition of 100 μM of the redox dye 2,6-dichloroindophenol (DCPIP). A 2x loading buffer was made using 1 mM DCPIP and 10% glycerol in running buffer. Wells were loaded to maximum capacity with ~ 300 μg protein in 1x loading buffer. Gels were run at 100 V for 150 minutes at 4°C. Gels were then removed from their cassette and washed briefly in 25 mM Tris-HCl. Gels were then incubated in 15 ml of 25 mM Tris-HCl, 200 μM NADPH, 200 μM idebenone, and 100 μM DCPIP for 5-10 minutes. Pictures of gels were taken using an iPhone 6 (Apple). Images were converted to grayscale for clarity. Enzyme activity is indicated by the absence of color after enzymatic reduction of the dye.

4.6.8 Identification of proteins by mass spectrometry

Gel bands showing DCPIP turnover were excised from the native PAGE and cut into 1 × 1 mm pieces. The gel pieces were destained in 50 % acetonitrile with 50 mM ammonium bicarbonate. Proteins in the gel pieces were reduced by 50 mM Tris(2-carboxyethyl) phosphine and alkylated by 100 mM iodoacetamide in the dark. The gel pieces were shrunk by neat acetonitrile and air dried. Proteins were digested and extracted by incubating the gel pieces with sequencing grade trypsin in 50 mM ammonium bicarbonate overnight. Tryptic peptides from the supernatant were separated on a nanoACQUITY UPLC analytical column (BEH130 C18, 1.7 μm, 75 μm x 200 mm, Waters) over a 165-minute linear acetonitrile gradient (3 – 40 %) with 0.1 % formic acid on a Waters nano-ACQUITY UPLC system and analyzed on a coupled Thermo Scientific Orbitrap Fusion Lumos Tribrid mass spectrometer as described by Williamson *et al.* [186]. Full scans were acquired at a resolution of 120,000, and precursors were selected for fragmentation by collision-induced dissociation (normalized collision energy at 35%) for a maximum 3-second cycle. Tandem mass spectra were searched against a UniProt *Rattus norvegicus* reference proteome using Sequest HT algorithm described by Eng *et al.* [187] with a maximum precursor mass error tolerance of 10 ppm. Carbamidomethylation of cysteine and deamidation of asparagine and glutamine were treated as static and dynamic modifications, respectively. Resulting hits were validated at a maximum false discovery rate of 0.01 using a semi-supervised machine learning algorithm Percolator developed by Käll *et al.* [188].

4.6.9 Griess Assay

Nitric oxide concentration was estimated indirectly by detecting the more stable nitric oxide derivative nitrite using a Griess assay (Thermo Fisher) according to the manufacturer's

protocol. Absorbance was measured at 560 nm and a standard curve of sodium nitrite was used to calculate concentrations.

4.6.10 Cell-based respirometry

Oxygen consumption rate (OCR) measurements were performed using a Seahorse XF24 Extracellular Flux Analyzer (Agilent Technologies, Santa Clara, CA) as previously described [189, 190]. HAPI cells were plated in XFe96 or XF24 plates (Agilent Technologies) at 8,000 or 12,000 cells per well, respectively, and cultured for ~24 hours before stimulation. Cells were either untreated or activated for 9-12 hours by LPS (10 ng/ml) plus IFN- γ (10 ng/ml) and then respiration was measured. Artificial cerebrospinal fluid (aCSF) assay medium for respiration measurements consisted of 1.3 mM CaCl₂, 0.4 mM KH₂PO₄, 1 mM MgCl₂, 120 mM NaCl, 3.5 mM KCl, 5 mM 4-(2-hydroxyethyl)-1-piperazineethanesulfonic acid (HEPES), and 15 mM glucose, pH 7.4. Fatty acid-free bovine serum albumin (0.1 mg/mL) was included in the injection port media for the permeabilized cell experiments in which recombinant enzymes were injected. Cell counts were obtained prior to oxygen consumption measurements using either a Celigo™ image cytometer (Revvity; Waltham, MA) or an ImageXpress™ Pico Automated Cell Imaging System (Molecular Devices; San Jose, CA).

4.6.11 Statistical analysis

Statistical analyses were performed using SigmaPlot 12.0 (Systat Software Inc, San Jose, CA). Two-way analysis of variance (ANOVA) was employed to evaluate statistical significance. A p value < 0.05 was considered significant. Tukey's post-hoc analysis was used to compare individual groups.

Chapter 5

Inhibition of Nitric Oxide (NO) Production Prevents the Loss of a Subset of Mitochondrial Electron Transport Chain Subunits During Pro-inflammatory Microglial Activation

5.1 Introduction

Microglia are the intrinsic innate immune cells of the central nervous system (CNS). Under physiological conditions, microglia patrol the CNS for local neuronal damage, cell death, and exogenous infections. In traumatic brain injury (TBI) and many neurodegenerative disorders such as Alzheimer's disease [191, 192] and Parkinson's disease [193], microglia-mediated persistent neuroinflammation is common and leads to progressive neuronal damage [54, 194]. During these pathological conditions, pattern recognition receptors (PRRs) residing on the surface of microglia, such as Toll-like receptors (TLRs), are activated by exogenous pathogens and endogenous ligands collectively referred to as damage-associated molecular patterns (DAMPs). Various DAMPs can induce the formation of the NLRP3 inflammasome [195] and transform the microglia into a pro-inflammatory state. Depending on the nature and extent of pro-inflammatory microglial activation, the microglia may become neurotoxic and promote neuronal death by releasing neuroinflammatory molecules such as nitric oxide (NO) [196, 197] and the pro-inflammatory cytokines TNF- α and IL-1 β [198].

Mitochondria are thought to contribute to the pro-inflammatory activation of microglia in multiple ways [55]. These include bioenergetic alterations and reactive oxygen species (ROS) production. ROS mediate separate interactions of NLRP3 protein and caspase-1 with the mitochondrial outer membrane (MOM), regulating NLRP3 inflammasome assembly [69]. Pharmacological inhibition of reverse electron transport (RET) driven by ETC Complex I or genetic depletion of the Complex I subunit NDUFS4 attenuates neuroinflammation and improves

functional outcomes in experimental autoimmune encephalomyelitis (EAE), a mouse model of multiple sclerosis [199]. Mitochondrial ETC complexes also support NLRP3 inflammasome activation through ATP generation [200]. These findings suggest that individual ETC complexes may play unique roles in neuroinflammation.

NO is also a known inducer of neuroinflammatory signaling. In both pro-inflammatory mouse microglia and bone marrow-derived macrophages—peripheral innate immune cells sharing some of the same signaling pathways—NO is generated by inducible nitric oxide synthase (iNOS). Recent studies showed that suppression of ETC complex activities and accompanying ETC protein loss in LPS/IFN- γ activated bone marrow-derived macrophages were induced by NO accumulation [86, 201]. In these studies, ETC subunits NDUFS1 and NDUF8 (Complex I), SDHB (Complex II), and MTCO1 (Complex IV) were protected in LPS/IFN- γ activated *Nos2* knockout (KO) macrophages compared to wild-type (WT) cells [86, 201]. Mitochondrial ETC deficits also occur in microglia following LPS/IFN- γ stimulation [85, 158, 202, 203], but whether these coincide with ETC subunit loss and exhibit NO-dependency are unknown. However, supporting this possibility, in experiments described in Chapter 4 we observed partial protection of maximal (uncoupled) mitochondrial respiration in LPS/IFN- γ -activated *Nos2* KO HAPI cells compared to the empty vector (EV) controls (see Figure 4.3B). Understanding the mechanisms of how ETC complex subunits are degraded in pro-inflammatory microglia is critical to prevent or reverse the loss of mitochondrial respiratory function, which may also suppress microglial pro-inflammatory activation phenotypes. Therefore, important goals are to identify the mechanisms underlying the ETC deficits in pro-inflammatory microglia and to identify therapeutic strategies for preserving mitochondrial bioenergetic function. The strategies may include preventing the degradation of ETC complex subunits by one or more proteases.

Caspase proteases belong to the cysteine protease family, and they play important roles not only in apoptotic cell death, but also inflammation [204]. Self-cleaved mature caspase-1 (p20), as produced by the NLRP3-dependent inflammasome assembly, mediates the cleavage and maturation of IL-1 β [205]. While pro-caspase-1 mostly resides in the cytoplasm, it also translocates into the nucleus and becomes activated in a process regulated by tumor necrosis factor (TNF) [72]. In addition, as part of the NLRP3-dependent inflammasome assembled on a mitochondrial membrane platform, caspase-1 is detected in mitochondria [69, 74, 206]. However, mitochondrial substrates of caspase-1 have yet to be described. Based on the mitochondrial localization during NLRP3 inflammasome assembly of this established LPS/IFN- γ -activated protease and our findings of mitochondrial functional protection in *Nos2* KO HAPI cells, we hypothesized that caspase-1 cleaves ETC subunits in LPS/IFN- γ -stimulated microglial cells downstream of iNOS-mediated NO production.

To test this hypothesis, several pharmacological approaches were employed, along with the genetic ablation of iNOS. We used 1400W, an iNOS-selective NO production inhibitor that does not affect the iNOS protein level [207], to complement the *Nos2* KO genetic approach. The caspase-1/-11 inhibitor VX-765 and the pan-caspase inhibitor Q-VD-OPh were employed to determine if caspase activities are required for the degradation of any of the investigated representative ETC complex subunits. Additionally, we tested MCC950, an NLRP3 protein inhibitor that is predicted to prevent LPS/IFN- γ -induced caspase-1 activation by blocking NLRP3 inflammasome assembly and ATP hydrolysis [70]. Finally, because LPS may directly bind and activate caspase-11 independently of TLR4 and/or NLRP3 signaling [208], we also tested TAK-242, an inhibitor of LPS-induced TLR4 activation [209-211]. Overall, results indicate that subunits of Complex I, II, and IV are diminished during LPS/IFN- γ -induced microglial activation. Contrary

to our hypothesis, only a subset of these ETC subunit losses—that of the Complex II subunit SDHB and the Complex IV subunit MTCO1—are NO-dependent and caspase proteases activities are not required. However, we identified a novel positive feedback loop between iNOS protein expression and caspase-1 activation that may amplify the neuroinflammatory cascade.

5.2 Materials and Methods

5.2.1 Cell culture, pro-inflammatory activation, and sample collection

The HAPI (highly aggressively proliferative immortalized) mouse microglial cell line was generously provided by Dr. James Connor (Penn State University). Cells were maintained in Dulbecco's Modified Eagle's Medium (Corning catalogue number (Cat#) 10-017-CV, Corning, NY) containing 10% fetal bovine serum (FBS) and 1x penicillin-streptomycin (both from Thermo Fisher Scientific; Waltham, MA) in a 5% CO₂ humidified incubator at 37°C. Cells were passaged at a 1:20 dilution in T75 culture flasks when they reached 90% confluency, which was typically every two days. Cells were seeded onto 6-well plates at 0.2×10^6 per well, followed by a 24-hour recovery prior to pro-inflammatory activation. Cells were then activated by the addition of 10 ng/mL lipopolysaccharide (LPS) and 10 ng/mL interferon gamma (IFN- γ) in a full medium change. After 18 hours of treatment, 1 mL of conditioned medium was collected from each well into Eppendorf tubes, followed by microfuge centrifugation (Fisherbrand accuSpin Micro 17R; Thermo Fisher) at 17,000 $\times g$ for 20 minutes at 4°C to remove the cellular debris. Supernatants were transferred to new Eppendorf tubes for detection of nitrite by Griess assay. Residual medium was removed by suction and the cells were washed once with room temperature phosphate-buffered saline (PBS, Thermo Fisher). The cells were then thoroughly scraped and harvested after adding ice-cold radioimmunoprecipitation assay (RIPA) lysis buffer (Thermo Fisher) with freshly added

protease/phosphatase inhibitor cocktail (Thermo Fisher, Cat# 78430). Cell lysates were collected into Eppendorf tubes and centrifuged at 17,000×g for 20 minutes at 4°C to remove insoluble material. Supernatants were transferred to new tubes and stored at -80°C for later detection of proteins by western blot.

5.2.2 *Protein detection by western blot*

Cell samples were thawed on ice, and the protein concentrations were measured with the bicinchoninic acid (BCA) protein quantification assay (Thermo Fisher). Fifty µg of protein per sample were loaded onto NuPAGE™ Bis-Tris 4-12% gradient mini protein gels (Thermo Fisher) in a 20 µL per well volume that was prepared in protein sample loading buffer (LI-COR Biosciences; Lincoln, NE). Five µLs of 10-250 kDa pre-stained Odyssey Protein Molecular Weight Marker (LI-COR Cat# 928-40000) were added to one lane of each mini gel. Gel electrophoresis was run for 21 minutes at 200 volts and a Trans-Blot turbo semi-dry transfer station (Bio-rad Laboratories; Hercules, CA) was then used at 25V for 11 minutes to transfer proteins from gels to Immuno-Blot Low Fluorescence PVDF Membranes (Bio-Rad).

After protein, transfer, membranes were dried on filter paper in a 37°C non-CO₂ incubator for 15 minutes and then stained for total protein using a Revert 700 kit (LI-COR). Following destaining using Revert Destaining Solution (LI-COR), membranes were blocked with 2.5% Blotting-Grade Blocker Non-Fat Dry Milk (Bio-Rad Cat# 1706404XTU) and 2.5% bovine serum albumin (BSA, Cat# A7906; Sigma-Aldrich; St. Louis, MO,) in 0.1% 0.1% Tween 20 in Tris-buffered saline (TBST) for 1 hour at room temperature. Membranes were then probed overnight on a rocker at 4°C with primary antibodies dissolved in blocking buffer. Primary antibodies were used at the following dilutions: 1:1000 mouse Total OXPHOS Rodent WB Antibody Cocktail

(Abcam, Cat# ab110413, RRID:AB_2629281), 1:1000 rabbit caspase-1 (Cell Signaling Technology, Cat# 2225, RRID:AB_2243894), 1:500 mouse iNOS (BD Biosciences, Cat# 610329, RRID:AB_397719), 1:500 rat caspase-11 (BioLegend, Cat# 647202, RRID:AB_1937281), and 1:20,000 hFAB Rhodamine-conjugated anti-Tubulin (Bio-Rad Cat# 12004166, RRID:AB_2884950). Membranes were washed three times for 10 minutes each in TBST, followed by the introduction of secondary antibodies. The LI-COR fluorescent secondary antibodies IRDye 680RD goat anti-mouse (LI-COR Biosciences Cat# 926-68070, RRID: AB_10956588) and IRDye 800CW goat anti-rabbit (LI-COR Biosciences Cat# 926-32211, RRID: AB_621843) were added to membranes at a 1:20,000 dilution and incubated at room temperature for 40 minutes. After an additional three 10-minute TBST washes, membranes were imaged with a LI-COR Odyssey Fc blot imager and proteins were quantified using LI-COR Image Studio 6.0 software.

5.2.3 *Griess assay*

Nitrite concentration in conditioned cell culture medium was measured in duplicate with a Griess Reagent kit (Invitrogen, Thermo Fisher). This colorimetric assay detects the nitrite in the medium when nitrite and sulfanilic acid react to form a diazonium salt which is coupled to N-(1-naphthyl)ethylenediamine. The azo dye formed during this reaction can then be detected spectrophotometrically by absorbance at 548 nm.

5.2.4 *Statistical analysis*

All experiments were replicated at least three times (n=3). Biological replicates are reported as mean \pm standard error of the mean (SEM). Statistical analyses were performed using GraphPad Prism 10.4.0 (GraphPad Software, LaJolla, CA). Griess assay and western blot data

were analyzed using two-way ANOVA with Dunnett's multiple comparisons. The significance level was set at $p < 0.05$.

5.3 Results

5.3.1 Pharmacological co-inhibition of TLR4 and caspase-1 may lead to partial rescue of the Complex IV subunit MTCO1

Protein levels of representative ETC complex subunits were examined by western blot in activated HAPI cells and non-activated controls. In wild-type (WT) control cells transduced with an empty vector (EV), we observed dramatic activation-induced decreases in the Complex II subunit SDHB and the Complex IV subunit MTCO1, as well as a significant decrease in the Complex I subunit NDUFB8. Neither individually inhibiting TLR4 with TAK-242 nor inhibiting caspase-1/-11 with VX-765 prevented the loss of the Complex I, II and IV subunits. However, the combination of TAK-242 and VX-765 appeared to partially inhibit the reduction in the Complex IV subunit MTCO1. In contrast to the partial protection observed with the TLR4/caspase-1/-11 inhibitor combination, we observed complete protection of not only MTCO1 but also the Complex II subunit SDHB in LPS/IFN- γ -treated *Nos2* KO HAPI cells compared with the activated WT EV cells. The Complex I subunit NDUFB8 was not protected from LPS/IFN- γ -induced loss by the absence of *Nos2*, as its level decreased to the same extent in EV and *Nos2* KO cells. This finding indicates that the degradation mechanism of this Complex I subunit is independent of NO. The Complex III subunit UQCRC2 and the Complex V subunit ATPA5 were unchanged following LPS/IFN- γ activation, regardless of the presence of iNOS. We observed that pro-caspase-1 (~50kDa) remained unchanged following LPS/IFN- γ treatment but the level of the "p20" active

form of caspase-1 (~20kDa) increased. We observed a slight decrease in the p20 band in the TAK-242 and VX-765 combination group, with simultaneous partial protection of the Complex IV subunit MTCO1. Although we did not probe for iNOS in this experiment, in subsequent experiments we observed that the sole addition of VX-765 decreased the induction of iNOS protein in LPS/IFN- γ activated cells. (Figure 5.2) The NLRP3 inhibitor MCC950 did not rescue the loss of any ETC complex subunits in activated HAPI cells. In addition, MCC950 failed to attenuate the LPS/IFN- γ -induced production of NO implicated in SDHB and MTCO1 degradation.

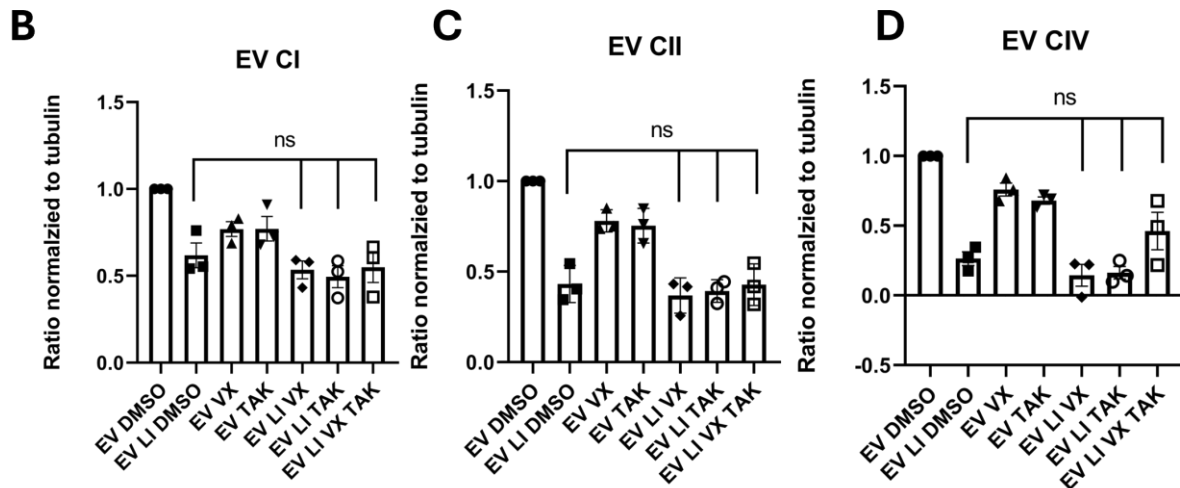
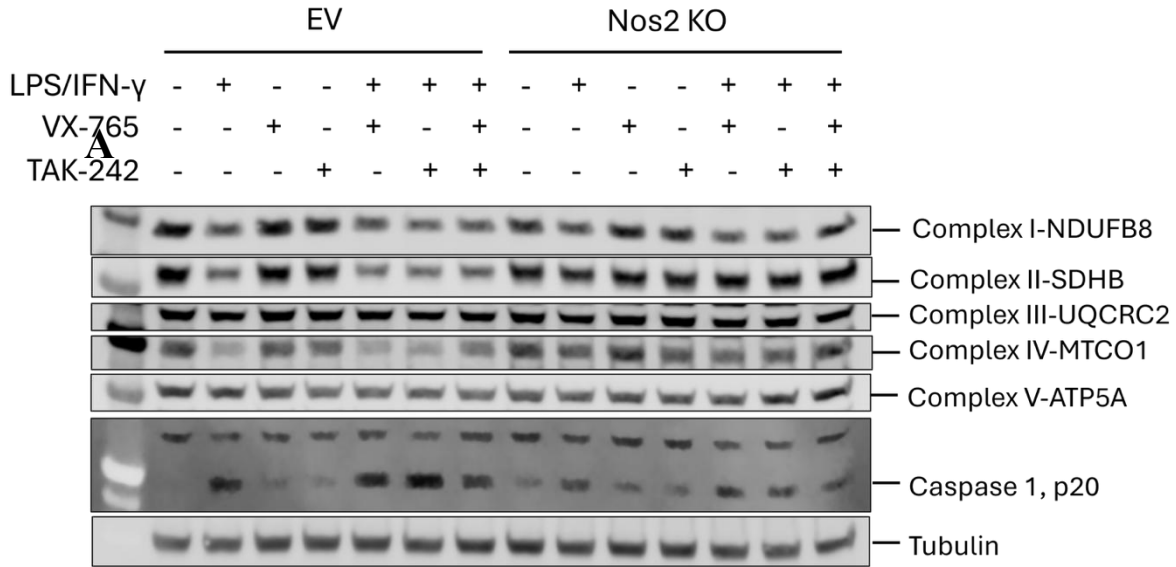


Figure 5.1 Co-inhibition of TLR4 inhibitor TAK-242 and caspase-1/11 inhibitor VX-765 partially rescued the Complex IV subunit MTCO1 loss in empty vector wildtype HAPI cells while Nos2 KO completely rescued the loss.

(A) Representative western blot images for rodent OXPHOS, caspase-1, and tubulin. Cells were treated with TAK-242 (1 μ M) and VX-765 (80 μ M) along with LPS/IFN- γ . ETC complex-origin and specific subunit names are labeled on the right. B-D. The relative levels of the representative Complex I (B), II (C), and IV (D) subunits. One-way ANOVA, Dunnett's multiple comparison test, n=3. Mean \pm SEM.

5.3.2 *Elimination of NO production rescues the Complex II and IV subunits SDHB and MTCO1, respectively, but not the Complex I subunit NDUFB8*

Having observed that the representative ETC Complex II and IV subunits are preserved in *Nos2* KO HAPI cells, we sought to confirm that NO produced by iNOS is required for the loss of these subunits. Therefore, we co-treated both EV and *Nos2* KO HAPI cells with the iNOS inhibitor 1400W upon LPS/IFN- γ addition, predicting protection against the ETC Complex II and IV losses in the EV cells. By measuring NO in the culture medium using the Griess assay, we verified that 1400W completely inhibited NO production (data not shown). As expected, we observed no loss of SDHB or MTCO1 protein in activated wild-type or *Nos2* KO cells when 1400W was present (Figure 5.2). However, neither 1400W treatment nor elimination of the *Nos2* gene rescued the protein level of the Complex I subunit NDUFB8.

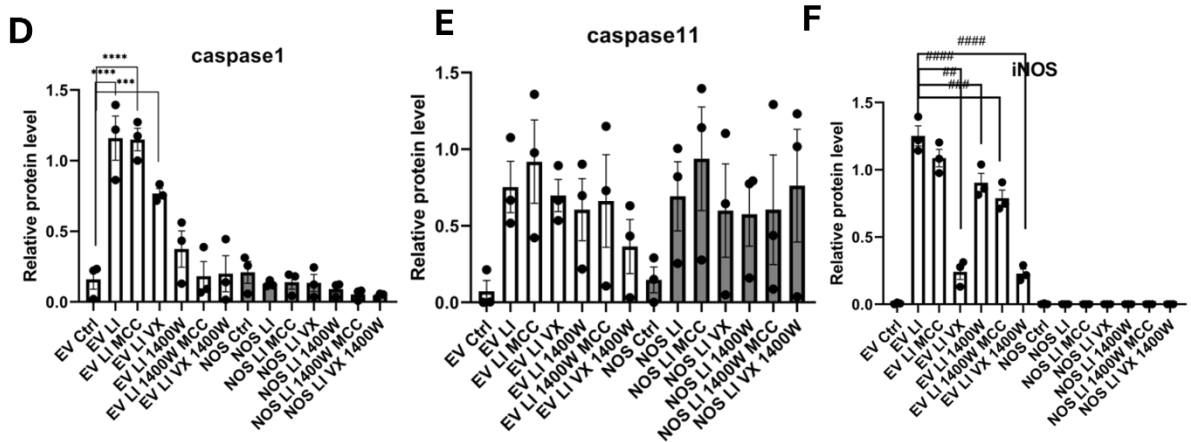
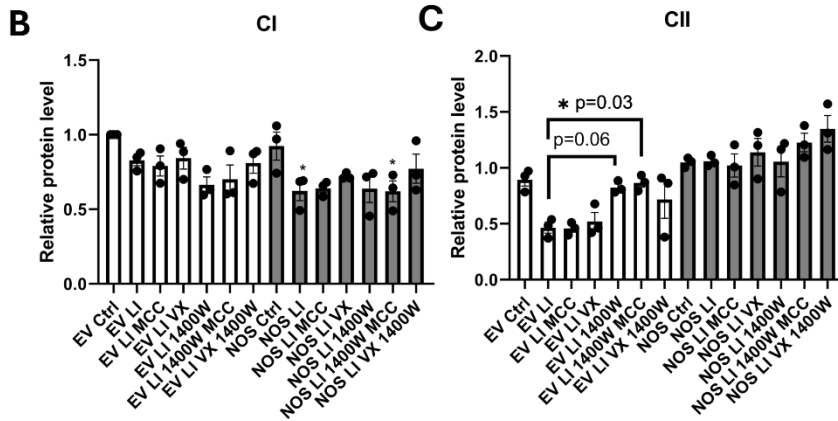
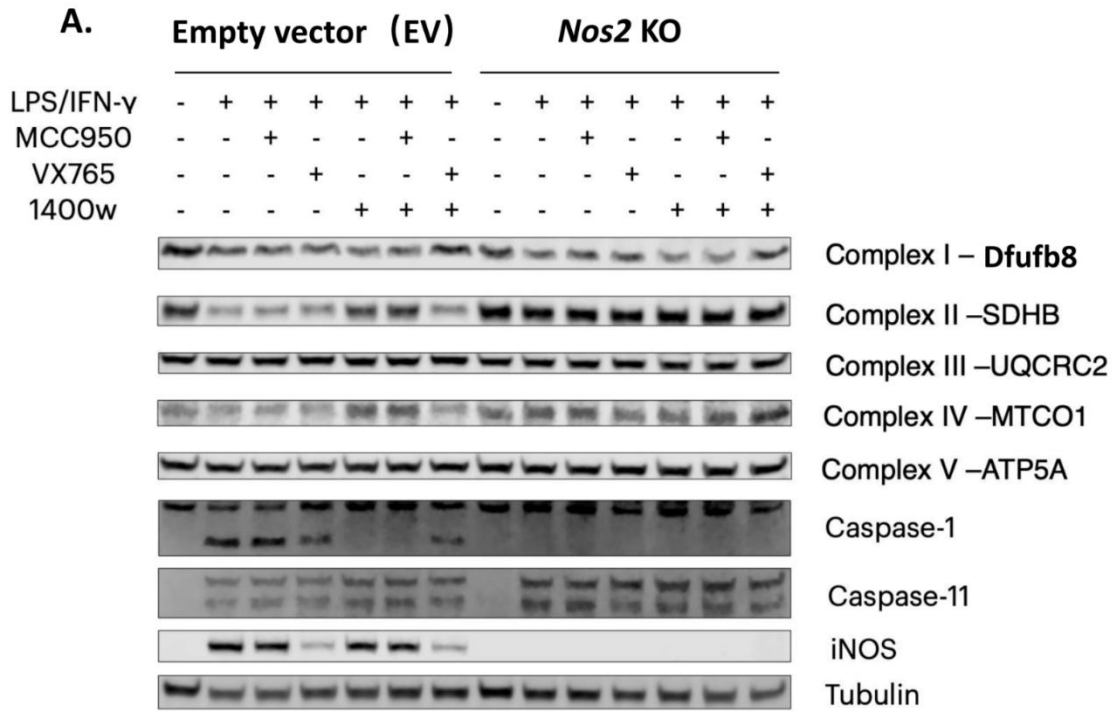


Figure 5.2 Either pharmacological iNOS inhibition or Nos2 KO rescues ETC complex subunits SDHB and MTCO1.

(A) Western blot analysis of representative ETC Complex subunits, iNOS and caspases when EV and *Nos2* KO cells were treated with caspase-1/11 inhibitor VX-765 (80 μ M), NLRP3 inhibitor MCC950 (20 μ M) and NO production inhibitor 1400W (100 μ M). ETC complex-origin and specific subunit names are labeled on the right. **B-F.** Complex I- (**B**), II- (**C**), caspase-1 (**D**), caspase-11 (**E**) and iNOS (**F**), two-way ANOVA with Tukey's multiple comparison test, n=3. # or * p<0.05, ** p<0.01, *** p<0.001, **** p<0.001, ##### p<0.001.

5.3.3 *Caspase activity is not required for the loss of ETC complex subunits*

Although we concluded that NO is required for the degradation of the representative Complex II and IV subunits evaluated, experiments with the caspase-1/-11 inhibitor VX-765 were not sufficient to demonstrate the hypothesized requirement for caspase-1. We then tested the pan-caspase inhibitor Q-VD-Oph to more broadly address the requirement for any of the caspase proteases in the activation-induced loss of ETC subunits. However, as was the case for the VX-765 treatment, we found that Q-VD-Oph failed to protect the representative Complex I, II, or IV subunits from LPS/IFN- γ -triggered loss (Figure 5.3A). This finding suggests that the loss of all three subunits in pro-inflammatory microglia occurs by caspase-independent mechanisms.

5.3.4 *A caspase-1/iNOS positive feedback loop may contribute to Complex II and IV degradation*

We observed an inhibition of LPS/IFN- γ -induced iNOS induction when VX-765 was used to inhibit caspase-1/-11 (Figure 5.3D). This finding suggests that caspase-1/-11 activity enhances iNOS expression. Although pan-caspase inhibitor Q-VD-Oph failed to rescue the loss of any of the ETC complex subunits, it decreased the iNOS protein level (Figure 5.3B) as well as NO secretion (Figure 5.3C) measured after 18 hours of LPS/IFN- γ treatment. We also observed a decrease of the p20 active caspase-1 band (Figure 5.2D) when we used 1400W to inhibit NO production in WT EV HAPI cells. This result suggests that the activation of caspase-1, reflected by the level of p20, is enhanced by iNOS-mediated NO production. We also observed decreased p20 caspase-1 in *Nos2* KO cells (Figure 5.2D), further supporting this conclusion. Thus, a positive feedback loop (Figure 5.3E) between iNOS and caspase-1 regulates their expression during pro-inflammatory microglial activation, resulting in the NO-dependent loss of Complex II and IV

subunits. The Complex I subunit NDUF8 is lost by a different mechanism that is both NO- and caspase-1/-11 independent.

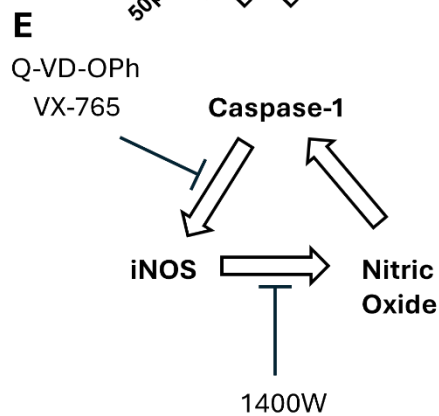
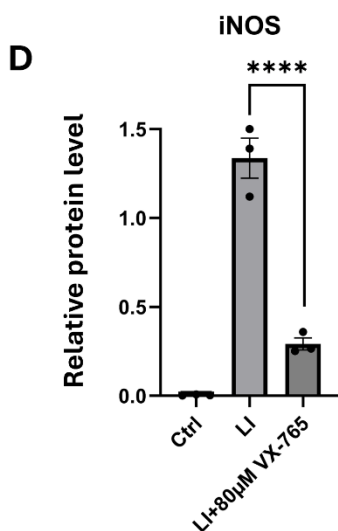
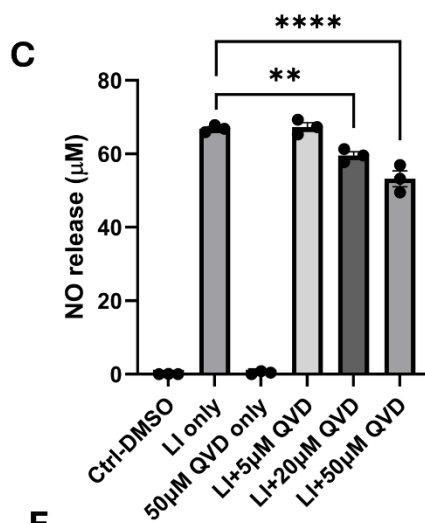
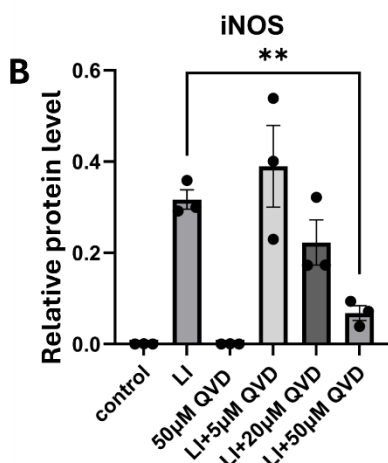
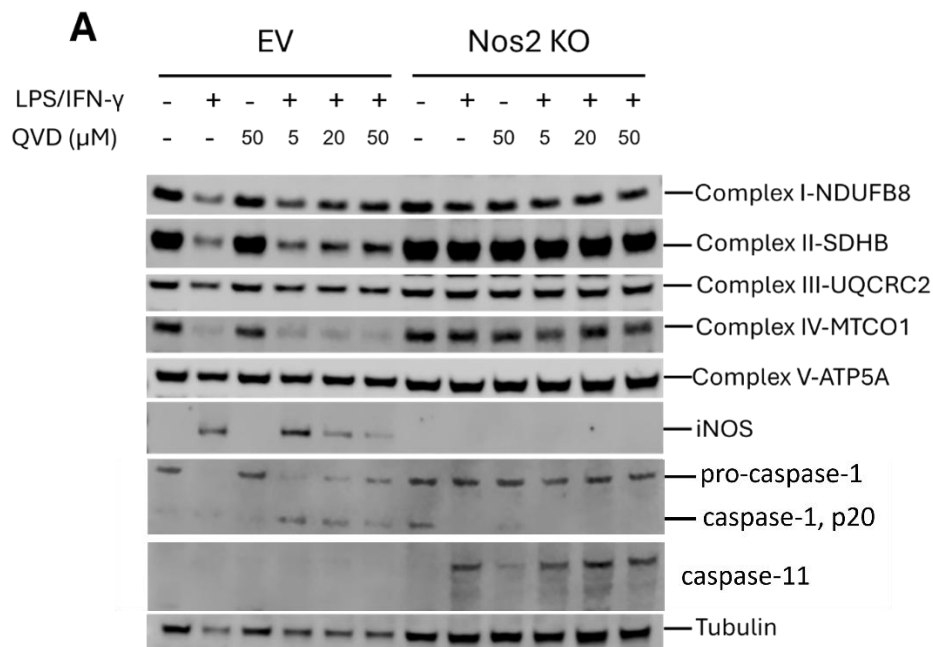


Figure 5.3 The pan-caspase inhibitor Q-VD-Oph decreases the iNOS enzyme level but fails to prevent the loss of ETC complex subunits.

QVD, Q-VD-Oph. LI, LPS/IFN- γ . (A) Western blot evaluation of ETC complex subunits and analysis of caspases and iNOS, with a titration of Q-VD-Oph (5~50 μ M) in empty vector (EV) and Nos2 KO HAPI cells. (B) iNOS protein level decreased in Q-VD-Oph treatment with a dose-dependent manner. (C) Relevant NO release showed milder decrease than iNOS protein level. (D) iNOS protein level also decreased with 80 μ M caspase-1/-11 inhibitor VX-765 treatment. (E) Schematic model explaining the positive feedback loop between iNOS and caspase-1. One-way ANOVA with Dunnett's multiple comparisons test. n=3. Mean \pm SEM, * p<0.05, ** p<0.01, **** p<0.0001.

5.4 Discussion

In this study, we found that the loss of ETC subunits in HAPI microglia activated with the pro-inflammatory stimulus of LPS/IFN- γ occurs by multiple mechanisms. First, we observed that the degradation of SDHB (CII) and MTCO1 (CIV), but not NDUFB8 (CI), was prevented by pharmacologically inhibiting NO synthesis or by genetically ablating the iNOS-encoding *Nos2* gene. In experiments described earlier in this dissertation, we also observed a partial protection of respiratory impairment in *Nos2* KO HAPI cells relative to WT EV at 12 hours of LPS/IFN- γ treatment (see Figure 4.3), consistent with the rescue of the ETC subunits SDHB and MTCO1. This evidence indicates that NO is required for the activation-induced loss of SDHB (CII) and MTCO1 (CIV), but not that of NDUFB8 (CI). Another group also showed NO-dependency of SDHB (CII) degradation in LPS/IFN- γ -activated macrophages, but found that the Complex II subunit SDHA was stable, indicating differential regulation of subunits belonging to the same ETC complex [86]. The authors showed that SDHB protein decreases in WT but not *Nos2* KO primary macrophages, consistent with our results in HAPI microglia. The authors also reported a MTCO1 (CIV) subunit decrease in activated WT macrophages and a protection in *Nos2* KO cells, also consistent with our HAPI microglial cell results. Finally, also consistent with our HAPI cell findings, the ATP5A (CV) and UQCRC2 (CIII) ETC subunits were unaltered in LPS/IFN- γ -treated macrophages. Collectively, these results suggest that there is a common NO-dependent ETC degradation mechanism employed by these two myeloid cell types.

Among the ETC complexes, it appears that the degradation mechanisms of Complex I, the largest complex consisting of 45 subunits, may be the most complex. In our study, we observed that the NDUFB8 (CI) subunit decrease in LPS/IFN- γ -treated HAPI microglial cells was not rescued by genetic depletion of *Nos2*. Palmieri et al. reported that a decrease in a different Complex

I subunit, NDUFS1, was rescued in LPS/IFN- γ -activated macrophages by *Nos2* KO. [86] In addition, they found that the LPS/IFN-g induced loss of NDUF8 was rescued in *Nos2* KO macrophages, in contrast to what we observed in activated HAPI cells. These results indicate that different subunits within the ETC can undergo different mechanisms of degradation and that the specific degradation mechanisms may be cell-type-dependent.

A limitation of our study is that we only measured one representative subunit of each ETC complex. This is insufficient to draw conclusions on the overall regulation of the ETC complexes. For example, although we found that the Complex III subunit UQCRC2 was stable following LPS/IFN- γ stimulation of HAPI cells, it is possible that one or more of the unmeasured Complex III subunits underwent degradation.

In future studies, the activity of each ETC complex in LPS/IFN- γ -activated WT EV and *Nos2* KO HAPI cells should be examined by blue native gel electrophoresis. In addition, the protein levels of more key subunits of each complex should be measured by western blot or mass spectrometry for a thorough evaluation of the structural integrity of each complex. It is also necessary to measure time-dependent changes to the individual Complex I, II, and IV respiratory capacities for LPS/IFN- γ -activated WT EV and *Nos2* KO HAPI cells using the newly optimized CRABS-ROC protocol (described in Chapter 2). With the activity measurements of each complex, we can associate the onset of functional deficits with structural degradation of the various ETC complexes at the individual subunit level.

Chapter 6

Evaluation of idebenone's ability to reduce two-week post-injury lesion size following adult mouse TBI

6.1 Introduction

Although idebenone is not yet an FDA-approved drug, it has been approved since 2015 by the European Medicines Agency (EMA) for the treatment of Leber's hereditary optic neuropathy (LHON) [28], a mitochondrial disease. Including LHON, idebenone has been preclinically tested in many neurological diseases, also including testing in Alzheimer's disease and Parkinson's disease mouse models. In 5xFAD Alzheimer's mice, 7-day idebenone treatment rescues impaired NRF2 expression, improved spatial and recognition memory impairments caused by LPS injection, and decreased NLRP3 level as well as subsequent neuroinflammation [212]. In the 1-methyl-4-phenyl-1,2,3,6-tetrahydropyridine (MPTP) mouse model of Parkinson's disease, idebenone protected against the loss of tyrosine hydroxylase-positive dopaminergic neurons in the substantia nigra and improved motor deficits [213].

Idebenone has also been tested in preclinical rodent studies for protection against acute brain injuries, however, there is no evidence showing whether idebenone has a protective effect against long-term secondary injury after TBI. At a 24-hour acute time point after mouse CCI, a microglial gene signature was increased in response to post-TBI idebenone treatment, suggesting amplification of the early, adaptive microglial response, while TBI-induced alterations to the expression of ephrin-A and dopamine signaling pathway genes were attenuated by idebenone [44]. Additionally, a recent study showed that idebenone mitigates oxidative stress and neuroinflammation in a mouse intracerebral hemorrhage (ICH) model by reducing microglial pro-inflammatory activation within three days during the acute injury phase [214]. *In vitro*, idebenone

reduces pro-inflammatory cytokine secretion in the RAW 264.7 macrophage cell line [215] and the BV2 microglial cell line [213]. In experiments described in Chapter 4, we observed that idebenone restores respiration in microglia activated to a pro-inflammatory state and identified a contribution of the enzyme iNOS to the cytoplasmic-reduction-mediated activation of idebenone in the HAPI microglial cell model. The significant restoration of microglial mitochondrial respiratory function by idebenone suggests that the compound has therapeutic potential for alleviating the microglia-induced secondary injury after TBI.

Based on the existing preclinical literature and our *in vitro* mechanistic studies described in Chapter 4, we hypothesized that idebenone alleviates secondary injury following TBI by restoring microglial respiration and inhibiting the pro-inflammatory activation of microglia. As neuroinflammation-induced secondary injury enlarges lesion volume following TBI, we selected histological quantification of lesion volume as an initial straightforward way to evaluate idebenone's potential for long-term neuroprotection. In this study, we administered idebenone by intraperitoneal (i.p.) injection twice daily for two weeks after mouse CCI and performed hematoxylin and eosin (H&E) staining to determine whether idebenone treatment mitigates the enlargement of lesion volume caused by secondary injury.

6.2 Materials and methods

6.2.1 Reagents

The following reagents were obtained from Sigma-Aldrich (Saint Louis, MO): 4% paraformaldehyde (PFA); 30% sucrose; 200 proof ethyl alcohol; Eosin Y Solution, Alcoholic (Cat# HT110132-1L); Harris Hematoxylin Solution, Modified (Cat# HHS16-500ML); and DPX Mountant for histology (Cat# 06522).

6.2.2 *Animal husbandry*

All procedures were approved by the University of Maryland Institutional Animal Care and Use Committee (IACUC) and were compliant with the NIH Guide for the Care and Use of Laboratory Animals. C57BL/6J (B6) mice were maintained under 12-hour light and dark cycles.

6.2.3 *Controlled cortical impact (CCI)*

8~10-month-old B6 male and female mice were mounted on a stereotaxic frame (Stoelting) and subjected to CCI or sham. Mice were anesthetized with 5 mg/mL isoflurane for initial anesthesia until losing reflection to a deep toe pinch. The concentration of isoflurane was then adjusted to and maintained at 2 mg/mL during the procedure. After multiple scrubs with 70% ethanol and betadine, a 1-cm-long incision in the midline of the scalp was made from the base of the skull to above the ears using a sterile surgical blade. A few drops (~100 μ L) of bupivacaine (1.5mg/kg) were applied with a needle to the periosteum/wound edges, followed by waiting for 3-5 minutes for effective analgesia. The skull was then dried with sterile Q-tips/cotton swabs and the left temporoparietal bone, between bregma and lambda, was exposed. A 5-mm craniotomy was made with a small drill with a sterile bit. The injury device consisted of a microprocessor-controlled pneumatic impactor (Impact One TM Stereotaxic Impactor for CCI, Leica Microsystems, Buffalo Grove, Illinois) with an interchangeable tip (2.5 mm diameter). Mild-to-moderate-level TBI was induced by an impactor velocity of 5 m/sec and deformation depths of 1-2 mm. Immediately following sham or impact injury, the skin was sealed with 5-0 nylon sutures (AD surgical; Sunnyvale, CA). Skull flaps were not re-sealed with dental acrylics due to the potential for induction of secondary injury.

6.2.4 Intraperitoneal (i.p.) injection

Idebenone was freshly reconstituted from a 100 mM DMSO stock solution and further diluted with corn oil (Sigma-Aldrich). Immediately after vortex for at least 10 seconds, idebenone or vehicle (DMSO in corn oil) was loaded in a Tuberculin Syringe with Needle (BD Biosciences; San Diego, CA; Cat # 309626) and injected intraperitoneally at 100 mg/kg. The first injection was given at one hour post-injury, and the remainder of injections were administered twice daily at an 8-12-hour interval for 14 days. The mice were subjected to vital perfusion on post-TBI day 15, and the brains were carefully removed for further fixation in 10 mL of 4% PFA at 4 °C, incubated overnight. Brains were then transferred into 30% sucrose in PBS at 4 °C.

6.2.5 Hematoxylin and eosin (H&E) staining

When the brains in sucrose were well-rehydrated, brains were sectioned at 40 µm thickness using a Leica microtome and the sections were stored in cryoprotectant at -20°C. One in every 12 adjacent sections was attached on to a glass slide (super frosted; VWR; Radnor, PA), stained with H&E, and mounted with PDX Mountant and coverslip (VWR).

6.2.6 Microscopy imaging and quantification of lesion volumes

H&E-stained brain sections were imaged using an Axio Imager 2 motorized microscope (Zeiss, Germany) under 10x magnification. A randomly generated and placed 25 micrometers (µm) × 25 µm grid by Stereo Investigator software (MBF Bioscience; Williston, VT) was then used to estimate the lesion volumes (mm³) based on Cavalieri's principle.

6.3 Results

6.3.1 CCI with a 1.5 mm depth is optimal for the induction of moderate TBI

Previously, we tested the CCI model set at a 2 mm impact depth, however, the initial penetration pierced through the corpus callosum and induced severe damage. Therefore, for this study we tested 1.0 mm and 1.5 mm depths in male and female mice and observed that neither depth penetrated through the corpus callosum despite the 1.5mm depth causing a relatively large lesion size (Figure 6.1). We therefore chose 1.5 mm as an appropriate depth setting to deliver “moderate” TBI.

6.3.2 Idebenone failed to decrease the lesion volume at 14 days post-injury

No significant difference in the estimated CCI-induced lesion volume was observed between the idebenone-treated group and the vehicle control group in either males or females (Figure 6.2). There was also no sex difference in lesion volume despite the appearance of a slight trend toward a smaller lesion size in males.

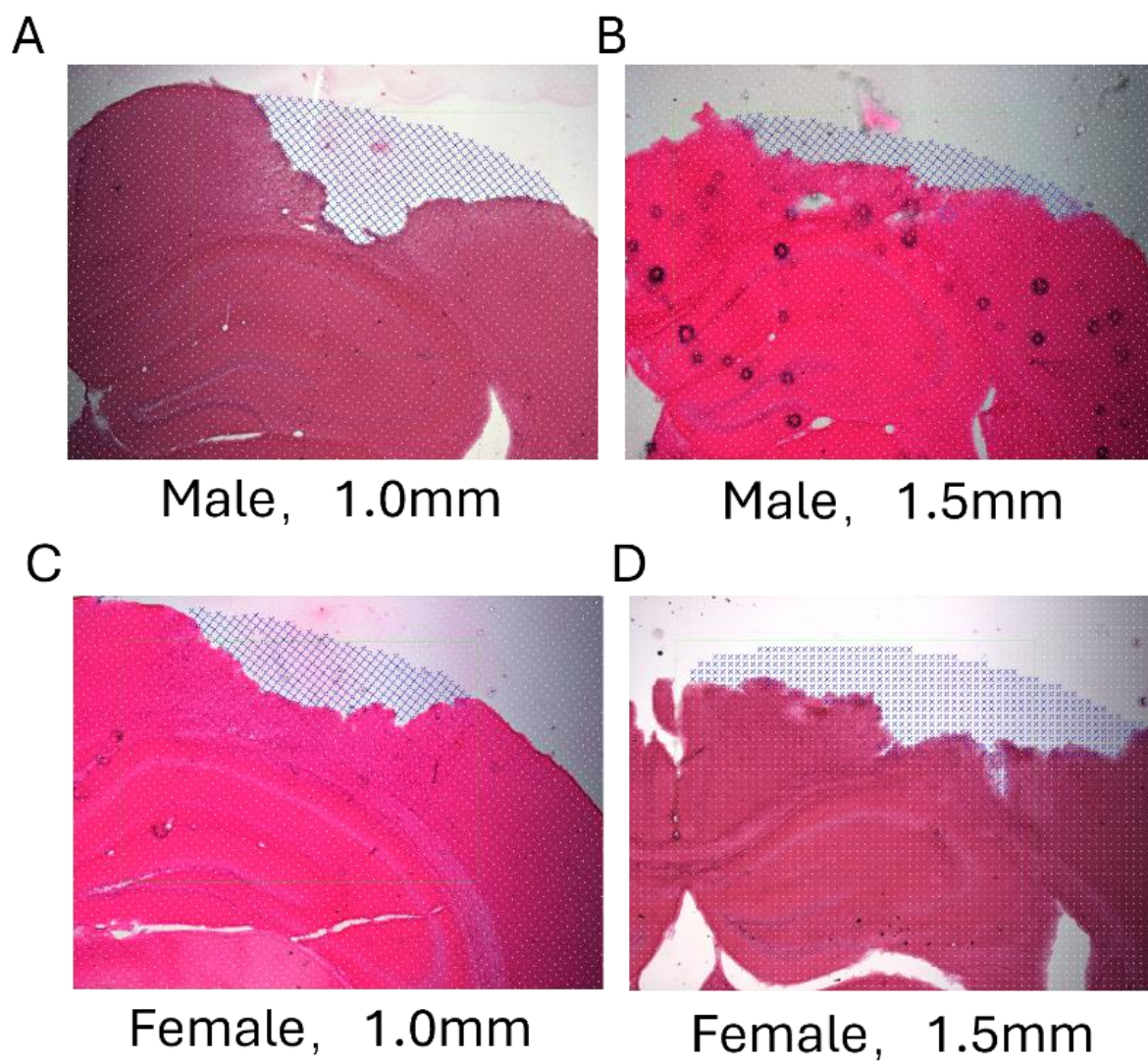


Figure 6.1 Comparisons of lesion size for CCI impact depths of 1.0 mm and 1.5 mm in male and female mice. The dotted area is masking the injured area by the Montage software.

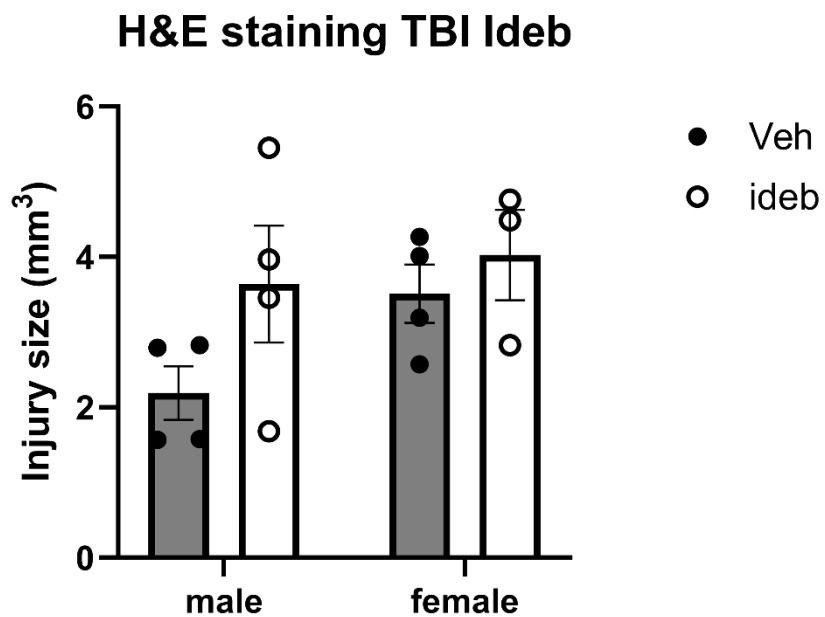


Figure 6.2 Effect of idebenone treatment on lesion size in CCI mice at 14 days post-injury. Idebenone (100 mg/kg) was administered by intraperitoneal injection twice a day at an 8-12-hour interval for 14 days. The first injection was delivered one hour after injury. Data is mean \pm SEM.

6.4 Discussion

A protective effect of idebenone treatment against lesion size at 14 days after CCI was not observed. We found that a few sections exhibited very high variability in the apparent injury across the rostral-caudal axis, showing an obvious inconsistency of lesion size. Extending the stereology from a twelve-section interval to an eight-section interval may improve the accuracy of quantification. Otherwise, a parallel 2,3,5-triphenyltetrazolium chloride (TTC) staining could be used as an alternative method to quantify lesion size.

The axis of improving microglial mitochondrial respiration – alleviating microglial neurotoxic factors release – mitigating secondary neuronal death – protection against behavioral impairments is yet to be established. Notably, idebenone has distinct effects on non-microglial cell types in culture, which may contribute to offsetting effects *in vivo*: idebenone supports NQO1-dependent respiration in astrocytes but inhibits Complex I-dependent spare respiratory capacity in neurons [47].

To further study the protective effect of idebenone in TBI, we plan to immunostain the harvested brain sections for the microglial marker IBA-1 to evaluate whether idebenone reduces the number of activated/pro-inflammatory microglial cells persisting at two weeks post-injury. Microglial and neuronal mitochondrial respiratory function should also be examined in the idebenone study. Finally, behavioral experiments should be performed to see whether idebenone improves the performance of TBI mice in cognitive tests. More time points following TBI should be considered to reveal if prolonged idebenone treatment is neuroprotective.

Chapter 7

Discussion

The research for the development of TBI therapeutic strategies that target mitochondria focused on ROS [25], apoptosis signaling such as Bcl-2 and AIF [216, 217], mitochondrial fission/fusion [218], impaired mitophagy [219] as a reflection of acute response. However, the long-term management of TBI survivors is undermined and requires advancements to ameliorate progressive neurological decline[217, 220]. Rescuing mitochondrial dysfunction is increasingly considered a promising therapeutic strategy for post-TBI treatment[221-223]. This dissertation focused on strategies for mitigating the mitochondrial respiratory dysfunction in the TBI brain and for preventing the degradation of ETC complexes in pro-inflammatory microglia. To help achieve these goals, we established a robust protocol for assessing individual ETC complex-dependent respiratory capacities and developed an *in vitro* model for investigating the mechanisms of ETC complexes degradation in pro-inflammatory microglia. Among key discoveries, we found that not only is NO required for the loss of specific Complex II and IV subunits in pro-inflammatory microglia, the relative enzyme iNOS is also one of the main enzymes that catalyzes the reduction of idebenone, a potential neurotherapeutic which can partially restore respiration in these cells.

In Chapter 2, we described the development of a new Seahorse-based protocol CRABS-ROC (Complex Respirometry Assay Bypassing Substrate-Restricted Oxygen Consumption), which can be used to investigate respiratory dysfunction at the level of individual ETC complexes. The main contribution of this method is that it assesses the total respiratory capacity of each ETC complex by using saturating levels of complex-specific substrates, overcoming the oxygen consumption rate restrictions caused by endogenous substrate limitations. The schematic diagrams in Figure 1.3 showed the evolution of Seahorse protocols assessing respiratory dysfunction. In the

classical Mito Stress Test protocol, FCCP is added to cells metabolizing glucose (Figure 1.2A). Glycolysis is a rate-limiting factor for the provision of mitochondrial substrates, and this can be bypassed by adding a supraphysiological amount of the cell-permeable Complex I-linked substrate pyruvate in combination with FCCP (Figure 1.2B). Using the CRABS-ROC protocol, the glycolysis rate limitation and additional rate limitations by NADH-generating dehydrogenase enzymes such as PDH can be bypassed by directly delivering a saturating amount of NADH, the immediate substrate of ETC Complex I (Figure 1.2C). Using this method, we revealed the total Complex I respiratory capacity, with the removal of substrate limitations unmasking a hidden Complex I deficit in isolated brain mitochondria from harlequin mutant mice.

Similar studies have also shown that the re-supplement of NADH and cytochrome c restored the lost respiratory activity from frozen tissue samples [224]. However, in their study, they conducted the Seahorse-based respirometry assay with 10 μ M of cytochrome c without a proof of abundance. Insufficient cytochrome c re-supplement could become a rate-limiting factor failing to support the full respiratory capacity, causing unreliable measurements of OCR. In our study, we titrated the amount of cytochrome c with frozen mouse brain homogenates, revealing that 10 μ M isn't sufficient (Figure 2.5A). We recommend titrating the amount of cytochrome c when different types of frozen tissue are being measured. We also titrated alamethicin (Figure 2.5B) and NADH (data not shown) in our study.

The CRABS-ROC protocol allows measurements of the Complex I-, II- and IV-dependent respiration in one experiment, showing potential of quick evaluation of mitochondrial respiratory capacity in pathological conditions compared to their physiological controls. Assessing individual ETC complex-dependent respiratory deficiencies provides clues for a next-level examination of ETC stability on structural impairments and protein turnovers. Tissue from multiple organs have

been tested before and after frozen and showed feasibility of assessing mitochondrial respiratory capacity in frozen tissue [224]. Combined with the quick screening for each representative ETC complex subunits by western blot, mitochondrial impairments will be quickly located at functional level and structural level. In the experiments described in Chapter 3, the CRABS-ROC protocol was employed to reveal male-specific decreases in Complex I-dependent and Complex IV-dependent respiration in pediatric rat brain homogenates post-TBI. Interestingly, we didn't observe significant protein level changes of representative ETC complex subunits, indicating a possibility that the respiratory deficiency may be caused by perturbations on post-translational level. Notably, the rodent OXPHOS (Abcam) antibody cocktail we used in western blot experiment only detects one representative subunit of each ETC complex. We won't conclude full integrity of the ETC complexes until more key subunits are tested. However, these findings are sufficient to reinforce the strength of the CRABS-ROC protocol for resolving functional differences at the level of individual ETC complexes.

Briefly mentioned in the Introduction Chapter, many mitochondrial impairments in TBI were measured with respiration States (Table 1.1). To measure the Complex I- and II-dependent respiratory capacity, the uncoupled respiration is measured when Complex I- and II-specific substrates are added (Figure 1.2). These uncoupled respirations were also recognized as Complex I- or II-dependent State V respiration. These outcomes are used as good estimation but not precise reflection of Complex I- and II-dependent respiration, for the inclusion of extra respiration supplied by several dehydrogenase enzymes discussed in Chapter 2.

In Chapter 4, we described experiments demonstrating the contribution of iNOS to the cytoplasmic reduction of the potential neurotherapeutic idebenone in pro-inflammatory microglia. Former lab member Sausan Jaber reported that the NQO1 inhibitor dicoumarol did not inhibit the

reduction of idebenone in pro-inflammatory microglia. This finding indicated that there was an enzyme other than NQO1, the enzyme responsible for idebenone reduction in astrocytes, that catalyzes idebenone's reduction in the cytoplasm of pro-inflammatory microglia. The iNOS enzyme was identified as a strong candidate by an in-gel activity assay combined with mass-spectrometry. To investigate whether iNOS contributes to the reduction of idebenone in activated microglial cells, we generated *Nos2* KO HAPI cells, along with an empty vector control cell line. An indirect idebenone reduction assay based on NADPH oxidation rate demonstrated an ~70% decrease in *Nos2* KO cell extracts compared to EV control extracts, suggesting that iNOS catalyzes the majority of idebenone reduction in LPS/IFN- γ -activated HAPI microglia. Although the respirometry data showed abolished respiratory stimulation by idebenone in activated *Nos2* KO cells relative to EV controls, we could not distinguish whether this loss of activity was due to inadequate idebenone reduction when iNOS was absent or because iNOS deficiency prevented the portion of the LPS/IFN- γ -induced respiratory deficit that was rescuable by idebenone.

Within the study, HAPI microglial cell line was established as a model for microglia, because of the limitation in availability in studying primary microglia. To understand the role of iNOS in reducing idebenone, we also generated CRISPR knockout cell lines with HAPI cell line. However, to improve the scientific significance of this study, we plan to test our conclusion with mouse primary microglia isolated from wild type and *Nos2* KO strains. We also plan to test more candidates that are catalyzing the redox reaction of idebenone.

In the experiments described in Chapter 5, we investigated the stability of representative ETC complex subunits upon pro-inflammatory activation of EV or *Nos2* KO HAPI microglial cells using an OXPHOS antibody cocktail. First, we saw different patterns of stability across the different ETC complexes in the LPS/IFN- γ -activated EV HAPI cells. The UQCRC2 and ATP5A

(Complex III and V subunits, respectively) protein levels remained unchanged in activated EV cells, but the NDUFB8 (CI), SDHB (CII) and MTCO1 (CIV) levels decreased. Then, among the three altered complexes, we observed that SDHB (CII) and MTCO1 (CIV) degradation was NO-dependent whereas NDUFB8 (CI) was not. Another group conducted a similar study on BMDMs from wild-type and *Nos2* KO mice, showing similar results for CII-CV subunits[86]. However, they found that the LPS/IFN- γ -triggered loss of the Complex I subunit NDUF51 was prevented in *Nos2* KO BMDMs, while we did not observe a protection of NDUFB8 degradation in *Nos2* KO HAPI cells. SDHA remained intact in activated wild-type macrophages, while SDHB exhibited the same pattern of degradation we observed in HAPI cells: it decreased in wild-type BMDMs and this decrease was prevented by genetic *Nos2* depletion. Taken together, the results of our studies and others indicate that there is differential stability of ETC Complex subunits and that multiple mechanisms contribute to ETC subunits loss upon pro-inflammatory activation.

While in this dissertation we focused on their bioenergetic roles, it is also possible that some Complex I and II subunits have other functions under inflammatory conditions. Notably, one group recently reported that Complex I activity is required to sustain neuroinflammation through ROS production [199]. Modeling the hypothesized ROS generation mechanism *in vitro*, the authors treated LPS/IFN- γ -activated primary microglia with oligomycin and succinate to induce reverse electron transport (RET) and found that ROS production and increased membrane potential were both prevented by rotenone. Others showed that microglia from Complex I-deficient *Ndufs4* KO mice exhibited protection against oxidative stress, pro-inflammatory activation, and secondary axonal damage in an experimental autoimmune encephalomyelitis (EAE) model of multiple sclerosis. There is also a cancer study in 2007 which suggested that the Complex II subunits SDHA and SDHB have distinct effects on ROS production and HIF- α stabilization when inhibited

pharmacologically or via RNA interference [225]. Inhibiting SDHB resulted in an increase in ROS and HIF- α , which are also observed during pro-inflammatory microglial activation. These findings suggest that SDHB's normal activity may counteract pro-inflammatory activation. Further research is crucial to understand the individual and combined roles of ETC subunit alterations in neuroinflammation.

In this project, we also provided novel evidence for a positive feedback loop between the induction of iNOS expression and the activation of caspase-1 in pro-inflammatory microglia. Our evidence indicates that inhibition of iNOS-mediated NO production reduces the appearance of the activated caspase-1 p20 protein during LPS/IFN- γ -induced activation. The caspase-1 inhibitor VX-765, in turn, inhibited the iNOS protein level in activated cells. In contrast to what we observed in HAPI microglial cells, in LPS/ATP-stimulated murine peritoneal macrophages, both exogenously added NO donor (SNAP or GSNO) and endogenous NO produced by iNOS inhibited the formation of the NLRP3 inflammasome and the subsequent activation of caspase-1 [226]. The authors concluded that caspase-1 is negatively regulated by iNOS. Factors that may explain this apparently conflicting result include the different cell types, the different activation stimulus, the different methods of NO delivery, and the different methods of iNOS protein depletion.

Next, to clarify whether caspase-1 is involved during the ETC complexes degradation in pro-inflammatory stage immune cells, we plan to test the ETC degradation in caspase-1 KO BMDMs isolated from caspase-1 knockout mice, provided by Dr. Stefanie Vogel. Most of the traditional caspase-1 mouse line was indeed a caspase-1/-11 double knockout line[227], but the line we plan to use is pure caspase-1 KO. We hypothesize that the degradation of ETC complex subunits, such as Complex II subunit SDHB and Complex IV subunit MTCO1, is still observed in LPS/IFN- γ activated, caspase-1 KO BMDMs, but can be reversed by the addition of 1400W. ETC

subunit degradation, levels of caspase-1, caspase-11 and iNOS will be detected by western blot. Griess assay will be performed in parallel in the conditioned culture medium as a hallmark of successful activation of BMDMs, and an indicator of NO inhibition efficiency by 1400W.

Collectively, in this dissertation, we introduced a reliable fast-screen pipeline studying mitochondrial dysfunction including respiratory deficiency and ETC complexes impairments in rodent neurotrauma models. The CRABS-ROC Seahorse protocol and western blot with OXPHOS antibody, will guide the direction exploring mitochondrial pathology in neurotrauma. Unmasking the true respiratory capacity of each ETC complex provides reliable potential for restoring the impaired respiration. The downstream western blot scan helps to locate the pathological sites associated with the impaired mitochondrial respiration.

Another key discovery of this dissertation lies on idebenone, a potential solution of mitochondrial dysfunction in neurotrauma, for its supporting role in re-boosting mitochondrial respiration and bioenergetics. By understanding the mechanism of cytoplasmic reduction of idebenone in microglia, we demonstrated a target, iNOS, that may contribute to maximizing the therapeutic potential of idebenone. Meanwhile, because microglia is such a key immune cell type, which regulates brain immunity through multiple signaling pathways, ameliorating pro-inflammatory polarization of microglia by restoring mitochondrial respiratory functions may become a strategy to mitigate secondary inflammation in the injured brain. We hope these findings be helpful to future neurotrauma studies.

References

1. Prevention, C.f.D.C.a., *TBI in the United States*. 2024.
2. Corps, K.N., T.L. Roth, and D.B. McGavern, *Inflammation and neuroprotection in traumatic brain injury*. *JAMA Neurol*, 2015. **72**(3): p. 355–62.
3. Riechers, R.G., 2nd, M.F. Walker, and R.L. Ruff, *Post-traumatic headaches*. *Handb Clin Neurol*, 2015. **128**: p. 567–78.
4. Izzy, S., et al., *Association of Traumatic Brain Injury With the Risk of Developing Chronic Cardiovascular, Endocrine, Neurological, and Psychiatric Disorders*. *JAMA Network Open*, 2022. **5**(4): p. e229478–e229478.
5. Brett, B.L., et al., *Traumatic Brain Injury and Risk of Neurodegenerative Disorder*. *Biol Psychiatry*, 2022. **91**(5): p. 498–507.
6. R, A.A., *Risk factors for Alzheimer's disease*. *Folia Neuropathol*, 2019. **57**(2): p. 87–105.
7. Sperl, M.A., et al., *Long-Term Risk of Stroke after Traumatic Brain Injury: A Population-Based Medical Record Review Study*. *Neuroepidemiology*, 2022. **56**(4): p. 283–290.
8. Ramos-Cejudo, J., et al., *Traumatic Brain Injury and Alzheimer's Disease: The Cerebrovascular Link*. *EBioMedicine*, 2018. **28**: p. 21–30.
9. Delic, V., et al., *Biological links between traumatic brain injury and Parkinson's disease*. *Acta Neuropathol Commun*, 2020. **8**(1): p. 45.
10. Norat, P., et al., *Mitochondrial dysfunction in neurological disorders: Exploring mitochondrial transplantation*. *npj Regenerative Medicine*, 2020. **5**(1): p. 22.
11. Stovell, M.G., et al., *Assessing Metabolism and Injury in Acute Human Traumatic Brain Injury with Magnetic Resonance Spectroscopy: Current and Future Applications*. *Front Neurol*, 2017. **8**: p. 426.
12. Donat, C.K., et al., *Microglial Activation in Traumatic Brain Injury*. *Front Aging Neurosci*, 2017. **9**: p. 208.
13. Lumba-Brown, A., et al., *Diagnosis and Management of Mild Traumatic Brain Injury in Children: A Systematic Review*. *JAMA Pediatr*, 2018. **172**(11): p. e182847.
14. Andraos, C., et al., *Limitations of the Glasgow Coma Scale: Challenges and Considerations*. *Cureus*, 2025. **17**(2): p. e78900.
15. Thapak, P. and F. Gomez-Pinilla, *The bioenergetics of traumatic brain injury and its long-term impact for brain plasticity and function*. *Pharmacol Res*, 2024. **208**: p. 107389.
16. LIGHTHALL, J.W., *Controlled Cortical Impact: A New Experimental Brain Injury Model*. *Journal of Neurotrauma*, 1988. **5**(1): p. 1–15.
17. Edward Dixon, C., et al., *A controlled cortical impact model of traumatic brain injury in the rat*. *Journal of Neuroscience Methods*, 1991. **39**(3): p. 253–262.
18. FOX, G.B., et al., *Sustained Sensory/Motor and Cognitive Deficits With Neuronal Apoptosis Following Controlled Cortical Impact Brain Injury in the Mouse*. *Journal of Neurotrauma*, 1998. **15**(8): p. 599–614.
19. Chance, B. and G.R. Williams, *Respiratory enzymes in oxidative phosphorylation. III. The steady state*. *J Biol Chem*, 1955. **217**(1): p. 409–27.
20. Lyons, D.N., et al., *A Mild Traumatic Brain Injury in Mice Produces Lasting Deficits in Brain Metabolism*. *J Neurotrauma*, 2018. **35**(20): p. 2435–2447.

21. Kalimon, O.J. and P.G. Sullivan, *Sex Differences in Mitochondrial Function Following a Controlled Cortical Impact Traumatic Brain Injury in Rodents*. *Front Mol Neurosci*, 2021. **14**: p. 753946.
22. Kalimon, O.J., et al., *Characterizing Sex Differences in Mitochondrial Dysfunction After Severe Traumatic Brain Injury in Mice*. *Neurotrauma Rep*, 2023. **4**(1): p. 627–642.
23. Gilmer, L.K., et al., *Early mitochondrial dysfunction after cortical contusion injury*. *J Neurotrauma*, 2009. **26**(8): p. 1271–80.
24. Singh, I.N., et al., *Time Course of Post-Traumatic Mitochondrial Oxidative Damage and Dysfunction in a Mouse Model of Focal Traumatic Brain Injury: Implications for Neuroprotective Therapy*. *Journal of Cerebral Blood Flow & Metabolism*, 2006. **26**(11): p. 1407–1418.
25. Hill, R.L., et al., *Time courses of post-injury mitochondrial oxidative damage and respiratory dysfunction and neuronal cytoskeletal degradation in a rat model of focal traumatic brain injury*. *Neurochem Int*, 2017. **111**: p. 45–56.
26. Kulbe, J.R., et al., *Synaptic Mitochondria Sustain More Damage than Non-Synaptic Mitochondria after Traumatic Brain Injury and Are Protected by Cyclosporine A*. *J Neurotrauma*, 2017. **34**(7): p. 1291–1301.
27. Haworth, R.A. and D.R. Hunter, *The Ca²⁺-induced membrane transition in mitochondria: II. Nature of the Ca²⁺ trigger site*. *Archives of Biochemistry and Biophysics*, 1979. **195**(2): p. 460–467.
28. Gueven, N., *Idebenone for Leber's hereditary optic neuropathy*. *Drugs Today (Barc)*, 2016. **52**(3): p. 173–81.
29. Anderson, V., et al., *Intellectual ability 10 years after traumatic brain injury in infancy and childhood: what predicts outcome?* *J Neurotrauma*, 2012. **29**(1): p. 143–53.
30. Ragan, D.K., et al., *Alterations in cerebral oxygen metabolism after traumatic brain injury in children*. *J Cereb Blood Flow Metab*, 2013. **33**(1): p. 48–52.
31. Zhang, Z., et al., *Pediatric Traumatic Brain Injury Causes Long-Term Deficits in Adult Hippocampal Neurogenesis and Cognition*. *J Neurotrauma*, 2020. **37**(14): p. 1656–1667.
32. McKenna, M.C., S. Scafidi, and C.L. Robertson, *Metabolic Alterations in Developing Brain After Injury: Knowns and Unknowns*. *Neurochem Res*, 2015. **40**(12): p. 2527–43.
33. Prins, M.L. and J. Matsumoto, *Metabolic Response of Pediatric Traumatic Brain Injury*. *J Child Neurol*, 2016. **31**(1): p. 28–34.
34. Shi, A.C., et al., *Microglial Metabolism After Pediatric Traumatic Brain Injury - Overlooked Bystanders or Active Participants?* *Front Neurol*, 2020. **11**: p. 626999.
35. Robertson, C.L., et al., *The potential role of mitochondria in pediatric traumatic brain injury*. *Dev Neurosci*, 2006. **28**(4-5): p. 432–46.
36. Rubin, T.G. and M.L. Lipton, *Sex Differences in Animal Models of Traumatic Brain Injury*. *Journal of Experimental Neuroscience*, 2019. **13**: p. 1179069519844020.
37. Robertson, C.L. and M. Saraswati, *Progesterone protects mitochondrial function in a rat model of pediatric traumatic brain injury*. *J Bioenerg Biomembr*, 2015. **47**(1-2): p. 43–51.
38. Jaber, S.M., N. Yadava, and B.M. Polster, *Mapping mitochondrial respiratory chain deficiencies by respirometry: Beyond the Mito Stress Test*. *Exp Neurol*, 2020. **328**: p. 113282.
39. Weyer, G., et al., *A controlled study of 2 doses of idebenone in the treatment of Alzheimer's disease*. *Neuropsychobiology*, 1997. **36**(2): p. 73–82.
40. Gutzmann, H. and D. Hadler, *Sustained efficacy and safety of idebenone in the treatment*

- of Alzheimer's disease: update on a 2-year double-blind multicentre study.* J Neural Transm Suppl, 1998. **54**: p. 301–10.
41. Thal, L.J., et al., *Idebenone treatment fails to slow cognitive decline in Alzheimer's disease.* Neurology, 2003. **61**(11): p. 1498–502.
 42. Haefeli, R.H., et al., *NQO1-dependent redox cycling of idebenone: effects on cellular redox potential and energy levels.* PLoS One, 2011. **6**(3): p. e17963.
 43. Heitz, F.D., et al., *Idebenone protects against retinal damage and loss of vision in a mouse model of Leber's hereditary optic neuropathy.* PLoS One, 2012. **7**(9): p. e45182.
 44. Hwang, H., et al., *Idebenone Mitigates Traumatic-Brain-Injury-Triggered Gene Expression Changes to Ephrin-A and Dopamine Signaling Pathways While Increasing Microglial Genes.* Cells, 2025. **14**(11).
 45. Gueven, N., K. Woolley, and J. Smith, *Border between natural product and drug: comparison of the related benzoquinones idebenone and coenzyme Q10.* Redox Biol, 2015. **4**: p. 289–95.
 46. Dinkova-Kostova, A.T. and P. Talalay, *NAD(P)H:quinone acceptor oxidoreductase 1 (NQO1), a multifunctional antioxidant enzyme and exceptionally versatile cytoprotector.* Arch Biochem Biophys, 2010. **501**(1): p. 116–23.
 47. Jaber, S.M., et al., *Idebenone Has Distinct Effects on Mitochondrial Respiration in Cortical Astrocytes Compared to Cortical Neurons Due to Differential NQO1 Activity.* J Neurosci, 2020. **40**(23): p. 4609–4619.
 48. Loane, D.J. and A. Kumar, *Microglia in the TBI brain: The good, the bad, and the dysregulated.* Exp Neurol, 2016. **275 Pt 3**(0 3): p. 316–327.
 49. Li, Y., et al., *Mitochondrial dysfunction in microglia: a novel perspective for pathogenesis of Alzheimer's disease.* Journal of Neuroinflammation, 2022. **19**(1): p. 248.
 50. Ye, J., et al., *Electron transport chain inhibitors induce microglia activation through enhancing mitochondrial reactive oxygen species production.* Exp Cell Res, 2016. **340**(2): p. 315–26.
 51. SM., J.T., *Effects of Idebenone on the Mitochondrial Respiration of Neurons, Astrocytes, and Microglia.* ProQuest Dissertations & Theses, 2018.
 52. jaber, S., 2018.
 53. Burda, J.E. and M.V. Sofroniew, *Reactive gliosis and the multicellular response to CNS damage and disease.* Neuron, 2014. **81**(2): p. 229–48.
 54. Gao, C., et al., *Microglia in neurodegenerative diseases: mechanism and potential therapeutic targets.* Signal Transduction and Targeted Therapy, 2023. **8**(1): p. 359.
 55. Strogulski, N.R., et al., *Fundamental Neurochemistry Review: Microglial immunometabolism in traumatic brain injury.* J Neurochem, 2023. **167**(2): p. 129–153.
 56. Xu, L., D. He, and Y. Bai, *Microglia-Mediated Inflammation and Neurodegenerative Disease.* Mol Neurobiol, 2016. **53**(10): p. 6709–6715.
 57. Cheepsunthorn, P., et al., *Characterization of a novel brain-derived microglial cell line isolated from neonatal rat brain.* Glia, 2001. **35**(1): p. 53–62.
 58. Woolf, Z., et al., *In vitro models of microglia: a comparative study.* Scientific Reports, 2025. **15**(1): p. 15621.
 59. McCarthy, R.C., et al., *Characterization of a novel adult murine immortalized microglial cell line and its activation by amyloid-beta.* J Neuroinflammation, 2016. **13**: p. 21.
 60. Nagamoto-Combs, K., J. Kulas, and C.K. Combs, *A novel cell line from spontaneously immortalized murine microglia.* Journal of Neuroscience Methods, 2014. **233**: p. 187–198.

61. Papageorgiou, I.E., et al., *TLR4-activated microglia require IFN- γ to induce severe neuronal dysfunction and death in situ*. Proc Natl Acad Sci U S A, 2016. **113**(1): p. 212–7.
62. Zhang, Y., et al., *Toll-like receptor 4 (TLR4) inhibitors: Current research and prospective*. Eur J Med Chem, 2022. **235**: p. 114291.
63. Ahmad, A., et al., *Absence of TLR4 reduces neurovascular unit and secondary inflammatory process after traumatic brain injury in mice*. PLoS One, 2013. **8**(3): p. e57208.
64. Yao, X., et al., *TLR4 signal ablation attenuated neurological deficits by regulating microglial M1/M2 phenotype after traumatic brain injury in mice*. J Neuroimmunol, 2017. **310**: p. 38–45.
65. Barochia, A., et al., *Eritoran tetrasodium (E5564) treatment for sepsis: review of preclinical and clinical studies*. Expert Opin Drug Metab Toxicol, 2011. **7**(4): p. 479–94.
66. Kobayashi, S., et al., *Suppression of murine endotoxin response by E5531, a novel synthetic lipid A antagonist*. Antimicrob Agents Chemother, 1998. **42**(11): p. 2824–9.
67. Rice, T.W., et al., *A randomized, double-blind, placebo-controlled trial of TAK-242 for the treatment of severe sepsis**. Critical Care Medicine, 2010. **38**(8): p. 1685–1694.
68. Swanson, K.V., M. Deng, and J.P.Y. Ting, *The NLRP3 inflammasome: molecular activation and regulation to therapeutics*. Nature Reviews Immunology, 2019. **19**(8): p. 477–489.
69. Elliott, E.I., et al., *Cutting Edge: Mitochondrial Assembly of the NLRP3 Inflammasome Complex Is Initiated at Priming*. J Immunol, 2018. **200**(9): p. 3047–3052.
70. Coll, R.C., et al., *MCC950 directly targets the NLRP3 ATP-hydrolysis motif for inflammasome inhibition*. Nat Chem Biol, 2019. **15**(6): p. 556–559.
71. Wang, L., et al., *Novel extracellular and nuclear caspase-1 and inflammasomes propagate inflammation and regulate gene expression: a comprehensive database mining study*. Journal of Hematology & Oncology, 2016. **9**(1): p. 122.
72. Mao, P.L., et al., *Activation of caspase-1 in the nucleus requires nuclear translocation of pro-caspase-1 mediated by its prodomain*. J Biol Chem, 1998. **273**(37): p. 23621–4.
73. Park, S., et al., *Defective mitochondrial fission augments NLRP3 inflammasome activation*. Scientific Reports, 2015. **5**(1): p. 15489.
74. Yu, J., et al., *Inflammasome activation leads to Caspase-1-dependent mitochondrial damage and block of mitophagy*. Proc Natl Acad Sci U S A, 2014. **111**(43): p. 15514–9.
75. Liu, X., et al., *Inflammasome-activated gasdermin D causes pyroptosis by forming membrane pores*. Nature, 2016. **535**(7610): p. 153–158.
76. Miao, R., et al., *Gasdermin D permeabilization of mitochondrial inner and outer membranes accelerates and enhances pyroptosis*. Immunity, 2023. **56**(11): p. 2523–2541.e8.
77. Heilig, R., et al., *Caspase-1 cleaves Bid to release mitochondrial SMAC and drive secondary necrosis in the absence of GSDMD*. Life Sci Alliance, 2020. **3**(6).
78. Flores, J., et al., *Caspase-1 inhibition alleviates cognitive impairment and neuropathology in an Alzheimer's disease mouse model*. Nat Commun, 2018. **9**(1): p. 3916.
79. Sun, Z., et al., *VX765 Attenuates Pyroptosis and HMGB1/TLR4/NF- κ B Pathways to Improve Functional Outcomes in TBI Mice*. Oxid Med Cell Longev, 2020. **2020**: p. 7879629.
80. Chen, K., et al., *Endothelial cell dysfunction and targeted therapeutic drugs in sepsis*. Heliyon, 2024. **10**(13): p. e33340.
81. Xue, Q., et al., *Regulation of iNOS on Immune Cells and Its Role in Diseases*. International

- Journal of Molecular Sciences, 2018. **19**(12): p. 3805.
82. Riobo, N.A., et al., *The modulation of mitochondrial nitric-oxide synthase activity in rat brain development*. J Biol Chem, 2002. **277**(45): p. 42447–55.
 83. Stuehr, D.J. and C.F. Nathan, *Nitric oxide. A macrophage product responsible for cytostasis and respiratory inhibition in tumor target cells*. Journal of Experimental Medicine, 1989. **169**(5): p. 1543–1555.
 84. Moss, D.W. and T.E. Bates, *Activation of murine microglial cell lines by lipopolysaccharide and interferon-gamma causes NO-mediated decreases in mitochondrial and cellular function*. Eur J Neurosci, 2001. **13**(3): p. 529–38.
 85. Chénais, B., H. Morjani, and J.C. Drapier, *Impact of endogenous nitric oxide on microglial cell energy metabolism and labile iron pool*. J Neurochem, 2002. **81**(3): p. 615–23.
 86. Palmieri, E.M., et al., *Nitric oxide orchestrates metabolic rewiring in M1 macrophages by targeting aconitase 2 and pyruvate dehydrogenase*. Nature Communications, 2020. **11**(1): p. 698.
 87. Jafarian-Tehrani, M., et al., *1400W, a potent selective inducible NOS inhibitor, improves histopathological outcome following traumatic brain injury in rats*. Nitric Oxide, 2005. **12**(2): p. 61–69.
 88. Nicholls, D.G. and S.J. Ferguson, *Bioenergetics 4*. 4 ed. 2013, London: Academic Press.
 89. Brand, M.D. and D.G. Nicholls, *Assessing mitochondrial dysfunction in cells*. Biochem J, 2011. **435**(2): p. 297–312.
 90. Patel, M.S. and L.G. Korotchkina, *Regulation of the pyruvate dehydrogenase complex*. Biochem Soc Trans, 2006. **34**(Pt 2): p. 217–22.
 91. Vahsen, N., et al., *AIF deficiency compromises oxidative phosphorylation*. EMBO J, 2004. **23**(23): p. 4679–89.
 92. Perier, C., et al., *Apoptosis-inducing factor deficiency sensitizes dopaminergic neurons to parkinsonian neurotoxins*. Ann Neurol, 2010. **68**(2): p. 184–92.
 93. Chinta, S.J., et al., *Reactive oxygen species regulation by AIF- and complex I-depleted brain mitochondria*. Free Radical Biology and Medicine, 2009. **46**(7): p. 939–947.
 94. Polster, B.M., *AIF, reactive oxygen species, and neurodegeneration: a "complex" problem*. Neurochem Int, 2013. **62**(5): p. 695–702.
 95. Meyer, K., et al., *Loss of apoptosis-inducing factor critically affects MIA40 function*. Cell Death Dis, 2015. **6**: p. e1814.
 96. Hangen, E., et al., *Interaction between AIF and CHCHD4 Regulates Respiratory Chain Biogenesis*. Mol Cell, 2015. **58**(6): p. 1001–14.
 97. Salscheider, S.L., et al., *AIFM1 is a component of the mitochondrial disulfide relay that drives complex I assembly through efficient import of NDUFS5*. Embo j, 2022. **41**(17): p. e110784.
 98. Murari, A., et al., *An antibody toolbox to track complex I assembly defines AIF's mitochondrial function*. J Cell Biol, 2020. **219**(10).
 99. Yakovlev, A.G., et al., *Differential expression of apoptotic protease-activating factor-1 and caspase-3 genes and susceptibility to apoptosis during brain development and after traumatic brain injury*. J Neurosci, 2001. **21**(19): p. 7439–7446.
 100. Stoica, B.A., et al., *Ceramide induces neuronal apoptosis through mitogen-activated protein kinases and causes release of multiple mitochondrial proteins*. Mol Cell Neurosci, 2005. **29**(3): p. 355–371.
 101. Sims, N.R., *Rapid isolation of metabolically active mitochondria from rat brain and*

- subregions using Percoll density gradient centrifugation.* J. Neurochem, 1990. **55**(2): p. 698–707.
102. Clerc, P. and B.M. Polster, *Investigation of mitochondrial dysfunction by sequential microplate-based respiration measurements from intact and permeabilized neurons.* PLoS One, 2012. **7**(4): p. e34465.
 103. Choi, S.W., A.A. Gerencser, and D.G. Nicholls, *Bioenergetic analysis of isolated cerebrocortical nerve terminals on a microgram scale: spare respiratory capacity and stochastic mitochondrial failure.* J Neurochem, 2009. **109**(4): p. 1179–91.
 104. Acin-Perez, R., et al., *A novel approach to measure mitochondrial respiration in frozen biological samples.* EMBO J, 2020. **39**(13): p. e104073.
 105. Gu, X., et al., *Measurement of mitochondrial respiration in adherent cells by Seahorse XF96 Cell Mito Stress Test.* STAR Protoc, 2021. **2**(1): p. 100245.
 106. Kauppinen, R.A. and D.G. Nicholls, *Synaptosomal bioenergetics. The role of glycolysis, pyruvate oxidation and responses to hypoglycaemia.* Eur. J. Biochem, 1986. **158**(1): p. 159–165.
 107. Laird, M.D., et al., *Augmentation of normal and glutamate-impaired neuronal respiratory capacity by exogenous alternative biofuels.* Transl. Stroke Res, 2013. **4**(6): p. 643–651.
 108. Mazzi, E. and K.F. Soliman, *Pyruvic acid cytoprotection against 1-methyl-4-phenylpyridinium, 6-hydroxydopamine and hydrogen peroxide toxicities in vitro.* Neurosci Lett, 2003. **337**(2): p. 77–80.
 109. Guarino, V.A., et al., *Reaction rate of pyruvate and hydrogen peroxide: assessing antioxidant capacity of pyruvate under biological conditions.* Sci Rep, 2019. **9**(1): p. 19568.
 110. Schuh, R.A., et al., *Adaptation of microplate-based respirometry for hippocampal slices and analysis of respiratory capacity.* J Neurosci Res, 2011. **89**(12): p. 1979–88.
 111. Bordt, E.A., et al., *The Putative Drp1 Inhibitor mdivi-1 Is a Reversible Mitochondrial Complex I Inhibitor that Modulates Reactive Oxygen Species.* Dev Cell, 2017. **40**(6): p. 583–594 e6.
 112. Klein, J.A., et al., *The harlequin mouse mutation downregulates apoptosis-inducing factor.* Nature, 2002. **419**(6905): p. 367–374.
 113. Vekaria, H.J., et al., *An efficient and high-throughput method for the evaluation of mitochondrial dysfunction in frozen brain samples after traumatic brain injury.* Front Mol Biosci, 2024. **11**: p. 1378536.
 114. Kim, C., et al., *An X-chromosome linked mouse model (Ndufa1(S55A)) for systemic partial Complex I deficiency for studying predisposition to neurodegeneration and other diseases.* Neurochem Int, 2017. **109**: p. 78–93.
 115. Frazier, A.E., et al., *Assessment of mitochondrial respiratory chain enzymes in cells and tissues.* Methods Cell Biol, 2020. **155**: p. 121–156.
 116. Brustovetsky, N., et al., *Calcium-induced cytochrome c release from CNS mitochondria is associated with the permeability transition and rupture of the outer membrane.* J. Neurochem, 2002. **80**(2): p. 207–218.
 117. Cohen, N.S., C.W. Cheung, and L. Rajjman, *Measurements of mitochondrial volumes are affected by the amount of mitochondria used in the determinations.* Biochem J, 1987. **245**(2): p. 375–9.
 118. Pozueta-Romero, J., et al., *A method for accurate analysis of intermembrane space in organelles enclosed by double envelope membranes.* Cell Struct Funct, 1992. **17**(1): p. 47–53.

119. González-Rodríguez, P., et al., *Disruption of mitochondrial complex I induces progressive parkinsonism*. *Nature*, 2021. **599**(7886): p. 650–656.
120. Keeney, P.M., et al., *Parkinson's disease brain mitochondrial complex I has oxidatively damaged subunits and is functionally impaired and misassembled*. *J Neurosci*, 2006. **26**(19): p. 5256–64.
121. Richardson, J.R., et al., *Obligatory role for complex I inhibition in the dopaminergic neurotoxicity of 1-methyl-4-phenyl-1,2,3,6-tetrahydropyridine (MPTP)*. *Toxicol Sci*, 2007. **95**(1): p. 196–204.
122. Jankovic, J., *Parkinson's disease: clinical features and diagnosis*. *J Neurol Neurosurg Psychiatry*, 2008. **79**(4): p. 368–76.
123. McCormack, A.L., et al., *Environmental Risk Factors and Parkinson's Disease: Selective Degeneration of Nigral Dopaminergic Neurons Caused by the Herbicide Paraquat*. *Neurobiology of Disease*, 2002. **10**(2): p. 119–127.
124. Paul, K.C., et al., *A pesticide and iPSC dopaminergic neuron screen identifies and classifies Parkinson-relevant pesticides*. *Nature Communications*, 2023. **14**(1): p. 2803.
125. Betarbet, R., et al., *Chronic systemic pesticide exposure reproduces features of Parkinson's disease*. *Nat. Neurosci*, 2000. **3**(12): p. 1301–1306.
126. Keenan, H.T. and S.L. Bratton, *Epidemiology and outcomes of pediatric traumatic brain injury*. *Dev Neurosci*, 2006. **28**(4-5): p. 256–63.
127. Kennedy, L., et al., *Moderate and severe TBI in children and adolescents: The effects of age, sex, and injury severity on patient outcome 6 months after injury*. *Front Neurol*, 2022. **13**: p. 741717.
128. Kilbaugh, T.J., et al., *Mitochondrial bioenergetic alterations after focal traumatic brain injury in the immature brain*. *Exp Neurol*, 2015. **271**: p. 136–44.
129. Kilbaugh, T.J., et al., *Mitochondrial response in a toddler-aged swine model following diffuse non-impact traumatic brain injury*. *Mitochondrion*, 2016. **26**: p. 19–25.
130. Kilbaugh, T.J., et al., *Cyclosporin A preserves mitochondrial function after traumatic brain injury in the immature rat and piglet*. *J Neurotrauma*, 2011. **28**(5): p. 763–74.
131. Casey, P.A., et al., *Early and sustained alterations in cerebral metabolism after traumatic brain injury in immature rats*. *J Neurotrauma*, 2008. **25**(6): p. 603–14.
132. Robertson, C.L., M. Saraswati, and G. Fiskum, *Mitochondrial dysfunction early after traumatic brain injury in immature rats*. *J Neurochem*, 2007. **101**(5): p. 1248–57.
133. Gagnard, P., et al., *Sex differences in brain mitochondrial metabolism: influence of endogenous steroids and stroke*. *J Neuroendocrinol*, 2018. **30**(2).
134. Robertson, C.L., et al., *The potential role of mitochondria in pediatric traumatic brain injury*. *Dev. Neurosci*, 2006. **28**(4-5): p. 432–446.
135. Fraunberger, E.A., T.E. Shutt, and M.J. Esser, *Sex-dependent and chronic alterations in behavior and mitochondrial function in a rat model of pediatric mild traumatic brain injury*. *Brain Inj*, 2019. **33**(4): p. 534–542.
136. Zhang, N., et al., *CRABS-ROC, A respirometry protocol for overcoming substrate limitations, reveals excess brain mitochondrial Complex I capacity*. *Free Radic Biol Med*, 2025. **241**: p. 24–31.
137. Pecinova, A., et al., *Evaluation of basic mitochondrial functions using rat tissue homogenates*. *Mitochondrion*, 2011. **11**(5): p. 722–8.
138. Almeida, A., et al., *Postnatal development of the complexes of the electron transport chain in synaptic mitochondria from rat brain*. *Dev Neurosci*, 1995. **17**(4): p. 212–8.

139. Bates, T.E., et al., *Postnatal development of the complexes of the electron transport chain in isolated rat brain mitochondria*. Dev Neurosci, 1994. **16**(5-6): p. 321–7.
140. McClatchy, D.B., et al., *Dynamics of subcellular proteomes during brain development*. J Proteome Res, 2012. **11**(4): p. 2467–79.
141. Li, Y., et al., *An Assembled Complex IV Maintains the Stability and Activity of Complex I in Mammalian Mitochondria**. Journal of Biological Chemistry, 2007. **282**(24): p. 17557–17562.
142. Suthammarak, W., et al., *Complex I function is defective in complex IV-deficient Caenorhabditis elegans*. J Biol Chem, 2009. **284**(10): p. 6425–35.
143. Srinivas Bharath, M.M., *Post-Translational Oxidative Modifications of Mitochondrial Complex I (NADH: Ubiquinone Oxidoreductase): Implications for Pathogenesis and Therapeutics in Human Diseases*. J Alzheimers Dis, 2017. **60**(s1): p. S69–s86.
144. Finelli, M.J., *Redox Post-translational Modifications of Protein Thiols in Brain Aging and Neurodegenerative Conditions—Focus on S-Nitrosation*. Frontiers in Aging Neuroscience, 2020. **Volume 12 - 2020**.
145. Lyseng-Williamson, K.A., *Idebenone: A Review in Leber's Hereditary Optic Neuropathy*. Drugs, 2016. **76**(7): p. 805–13.
146. James, A.M., R.A.J. Smith, and M.P. Murphy, *Antioxidant and prooxidant properties of mitochondrial Coenzyme Q*. Archives of Biochemistry and Biophysics, 2004. **423**(1): p. 47–56.
147. Suno, M. and A. Nagaoka, *Inhibition of lipid peroxidation by a novel compound, idebenone (CV-2619)*. Jpn. J. Pharmacol, 1984. **35**(2): p. 196–198.
148. Torii, H., et al., *Disposition of idebenone (CV-2619), a new cerebral metabolism improving agent, in rats and dogs*. J. Pharmacobiodyn, 1985. **8**(6): p. 457–467.
149. Nagai, Y., et al., *Brain distribution of idebenone and its effect on local cerebral glucose utilization in rats*. Arch. Gerontol. Geriatr, 1989. **8**(3): p. 257–272.
150. Sugiyama, Y. and T. Fujita, *Stimulation of the respiratory and phosphorylating activities in rat brain mitochondria by idebenone (CV-2619), a new agent improving cerebral metabolism*. FEBS Lett, 1985. **184**(1): p. 48–51.
151. Klopstock, T., et al., *A randomized placebo-controlled trial of idebenone in Leber's hereditary optic neuropathy*. Brain, 2011. **134**(Pt 9): p. 2677–2686.
152. Jaber, S. and B.M. Polster, *Idebenone and neuroprotection: antioxidant, pro-oxidant, or electron carrier?* J. Bioenerg. Biomembr, 2015. **47**(1-2): p. 111–118.
153. Giorgio, V., et al., *The effects of idebenone on mitochondrial bioenergetics*. Biochim Biophys Acta, 2012. **1817**(2): p. 363–9.
154. Suno, M. and A. Nagaoka, *Inhibition of lipid peroxidation by a novel compound (CV-2619) in brain mitochondria and mode of action of the inhibition*. Biochem. Biophys. Res. Commun, 1984. **125**(3): p. 1046–1052.
155. Varricchio, C., et al., *The ying and yang of idebenone: Not too little, not too much - cell death in NQO1 deficient cells and the mouse retina*. Free Radic Biol Med, 2020. **152**: p. 551–560.
156. Song, W.M. and M. Colonna, *The identity and function of microglia in neurodegeneration*. Nat Immunol, 2018. **19**(10): p. 1048–1058.
157. Bordt, E.A. and B.M. Polster, *NADPH oxidase- and mitochondria-derived reactive oxygen species in proinflammatory microglial activation: a bipartisan affair?* Free Radic Biol Med, 2014. **76**: p. 34–46.

158. Orihuela, R., C.A. McPherson, and G.J. Harry, *Microglial M1/M2 polarization and metabolic states*. *Br J Pharmacol*, 2016. **173**(4): p. 649–65.
159. Papageorgiou, I.E., et al., *TLR4-activated microglia require IFN-gamma to induce severe neuronal dysfunction and death in situ*. *Proc Natl Acad Sci U S A*, 2016. **113**(1): p. 212–7.
160. Mills, E.L., et al., *Itaconate is an anti-inflammatory metabolite that activates Nrf2 via alkylation of KEAP1*. *Nature*, 2018. **556**(7699): p. 113–117.
161. Briere, J.J., et al., *Quinone analogues regulate mitochondrial substrate competitive oxidation*. *Biochem Biophys Res Commun*, 2004. **316**(4): p. 1138–42.
162. Suno, M. and A. Nagaoka, *Inhibition of lipid peroxidation by idebenone in brain mitochondria in the presence of succinate*. *Arch. Gerontol. Geriatr*, 1989. **8**(3): p. 291–297.
163. Rauchova, H., M. Vokurkova, and Z. Drahota, *Idebenone-induced recovery of glycerol-3-phosphate and succinate oxidation inhibited by digitonin*. *Physiol Res*, 2012. **61**(3): p. 259–265.
164. Degli Esposti, M., et al., *The interaction of Q analogs, particularly hydroxydecyl benzoquinone (idebenone), with the respiratory complexes of heart mitochondria*. *Arch. Biochem. Biophys*, 1996. **330**(2): p. 395–400.
165. Stringer, J.L., et al., *Presence and induction of the enzyme NAD(P)H: quinone oxidoreductase 1 in the central nervous system*. *J Comp Neurol*, 2004. **471**(3): p. 289–97.
166. Prochaska, H.J., *Purification and crystallization of rat liver NAD(P)H:(quinone-acceptor) oxidoreductase by cibacron blue affinity chromatography: identification of a new and potent inhibitor*. *Arch Biochem Biophys*, 1988. **267**(2): p. 529–38.
167. Narayanaswamy, R.K.W., L.; Safinar I.I., *Molecular Docking Studies of Quinones against Human Inducible Nitric Oxide Synthase (iNOS)*. *Journal of Chemical and Pharmaceutical Research*, 2017. **9**(5): p. 39–44.
168. Jaber, S.M., et al., *Sex differences in the mitochondrial bioenergetics of astrocytes but not microglia at a physiologically relevant brain oxygen tension*. *Neurochem. Int*, 2018. **117**: p. 82–90.
169. Palmieri, E.M., et al., *Nitric oxide orchestrates metabolic rewiring in M1 macrophages by targeting aconitase 2 and pyruvate dehydrogenase*. *Nat Commun*, 2020. **11**(1): p. 698.
170. Bailey, J.D., et al., *Nitric Oxide Modulates Metabolic Remodeling in Inflammatory Macrophages through TCA Cycle Regulation and Itaconate Accumulation*. *Cell Rep*, 2019. **28**(1): p. 218–230 e7.
171. Van den Bossche, J., et al., *Mitochondrial Dysfunction Prevents Repolarization of Inflammatory Macrophages*. *Cell Rep*, 2016. **17**(3): p. 684–696.
172. Jiang, H.B., et al., *Reductive activation of mitomycin C by neuronal nitric oxide synthase*. *Biochem Pharmacol*, 2000. **60**(4): p. 571–9.
173. Hope, B.T. and S.R. Vincent, *Histochemical characterization of neuronal NADPH-diaphorase*. *J Histochem Cytochem*, 1989. **37**(5): p. 653–61.
174. Hope, B.T., et al., *Neuronal NADPH diaphorase is a nitric oxide synthase*. *Proc Natl Acad Sci U S A*, 1991. **88**(7): p. 2811–4.
175. Murphy, T.H., A.P. So, and S.R. Vincent, *Histochemical detection of quinone reductase activity in situ using LY 83583 reduction and oxidation*. *J Neurochem*, 1998. **70**(5): p. 2156–64.
176. Kumagai, Y., et al., *Inhibition of nitric oxide formation by neuronal nitric oxide synthase by quinones: nitric oxide synthase as a quinone reductase*. *Chem Res Toxicol*, 1998. **11**(6): p. 608–13.

177. Poderoso, J.J., et al., *The reaction of nitric oxide with ubiquinol: kinetic properties and biological significance*. Free Radic Biol Med, 1999. **26**(7-8): p. 925–35.
178. Suno, M. and A. Nagaoka, *Inhibition of lipid peroxidation by idebenone in brain mitochondria in the presence of succinate*. Archives of Gerontology and Geriatrics, 1989. **8**(3): p. 291–297.
179. Byrnes, K.R., et al., *Expression of two temporally distinct microglia-related gene clusters after spinal cord injury*. Glia, 2006. **53**(4): p. 420–433.
180. McKenna, M.C., *Substrate competition studies demonstrate oxidative metabolism of glucose, glutamate, glutamine, lactate and 3-hydroxybutyrate in cortical astrocytes from rat brain*. Neurochem Res, 2012. **37**(11): p. 2613–2626.
181. Danilov, C.A. and G. Fiskum, *Hyperoxia promotes astrocyte cell death after oxygen and glucose deprivation*. Glia, 2008. **56**(7): p. 801–808.
182. Bell-Temin, H., et al., *Proteomic analysis of rat microglia establishes a high-confidence reference data set of over 3000 proteins*. Proteomics, 2012. **12**(2): p. 246–50.
183. Feng, X., et al., *Glucocorticoid-Driven NLRP3 Inflammasome Activation in Hippocampal Microglia Mediates Chronic Stress-Induced Depressive-Like Behaviors*. Front Mol Neurosci, 2019. **12**: p. 210.
184. Sun, Y., et al., *High-Mobility Group Box 1 Contributes to Cerebral Cortex Injury in a Neonatal Hypoxic-Ischemic Rat Model by Regulating the Phenotypic Polarization of Microglia*. Front Cell Neurosci, 2019. **13**: p. 506.
185. Smith, P.K., et al., *Measurement of protein using bicinchoninic acid*. Anal Biochem, 1985. **150**(1): p. 76–85.
186. Williamson, J.C., et al., *High-performance hybrid Orbitrap mass spectrometers for quantitative proteome analysis: Observations and implications*. Proteomics, 2016. **16**(6): p. 907–914.
187. Eng, J.K., et al., *A fast SEQUEST cross correlation algorithm*. J Proteome Res, 2008. **7**(10): p. 4598–602.
188. Kall, L., et al., *Semi-supervised learning for peptide identification from shotgun proteomics datasets*. Nat. Methods, 2007. **4**(11): p. 923–925.
189. Gerencser, A.A., et al., *Quantitative microplate-based respirometry with correction for oxygen diffusion*. Anal Chem, 2009. **81**(16): p. 6868–6878.
190. Clerc, P. and B.M. Polster, *Investigation of mitochondrial dysfunction by sequential microplate-based respiration measurements from intact and permeabilized neurons*. PLoS. ONE, 2012. **7**(4): p. e34465.
191. Lee, E. and Y. Chang, *Modulating Neuroinflammation as a Prospective Therapeutic Target in Alzheimer's Disease*. Cells, 2025. **14**(3).
192. Valiukas, Z., et al., *Microglial activation states and their implications for Alzheimer's Disease*. J Prev Alzheimers Dis, 2025. **12**(1): p. 100013.
193. Jurcau, A., et al., *The Involvement of Neuroinflammation in the Onset and Progression of Parkinson's Disease*. Int J Mol Sci, 2023. **24**(19).
194. Yang, I., et al., *The role of microglia in central nervous system immunity and glioma immunology*. J Clin Neurosci, 2010. **17**(1): p. 6–10.
195. Kelley, N., et al., *The NLRP3 Inflammasome: An Overview of Mechanisms of Activation and Regulation*. Int J Mol Sci, 2019. **20**(13).
196. Yuste, J.E., et al., *Implications of glial nitric oxide in neurodegenerative diseases*. Front Cell Neurosci, 2015. **9**: p. 322.

197. Liy, P.M., et al., *Nitric oxide modulation in neuroinflammation and the role of mesenchymal stem cells*. *Exp Biol Med* (Maywood), 2021. **246**(22): p. 2399–2406.
198. Smith, J.A., et al., *Role of pro-inflammatory cytokines released from microglia in neurodegenerative diseases*. *Brain Res Bull*, 2012. **87**(1): p. 10–20.
199. Peruzzotti-Jametti, L., et al., *Mitochondrial complex I activity in microglia sustains neuroinflammation*. *Nature*, 2024. **628**(8006): p. 195–203.
200. Billingham, L.K., et al., *Mitochondrial electron transport chain is necessary for NLRP3 inflammasome activation*. *Nature Immunology*, 2022. **23**(5): p. 692–704.
201. Bailey, J.D., et al., *Nitric Oxide Modulates Metabolic Remodeling in Inflammatory Macrophages through TCA Cycle Regulation and Itaconate Accumulation*. *Cell Rep*, 2019. **28**(1): p. 218–230.e7.
202. Panigrahi, P.K., et al., *Ultrawide field angiography in proliferative diabetic retinopathy*. *Indian J Ophthalmol*, 2024. **72**(5): p. 754.
203. Jaber, S.M., et al., *Sex differences in the mitochondrial bioenergetics of astrocytes but not microglia at a physiologically relevant brain oxygen tension*. *Neurochem Int*, 2018. **117**: p. 82–90.
204. Fan, T.J., et al., *Caspase family proteases and apoptosis*. *Acta Biochim Biophys Sin* (Shanghai), 2005. **37**(11): p. 719–27.
205. Fu, J. and H. Wu, *Structural Mechanisms of NLRP3 Inflammasome Assembly and Activation*. *Annu Rev Immunol*, 2023. **41**: p. 301–316.
206. Paik, S., et al., *An update on the regulatory mechanisms of NLRP3 inflammasome activation*. *Cellular & Molecular Immunology*, 2021. **18**(5): p. 1141–1160.
207. Garvey, E.P., et al., *1400W is a slow, tight binding, and highly selective inhibitor of inducible nitric-oxide synthase in vitro and in vivo*. *J Biol Chem*, 1997. **272**(8): p. 4959–63.
208. Kayagaki, N., et al., *Caspase-11 cleaves gasdermin D for non-canonical inflammasome signalling*. *Nature*, 2015. **526**(7575): p. 666–71.
209. Matsunaga, N., et al., *TAK-242 (Resatorvid), a Small-Molecule Inhibitor of Toll-Like Receptor (TLR) 4 Signaling, Binds Selectively to TLR4 and Interferes with Interactions between TLR4 and Its Adaptor Molecules*. *Molecular Pharmacology*, 2011. **79**(1): p. 34–41.
210. Takashima, K., et al., *Analysis of binding site for the novel small-molecule TLR4 signal transduction inhibitor TAK-242 and its therapeutic effect on mouse sepsis model*. *Br J Pharmacol*, 2009. **157**(7): p. 1250–62.
211. Kawamoto, T., et al., *TAK-242 selectively suppresses Toll-like receptor 4-signaling mediated by the intracellular domain*. *European Journal of Pharmacology*, 2008. **584**(1): p. 40–48.
212. Lee, H.J., J.H. Park, and H.S. Hoe, *Idebenone Regulates A β and LPS-Induced Neurogliosis and Cognitive Function Through Inhibition of NLRP3 Inflammasome/IL-1 β Axis Activation*. *Front Immunol*, 2022. **13**: p. 749336.
213. Yan, A., et al., *Idebenone Alleviates Neuroinflammation and Modulates Microglial Polarization in LPS-Stimulated BV2 Cells and MPTP-Induced Parkinson's Disease Mice*. *Front Cell Neurosci*, 2018. **12**: p. 529.
214. Chen, C., et al., *Idebenone Orchestrates Anti-Inflammatory and Antioxidant Responses to Alleviate Brain Injury After Intracerebral Hemorrhage in Mice*. *J Integr Neurosci*, 2025. **24**(6): p. 37182.

215. Choi, Y., et al., *Anti-Inflammatory Effects of Idebenone Attenuate LPS-Induced Systemic Inflammatory Diseases by Suppressing NF- κ B Activation*. *Antioxidants*, 2024. **13**(2): p. 151.
216. Cheng, G., et al., *Mitochondria in traumatic brain injury and mitochondrial-targeted multipotential therapeutic strategies*. *Br J Pharmacol*, 2012. **167**(4): p. 699–719.
217. Tabassum, S., et al., *Mitochondrial-targeted therapies in traumatic brain injury: From bench to bedside*. *Neurotherapeutics*, 2025. **22**(1): p. e00515.
218. Sridharan, P.S., et al., *Acutely blocking excessive mitochondrial fission prevents chronic neurodegeneration after traumatic brain injury*. *Cell Reports Medicine*, 2024. **5**(9).
219. Zhu, M., et al., *Mitophagy in Traumatic Brain Injury: A New Target for Therapeutic Intervention*. *Oxid Med Cell Longev*, 2022. **2022**: p. 4906434.
220. Olatona, O.A., et al., *Mitochondria: the hidden engines of traumatic brain injury-driven neurodegeneration*. *Front Cell Neurosci*, 2025. **19**: p. 1570596.
221. Simmons, E.C., N.E. Scholpa, and R.G. Schnellmann, *Mitochondrial biogenesis as a therapeutic target for traumatic and neurodegenerative CNS diseases*. *Exp Neurol*, 2020. **329**: p. 113309.
222. Cheng, X.T., N. Huang, and Z.H. Sheng, *Programming axonal mitochondrial maintenance and bioenergetics in neurodegeneration and regeneration*. *Neuron*, 2022. **110**(12): p. 1899–1923.
223. Ahluwalia, M., et al., *Rescuing mitochondria in traumatic brain injury and intracerebral hemorrhages - A potential therapeutic approach*. *Neurochem Int*, 2021. **150**: p. 105192.
224. Acin-Perez, R., et al., *A novel approach to measure mitochondrial respiration in frozen biological samples*. *The EMBO Journal*, 2020. **39**(13): p. e104073.
225. Guzy, R.D., et al., *Loss of the SdhB, but Not the SdhA, subunit of complex II triggers reactive oxygen species-dependent hypoxia-inducible factor activation and tumorigenesis*. *Mol Cell Biol*, 2008. **28**(2): p. 718–31.
226. Mao, K., et al., *Nitric oxide suppresses NLRP3 inflammasome activation and protects against LPS-induced septic shock*. *Cell Research*, 2013. **23**(2): p. 201–212.
227. Man, S.M., et al., *Differential roles of caspase-1 and caspase-11 in infection and inflammation*. *Scientific Reports*, 2017. **7**(1): p. 45126.